DISSERTATION

SIMULTANEOUS WIRELESS INFORMATION AND POWER TRANSFER (SWIPT) IN COOPERATIVE NETWORKS

Submitted by

Dexin Wang

Department of Electrical and Computer Engineering

In partial fulfillment of the requirements

For the Degree of Doctor of Philosophy

Colorado State University

Fort Collins, Colorado

Spring 2019

Doctoral Committee:

Advisor: Liuqing Yang

Edwin K. P. Chong
Jie Luo
Haonan Wang

ABSTRACT

SIMULTANEOUS WIRELESS INFORMATION AND POWER TRANSFER (SWIPT) IN COOPERATIVE NETWORKS

In recent years, the capacity and charging speed of batteries have become the bottleneck of mobile communications systems. Energy harvesting (EH) is regarded as a promising technology to significantly extend the lifetime of battery-powered devices. Among many EH technologies, simultaneous wireless information and power transfer (SWIPT) proposes to harvest part of the energy carried by the wireless communication signals. In particular, SWIPT has been successfully applied to energy-constrained relays that are mainly or exclusively powered by the energy harvested from the received signals. These relays are known as EH relays, which attract significant attention in both the academia and the industry.

In this research, we investigate the performance of SWIPT-based EH cooperative networks and the optimization problems therein. Due to hardware limitations, the energy harvesting circuit cannot decode the signal directly. Time-switching (TS) and power splitting (PS) are the most popular solutions to this problem. In this research, we focus on PS-based SWIPT because of its superier performance.

First, different from existing work that employs TS-based SWIPT, we propose to employ PS based SWIPT for a truly full-duplex (FD) EH relay network, where the information reception and transmission take place simultaneously at the relay all the time. This more thorough exploitation of the FD feature consequently leads to a significant capacity improvement compared with existing alternatives in the literature.

Secondly, when multiple relays are available in the network, we explore the relay selection (RS) and network beamforming techniques in EH relay networks. Assuming orthogonal bandwidth allocation, both single relay selection (SRS) and general relay selection (GRS) without the limit on the number of cooperating relays are investigated and the corresponding RS methods are proposed. We will show that our proposed heuristic GRS methods outperform the SRS methods and achieve very similar performance compared with the optimal RS method achieved by exhaustive search but with dramatically reduced complexity. Under the shared bandwidth assumption, network beamforming among EH relays is investigated. We propose a joint PS factor optimization method based on semidefinite relaxation. Simulations show that network beamforming achieves the best performance among all other cooperative techniques.

Finally, we study the problem of power allocation and PS factor optimization for SWIPT over doubly-selective wireless channels. In contrast to existing work in the literature, we take the channel variation in both time and frequency domains into consideration and jointly optimize the power allocation and the PS factors. The objective is to maximize the achievable data rate with constraints on the delivered energy in a time window. Since the problem is difficult to solve directly due to its nonconvexity, we proposed a two-step approach, named joint power allocation and splitting (JoPAS), to solve the problem along the time and frequency dimensions sequentially. Simulations show significantly improved performance compared with the existing dynamic power splitting scheme. A suboptimal heuristic algorithm, named decoupled power allocation and splitting (DePAS), is also proposed with significantly reduced computational complexity and simulations demonstrate its near-optimum performance.

ACKNOWLEDGMENTS

First and foremost, thanks be to God, my Lord Jesus Christ, and the Holy Spirit. His guidance, comfort, and providence have been the source of my wisdom and strength during the entire pursuit of my Ph.D. degree.

I would like to sincerely express my gratitude, appreciation, and admiration to my advisor Dr. Liuqing Yang for her guidance and support, in both academic and personal aspects, throughout my Ph.D. study. Being an excellent teacher and researcher, she has taught and shown me the methodology and characters that are crucial to a researcher. Her insights, kindness, and patience have inspired me during my Ph.D. study and, I believe, beyond.

I would like to thank Dr. Edwin Chong, Dr. J. Rockey Luo and Dr. Haonan Wang, for their valuable time and efforts in serving on my supervisory committee. Their valuable insights and comments benefit my research a lot.

I am also very grateful for my friends and colleagues: Dr. Rongqing Zhang, Dr. Dongliang Duan, Dr. Xiang Cheng, Luoyang Fang, Dr. Xilin Cheng, Dr. Wenshu Zhang, Dr. Bo Yu, Pan Deng, Dr. Ning Wang, Robert Griffith, Dr. Jian Dang, Dr. Xiaotian Zhou, Dr. Yang Cao, Shijian Gao, Xinhu Zheng, Qiang Cui, Dr. Rui Hou, and Yupeng Li. I have benefited immensely from their friendship and support. I would like to express my special gratitude to Dr. Rongqing Zhang for his valuable expertise, time and efforts in guiding my research.

Finally, my heartiest thanks go to my wife Yanyan Zhu and my parents. They were always by my side, and their unconditioned love and encouragement have supported me throughout my Ph.D. study.

DEDICATION

To my Lord God Jesus Christ

and my wife, Yanyan

and my parents, Wenliang and Songxia

TABLE OF CONTENTS

LIST OF FIGURES

INDEX OF NOTATION

$(\cdot)^\top$	Transpose
$(\cdot)^*$	Complex conjugate
$(\cdot)^H$	Hermitian
$\mathbb{E}[\cdot]$	Expectation
$\lvert\cdot\rvert$	Absolue value
$\arg\max_x f(x)$	Argument of the maximum
$\arg\min_x f(x)$	Argument of the minimum
$\boldsymbol{A}_{ij}$	(i,j)-th entry of matrix $\boldsymbol{A}$
$\boldsymbol{A}^{-1}$	Inverse of matrix $\boldsymbol{A}$
$\det(\cdot)$	Determinant
$\mathrm{tr}\{\cdot\}$	Trace
$\mathrm{diag}(\boldsymbol{h})$	a diagonal matrix with elements of vector $\boldsymbol{h}$ on its diagonal
$\mathbf{0}_{M\times N}$	All-zero matrix of size $M \times N$
$\mathbf{1}_M$	All-one column vector of size $M \times 1$

CHAPTER 1

INTRODUCTION

Traditionally, mobile devices in wireless communication systems are powered by batteries. However, the development in the portable energy storage industry is stagnant compared with the vibrant wireless communications industry. In addition, the limited capacity of batteries significantly hinders the application of the rapidly developing wireless communication technologies [1]. On the other hand, for decades, the solutions to extend the lifetime of battery-powered wireless devices are confined to battery replacement or wired charging, which are inconvenient or sometimes even challenging for mobile devices. Energy harvesting (EH) attracts people's attention for its potential to provide a more convenient, safer, and more environment friendly alternative. EH has the potential to significantly extend the lifetime of battery-powered devices and, in some cases, to eliminate the necessity of batteries. Besides traditional energy harvesting from sources such as solar, wind, vibration, and heat, a new solution is to exploit the energy carried by radio-frequency (RF) signals. Simultaneous wireless information and power transfer (SWIPT) is one of the technologies that employs EH from RF signals.

1.1 Simultaneous Wireless Information and Power Transfer

It is recognized that both energy and information are carried by the same wireless signals. In conventional wireless communications, however, only the information is extracted at the receiving end. Energy cooperation exploits such a fact by transmitting power and information

over separate frequency bands [2]. However, the band allocated for power transfer cannot be used for information transmission. Consequently, the information transmission rate is significantly undermined by the reduced bandwidth. Therefore, SWIPT was proposed [3].

Different from energy cooperation, the transmitter in SWIPT transmits energy and information over the same frequency band. In [4], the study of fundamental tradeoffs in SWIPT was extended to frequency-selective channels. In the literature, SWIPT schemes can be classified into two categories. In one category, the receivers are assumed to be able to extract information and to harvest energy from the received signal simultaneously [3, 4]. However, practical circuits for energy harvesting from wireless signals are not yet able to directly process the information carried by the signals [5]. This triggers the study of the other category, in which the receivers adopt time switching (TS), shown in Fig. 1.1a, or power splitting (PS), shown in Fig. 1.1b, to coordinate the information processing (IP) and the energy harvesting (EH). Part of the time or power of the received signal is allocated to IP and the remaining part is used for EH.

(a) Time switching (b) Power splitting

Figure 1.1: Practical SWIPT schemes

1.2 Cooperative Communications and Relay Networks

Cooperative relaying has emerged as a coverage-extending technique in wireless communications networks. It is also a revolutionary technique that can greatly improve the energy efficiency (EE) by shortening the distances between Tx and Rx devices of each link. Energy efficient resource allocation/scheduling schemes in cooperative relaying networks have been intensively studied in the literature to achieve the desired tradeoff between spectrum efficiency (SE) and EE [6].

In a wireless network where multiple relays are available, relay selection (RS) is a practical solution to exploit the cooperative diversity. It has been a topic that attracts considerable attention in the academia [7–12]. Most existing work focused on the RS problem under the assumption that relays transmit over orthogonal channels and have independent power constraints. In this case, it is obvious that selecting only one relay is optimal in terms of spectrum efficiency, since the relay with the highest end-to-end signal-to-interference-and-noise ratio (SINR) can achieve the highest rate when acquiring the entire channel bandwidth exclusively. The concept of relay selection was extended to multiple selected relays for relays cooperating in a shared bandwidth in [8, 9]. In this case, single relay selection (SRS) is no longer optimal, since selecting multiple relays could enhance the signal-to-noise ratio (SNR) at the receiver without dividing the channel bandwidth as in the orthogonal channel allocation case.

1.3 Applications of SWIPT in Relay Networks

EH relaying is the combination of SWIPT and the relaying technique. In typical EH relay networks, the relays are the only nodes with the SWIPT capability. We will explain the concept of EH relaying with a simple example as follows. In a 3-node HD relay network with a source, a relay, and a destination, the source transmits signals to the relay in the first half of the transmission cycle. The relay separates the received signals, by time or power, into two parts for information and energy respectively. In the second half of the transmission cycle, the relay forwards the information obtained to the destination using the harvested energy.

In contrast to conventional relays, which consume their own energy to facilitate communications between other nodes, EH relays operate primarily or exclusively on the energy harvested from the received signals. Consequently, their dependence on batteries is significantly alleviated or completely removed. We will introduce various types of EH relaying techniques in Chapter 2.

1.4 Dissertation Organization

The organization of this dissertation is as follows. EH relaying is introduced in Chapter 2 in detail. The PS-SWIPT-based FD EH relay networks are studied in Chapter 3. The RS, as a orthogonal-channel cooperative technique, in FD EH one-way and two-way relay networks is investigated in Chapters 4 and 5, respectively. The network beamforming, as a shared-bandwidth cooperative technique, in EH relay networks is presented in Chapter 6. Finally, Chapter 7 presents the joint power allocation and splitting in point-to-point SWIPT

over doubly-selective channels. A summary and discussion of future works is presented in Chapter 8.

CHAPTER 2

ENERGY HARVESTING RELAY NETWORKS

Wireless relays can potentially extend the range of communications of the wireless transceivers without raising the transmit power [13, 14]. However, the power consumption of the relays limits their lifetime if constant power supply is not available. Among the technologies being studied, energy harvesting has the potential to significantly extend the lifetime of battery-powered devices and, in some cases, to eliminate the necessity of batteries.

SWIPT has been successfully applied at energy-constrained relay nodes that harvest the energy of the received wireless signals. Relays of this type operate mainly or exclusively based on the harvested energy. This topic has been well investigated in the academia [15]. TS based relaying and PS based relaying are two prevalent types of schemes. In HD EH relay networks, as shown in Fig. 2.1, each transmission cycle through the relay node is divided into two phases. In the first phase, the relay node receives signals from the source node with SWIPT, in either TS or PS manner. In the second phase, the relay node forwards the signals to the destination node with energy harvested in the first phase.

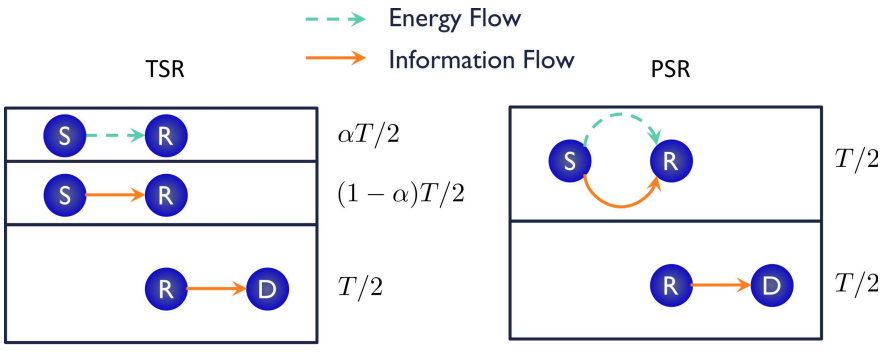

Figure 2.1: Half-duplex energy harvesting relay networks

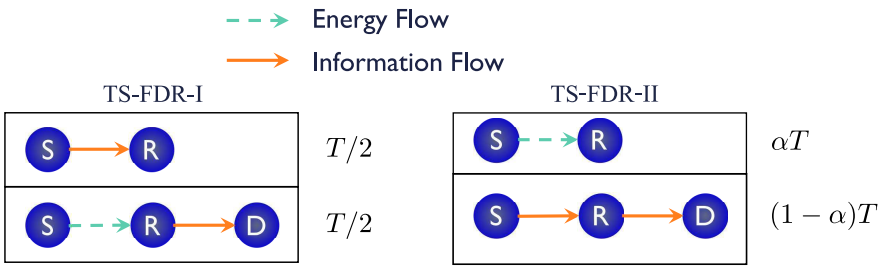

Figure 2.2: Full-duplex energy harvesting relay networks

Though existing work mostly focused on HD relaying, with the advancement in self-interference cancellation techniques [16–18], full-duplex (FD) relay networks are gaining increasing interest due to their significant performance advantages over HD ones [19]. Two representative FD EH relaying schemes are depicted in Fig. 2.2. A TS-based FD relaying scheme, termed as TS-FDR-I in this dissertation, was proposed in [20] and later extended in [21]. In this scheme, each transmission cycle T is divided into two phases by a TS factor $\alpha \in [0, 1]$. The source-to-relay (S-R) link is used for EH in the first phase, i.e. $t \in [0, \alpha T)$, and for IP in the second phase, i.e. $t \in [\alpha T, T)$. During the second phase, the relay not only receives information from the source, but also forwards information to the destination simultaneously. In [22], another FD EH relaying scheme, termed as TS-FDR-II, was proposed with equally divided phases. This scheme uses the S-R link for IP in the first phase and for EH in the second phase. Hence, the loopback self-interference becomes beneficial to the relaying network. These FD schemes utilize the spectral resource in a more efficient manner compared with the HD ones. Nevertheless, the relays in all these FD schemes can only transmit and/or receive information during a fraction of each transmission cycle. Therefore, we propose to further improve the relaying efficiency by fully exploiting the FD feature via PS-SWIPT [23]. This work will be presented in Chapter 3

CHAPTER 3

POWER-SPLITTING-BASED FULL-DUPLEX ENERGY-HARVESTING RELAY NETWORKS

In this chapter, we propose a PS-based full-duplex relaying (PS-FDR) scheme, in which the relay node simultaneously transmits and receives signals all the time, leading to a truly full-duplex information transfer. This is achieved by coordinating EH and IP via PS. We compare our proposed PS-FDR with TS-FDR alternatives in existing work under realistic settings. And the simulations show the capacity improvement of our proposed PS-FDR with most possible PS factor values. Our main contributions lie in the following three aspects.

- To the best of our knowledge, we are the first to apply PS-SWIPT to energy-harvesting full-duplex relay networks. The resultant relay node operation is truly full-duplex such that uninterrupted information flow is maintained on both S-R and R-D links simultaneously all the time. This is to be contrasted with existing TS alternatives, in which IP and EH share the time span of a transmission period.

- We investigate the optimum PS factor with various loopback interference levels. The quasi-convexity of the optimization problem is proved. Additionally, the closed-form optimal PS factor is derived when the residual self-interference channel gain is sufficiently small.

- We derive the ergodic capacity of our proposed PS-FDR and investigate the influence of the loopback interference by simulations.

The rest of this chapter is organized as follows. Section 3.1 introduces the system model of our proposed PS-FDR scheme. The optimization of the PS factor is discussed in Section 3.2. Then, the ergodic capacity of the relay network is derived in Section 3.3. Simulations and corresponding discussions are presented in Section 3.4 to verify the correctness of the derivation and the capacity enhancement of the proposed scheme over existing TS-based alternatives. Finally, Section 3.5 concludes the chapter.

3.1 System Model

As shown in Fig. 3.1, in this correspondence, we investigate an energy-harvesting relay network where the relay node operates in full-duplex amplify-and-forward (AF) mode. It receives signals from the source node and forwards the amplified signals to the destination node simultaneously. At the relay node, the received signals are split according to a power ratio of $\rho : (1 - \rho)$ for IP and EH respectively. The harvested energy is transfered to the battery for temporary storage and then used to power the transmission circuit.

The differences between our proposed scheme and the existing full-duplex energy-harvesting relaying schemes in the literature are depicted in Fig. 3.2. The major advantage of our proposed PS-FDR scheme is that both EH and information transmission are active for the entire transmission cycle, because power splitting is employed instead of time switching. In TS-FDR-I and TS-FDR-II, as shown in Figs. 3.2a and 3.2b respectively, the information transmission on both the S-R and the relay-to-destination (R-D) links is only performed in one of the two phases in each transmission cycle. In our proposed PS-FDR scheme, however, it is performed continuously all the time, as shown in Fig. 3.2c. Although a portion of the

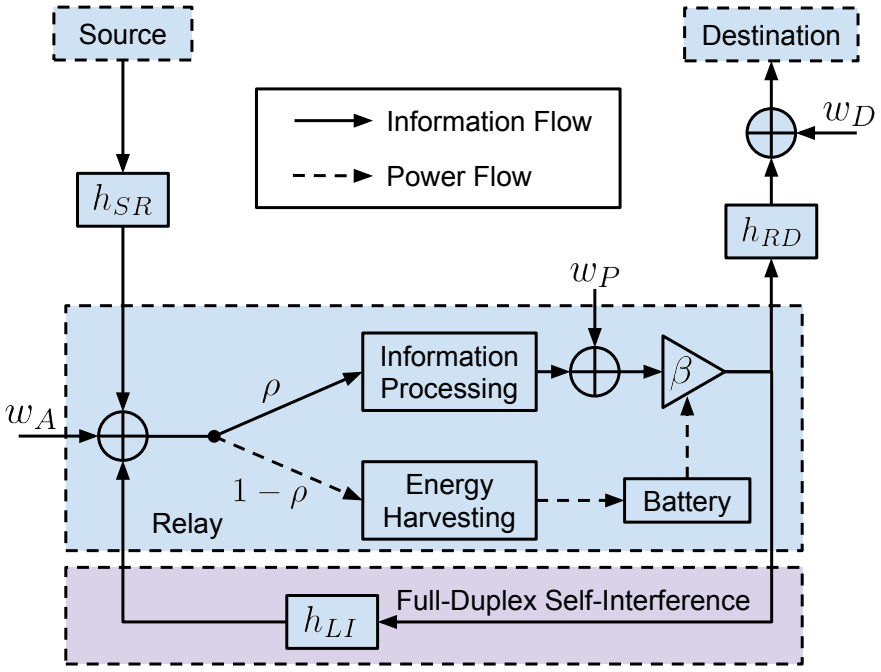

Figure 3.1: Proposed power-splitting based full-duplex energy-harvesting relaying scheme

received power at the relay node is split for EH, the overall capacity from the source node to the relay node will still benefit from the change from TS to PS, as the linear capacity gain from longer transmission time outweighs the logarithmic loss caused by power splitting because the SNR at the relay node is typically large in practical scenarios.

Note that the investigated relay node relies entirely on the harvested energy to forward signals to the destination node, and thus the transmit power at the relay node equals to that harvested from the received signals.

The channel between the source node and the relay node is denoted by h_{SR} and that between the relay node and the destination node is denoted by h_{RD}.

The received signal at the relay node is

$$y_R[n] = h_{SR}x_S[n] + h_{LI}x_R[n] + w_A[n] \tag{3.1}$$

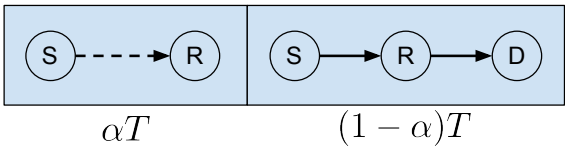

(a) TS-FDR-I [20]

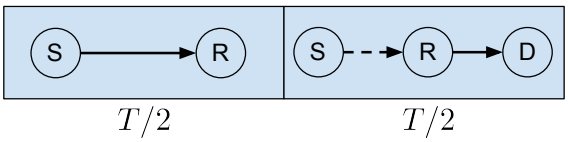

(b) TS-FDR-II [22]

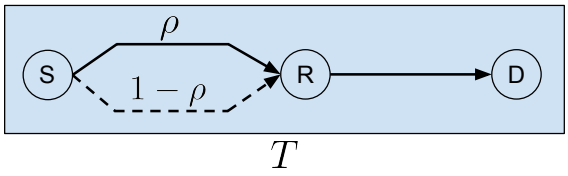

(c) Proposed scheme PS-FDR

Figure 3.2: Comparisons between our proposed scheme and the existing ones in the literature. R denotes the relay node. Solid arrows represent the information flow, and dashed arrows the power flow.

where x_R denotes the transmit signal at the relay node as

$$x_R[n] = \beta \left[y_{IP}[n-1] + w_P[n-1] \right] \tag{3.2}$$

and y_{IP} is the portion of the received signal that is split for IP.

The noise introduced by the receive antenna at the relay node, termed as the antenna noise, is represented by w_A and the processing noise, which is caused by the radio-frequency to baseband conversion, is represented by w_P [15]. β is the scaling factor at the AF relay node. In this paper, we study the AF relaying with fixed β [24]. The value of β is determined according to

$$P_R = \mathbb{E}[|x_R|^2] = \xi \, \mathbb{E}[|y_{EH}|^2] \tag{3.3}$$

where y_{EH} represents the signal for EH at the relay node, and ξ the energy havesting ef-

ficiency. This means, on average, the transmitted energy equals to the harvested energy. Therefore, the relay node could operate without extra power sources.[1]

The received signals for IP and EH are

$$y_{IP}[n] = \sqrt{\rho}\, y_R[n] \tag{3.4}$$

$$y_{EH}[n] = \sqrt{1-\rho}\, y_R[n] \tag{3.5}$$

so that they are split by a power ratio of $\rho : (1-\rho)$, $\rho \in [0,1]$, which plays a similar role as the TS factor α in TS-FDR-I. We can see from Fig. 3.1 that part of the power transmitted by the full-duplex relay node is harvested back in the form of loopback self-interference.

The received signal at the destination node is

$$y_D[n] = h_{RD} x_R[n] + w_D[n] \tag{3.6}$$

where w_D is the noise at the destination node.

Now we derive the amplification factor β that satisfies the power constraint in (3.3). The required transmit power at the relay node given the amplification factor β is

$$P_R = \mathbb{E}[|x_R|^2] = \beta^2 \left[\rho(|h_{SR}|^2 P_S + |h_{LI}|^2 P_R + \sigma_A^2) + \sigma_P^2\right] \tag{3.7}$$

[1]The power consumption of the signal processing circuitry in the relay node is assumed to be negligible in this paper. This is because the requirement of the self-interference mitigation in the investigated network is considerably relaxed compared with conventional FD relay nodes. In Fig. 3.3, the performance saturates when the residual self-interference channel gain is lower than -60 dB. Such a level of self-interference suppression can be achieved by passive mechanisms alone, which do not consume extra power [25].

and the power available for EH is

$$\mathbb{E}[|y_{EH}|^2] = (1-\rho)\left(|h_{SR}|^2 P_S + |h_{LI}|^2 P_R + \sigma_A^2\right). \tag{3.8}$$

By substituting (3.7) and (3.8) into (3.3), we obtain β as

$$\beta = \sqrt{\frac{\xi(1-\rho)\left(|h_{SR}|^2 P_S + |h_{LI}|^2 P_R + \sigma_A^2\right)}{\rho(|h_{SR}|^2 P_S + |h_{LI}|^2 P_R + \sigma_A^2) + \sigma_P^2}} \approx \sqrt{\frac{\xi(1-\rho)}{\rho}} \tag{3.9}$$

where the approximation is based on the assumption that the processing noise power is negligible compared with the power of the received signal at the relay node.

3.2 Power Splitting Factor Optimization

The PS factor plays an important role in the performance of the network. Therefore, optimizing ρ could significantly improve the system performance. This optimization problem is formulated as maximizing the SINR at the destination node, namely

$$\rho^* = \arg\max_{\rho} \gamma_{SD}. \tag{3.10}$$

To derive the expression of γ_{SD}, we first analyze the power of the received signal at the

destination node

$$\mathbb{E}[|y_D|^2] = \underbrace{\beta^2\rho|h_{SR}|^2 P_S|h_{RD}|^2}_{\text{Signal}} + \underbrace{\beta^2\rho\left(\sigma_A^2 + \frac{\sigma_P^2}{\rho}\right)|h_{RD}|^2 + \frac{|h_{LI}|^2\beta^4\rho^2}{1-|h_{LI}|^2\beta^2\rho}\left(|h_{SR}|^2 P_S + \sigma_A^2 + \frac{\sigma_P^2}{\rho}\right)|h_{RD}|^2 + \sigma_D^2}_{\text{Interference + Noise}}. \tag{3.11}$$

With the β obtained in (3.9), the SINR at the destination node can be presented as

$$\gamma_{SD} = \frac{P_S|h_{SR}|^2|h_{RD}|^2}{\left(\sigma_A^2 + \frac{\sigma_P^2}{\rho}\right)|h_{RD}|^2 + \frac{(1-\rho)\xi|h_{LI}|^2|h_{RD}|^2}{1-(1-\rho)\xi|h_{LI}|^2} \cdot \left(P_S|h_{SR}|^2 + \sigma_A^2 + \frac{\sigma_P^2}{\rho}\right) + \frac{\sigma_D^2}{(1-\rho)\xi}}. \tag{3.12}$$

Proposition 3.1 *The source-to-destination SINR γ_{SD} is quasi-concave with respect to the power splitting factor ρ.*

Proof. Let $\tilde{\gamma}_{SD}$ denote the denominator of γ_{SD} in (3.12). We have

$$\frac{\partial^2\tilde{\gamma}_{SD}}{\partial\rho^2} = \frac{\sigma_P^2|h_{RD}|^2}{\rho^3}(1+\xi|h_{LI}|^2) + \frac{\sigma_D^2}{(1-\rho)^3\xi}. \tag{3.13}$$

It is obvious that $\frac{\partial^2\tilde{\gamma}_{SD}}{\partial\rho^2} > 0$ for $\rho \in (0,1)$. Therefore, $\tilde{\gamma}_{SD}$ is convex for $\rho \in (0,1)$. Furthermore, $\gamma_{SD} = P_S|h_{SR}|^2|h_{RD}|^2/\tilde{\gamma}_{SD}$ and $f(x) = \frac{P_S|h_{SR}|^2|h_{RD}|^2}{x}$ is a decreasing function for $x > 0$. Since composition with a decreasing function preserves quasi-concavity, γ_{SD} is quasi-concave with respect to $\rho \in (0,1)$. ■

Proposition 3.1 guarantees that the optimal ρ that achieves the maximum γ_{SD} can be obtained efficiently by well-known one-dimensional search methods, such as the bisection method, the gradient descent method, and the Newton's method [26].

Proposition 3.2 *The optimal PS factor is* $\frac{|h_{RD}|\sigma_P}{|h_{RD}|\sigma_P+\sigma_D/\sqrt{\xi}}$ *when the residual self-interference channel gain is sufficiently small.*

Proof. Let $\tilde{\gamma}_{SD}$ denote the denominator of γ_{SD}. We have

$$\tilde{\gamma}_{SD} \xrightarrow{|h_{LI}|^2\to 0} |h_{RD}|^2\sigma_A^2 + \frac{|h_{RD}|^2\sigma_P^2}{\rho} + \frac{\sigma_D^2}{(1-\rho)\xi}. \tag{3.14}$$

Hence, to solve for the optimum ρ, we set

$$\frac{\partial\tilde{\gamma}_{SD}}{\partial\rho} \xrightarrow{|h_{LI}|^2\to 0} -\frac{|h_{RD}|^2\sigma_P^2}{\rho^2} + \frac{\sigma_D^2}{(1-\rho)^2\xi} = 0. \tag{3.15}$$

The optimum ρ is obtained by solving the above equation as

$$\rho = \frac{|h_{RD}|^2\sigma_P^2 \pm \sqrt{|h_{RD}|^2\sigma_P^2\sigma_D^2/\xi}}{|h_{RD}|^2\sigma_P^2 - \sigma_D^2/\xi} \tag{3.16}$$

$$= \frac{|h_{RD}|\sigma_P(|h_{RD}|\sigma_P \pm \sigma_D/\sqrt{\xi})}{(|h_{RD}|\sigma_P + \sigma_D/\sqrt{\xi})(|h_{RD}|\sigma_P - \sigma_D/\sqrt{\xi})} = \frac{|h_{RD}|\sigma_P}{|h_{RD}|\sigma_P \pm \sigma_D/\sqrt{\xi}}. \tag{3.17}$$

Since, in practice, σ_P and σ_D are similar in order of magnitude, and $0 < |h_{RD}| \ll 1$ and $1/\sqrt{\xi} > 1$, it is obvious that $0 < \rho_1 = \frac{|h_{RD}|\sigma_P}{|h_{RD}|\sigma_P+\sigma_D/\sqrt{\xi}} < 1$ and $\rho_2 = \frac{|h_{RD}|\sigma_P}{|h_{RD}|\sigma_P-\sigma_D/\sqrt{\xi}} < 0$. Therefore, the optimal power splitting factor is $\rho^* = \rho_1$ when the residual self-interference channel gain tends to 0. ■

Proposition 3.2 provides a closed-form solution of the optimal PS factor when the self-interference can be effectively mitigated to a certain extent. This theoretical observation is also verified in Section 3.4.1 through simulations.

3.3 Ergodic Capacity

We analyze the performance of the PS-FDR network by deriving the ergodic capacity from the source node to the destination node. It is defined as

$$C_E = \mathbb{E}[\log_2(1+\gamma_{SD})]. \tag{3.18}$$

We assume that the channel responses h_{SR}, h_{LI}, and h_{RD} are independent Rayleigh. Let f_X denote the probability density function (PDF) of a random variable X. Assuming all the channels are Rayleigh fading channels, $|h_{SR}|^2$ follows the exponential distribution and let $\bar{\eta}_{SR}$ denote its mean. The PDF of $|h_{SR}|^2$ is $f_{|h_{SR}|^2}(x) = \frac{1}{\bar{\eta}_{SR}} e^{-\frac{x}{\bar{\eta}_{SR}}}$. And similar statements can be made for $|h_{LI}|^2$ and $|h_{RD}|^2$ as well. The ergodic capacity of the proposed FD EH relay network can be computed [27, 3.352.4] as (3.20),

$$C_E = \iiint \log_2\left(1+\gamma_{SD}(x,y,z)\right) f_{|h_{SR}|^2}(x) f_{|h_{LI}|^2}(y) f_{|h_{RD}|^2}(z) \mathrm{d}x\mathrm{d}y\mathrm{d}z \tag{3.19}$$

$$\begin{aligned} =&\frac{1}{\ln 2 \cdot \bar{\eta}_{SR}\bar{\eta}_{LI}} \left[\iint \mathrm{e}^{\frac{B}{(A(x,y)+P_S x)\bar{\eta}_{RD}} - \frac{x}{\bar{\eta}_{SR}} - \frac{y}{\bar{\eta}_{LI}}} \cdot E_1\left(\frac{B}{(A(x,y)+P_S x)\bar{\eta}_{RD}}\right) \mathrm{d}x\mathrm{d}y \right. \\ &\left. - \iint e^{\frac{B}{A(x,y)\bar{\eta}_{RD}} - \frac{x}{\bar{\eta}_{SR}} - \frac{y}{\bar{\eta}_{LI}}} \cdot E_1\left(\frac{B}{A(x,y)\bar{\eta}_{RD}}\right) \mathrm{d}x\mathrm{d}y \right] \end{aligned} \tag{3.20}$$

where $E_1(\cdot)$ is the exponential integral function defined by $E_1(u) = \int_1^\infty \frac{e^{-tu}}{t}\mathrm{d}t$ and

$$A(x,y) = \left(\sigma_A^2 + \frac{\sigma_P^2}{\rho}\right) + \frac{(1-\rho)\xi y}{1-(1-\rho)\xi y}\left(P_S x + \sigma_A^2 + \frac{\sigma_P^2}{\rho}\right), \tag{3.21}$$

$$B = \frac{\sigma_D^2}{(1-\rho)\xi}. \tag{3.22}$$

Due to the complexity of the expression in (3.20), it is mathematically intractable to derive a closed-form solution. In order to evaluate the performance of our proposed PS-FDR in an analytical manner, in the following, we consider a mathematically tractable special case, which represents the scenario where the source and relay nodes are stationary and the destination node is mobile.

Proposition 3.3 *Given that h_{SR} and h_{LI} are static, and h_{RD} follows Rayleigh fading, the ergodic capacity can be obtained in closed form as in* (3.23).

$$\begin{aligned} C_E &= \frac{1}{\ln 2}\left[\mathrm{e}^{\frac{B}{(A(|h_{SR}|^2,|h_{LI}|^2)+P_S|h_{SR}|^2)\bar{\eta}_{RD}}} E_1\left(\frac{B}{(A(|h_{SR}|^2,|h_{LI}|^2)+P_S|h_{SR}|^2)\bar{\eta}_{RD}}\right)\right. \\ &\quad \left. - e^{\frac{B}{A(|h_{SR}|^2,|h_{LI}|^2)\bar{\eta}_{RD}}} E_1\left(\frac{B}{A(|h_{SR}|^2,|h_{LI}|^2)\bar{\eta}_{RD}}\right)\right] \end{aligned} \tag{3.23}$$

Proof. The channel gain $|h_{RD}|^2$ is the only random variable under such assumptions. Therefore,

$$C_E = \int_0^\infty \log_2(1+\gamma_{SD}(z)) f_{|h_{RD}|^2}(z)\mathrm{d}z. \tag{3.24}$$

By looking up the table [27, 3.352.4], it is straightforward to obtain (3.23) with some mathematical manipulations. ■

3.4 Simulations

3.4.1 Verification and Discussions

The purpose of this set of simulations is to validate the correctness of the ergodic capacity expression (3.23) and to investigate the characteristics of our proposed PS-FDR scheme. The transmit power is set to 30 dBm, $|h_{SR}|^2 = -60$ dB, $\mathbb{E}[|h_{RD}|^2] = -20$ dB, and the

EH efficiency $\xi = 90\%$. Noise power at the relay node and the destination node is set as $\sigma_A^2 = \sigma_P^2 = -93$ dBm, and $\sigma_D^2 = -90$ dBm, respectively. In our simulations, the intensity of loopback interference channel $|h_{LI}|^2$ varies from -85 dB to -15 dB. This is chosen as a pragmatic range because the loopback interference without self-interference cancelation is approximately -15 dB [22] and practical self-interference cancelation can already suppress the loopback interference by 70 dB or more [18]. The results are presented in Fig. 3.3, from which we can observe that with different values of the power splitting factor ρ, the average capacity obtained by simulations are perfectly aligned with the ergodic capacity we derived.

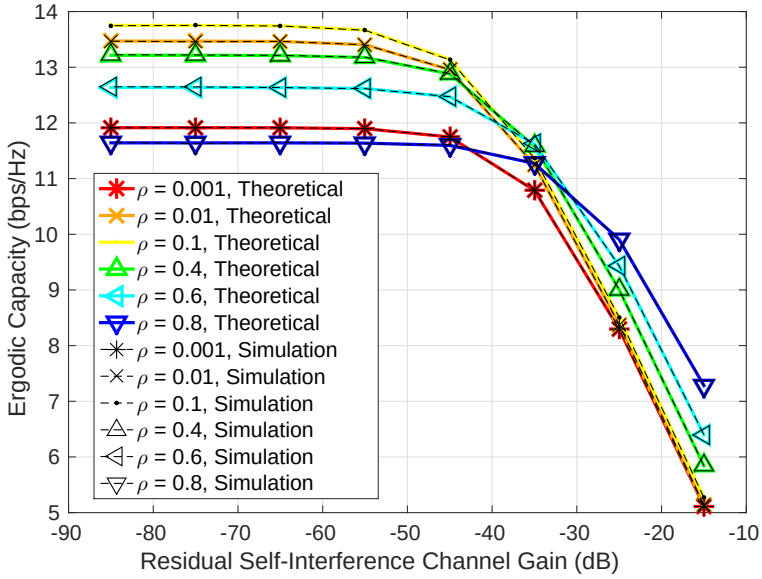

Figure 3.3: Ergodic capacity with different ρ and loopback interference level

In Fig. 3.3, it seems that the ergodic capacity is monotonically increasing while $|h_{LI}|^2$ is decreasing. And it begins to plateau when the loopback interference intensity is lowered to around -60 dB. In (3.12) that their relationship is monotonic. Intuitively, however, there should be a non-zero optimal $|h_{LI}|^2$ for our proposed scheme, since the system could benefit

from the loopback interference as it is also a source of EH. This is to be contrasted with full-duplex relaying without EH, where loopback interference is absolutely undesirable. The counter-intuitive results are caused by the approximation made in (3.9), which assumes the power of the received signals at the relay nodes is much larger than that of the processing noise for practical networks. In this case, the power harvested from the loopback interference is simply too little to overcome its unfavorable effect, namely the SINR degradation at the relay node.

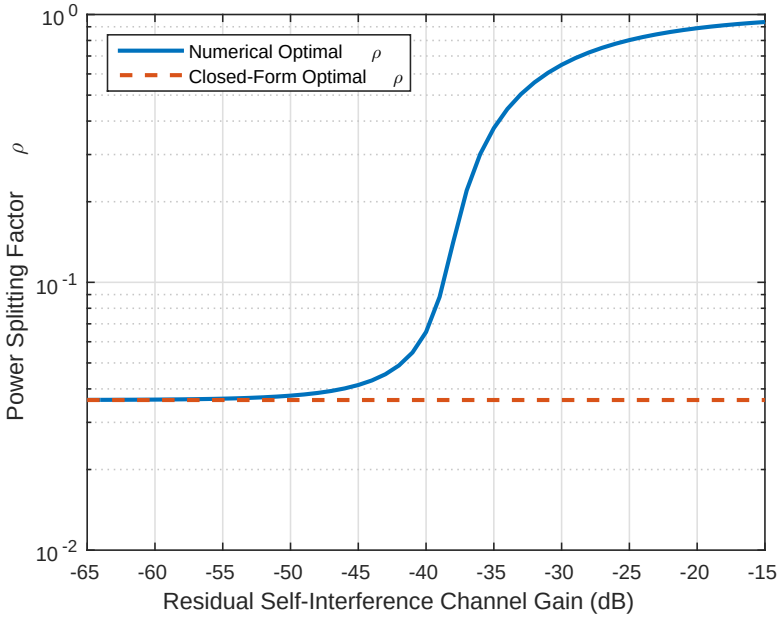

Figure 3.4: Optimal power splitting factor ρ vs. residual self-interference channel gain

Another interesting phenomenon is that the optimal ρ varies with the residual self-interference channel gain. The solid curve in Fig. 3.4 shows the optimal ρ that maximizes the source-to-destination capacity at different loopback interference levels under the same channel conditions. Larger ρ leads to better performance when the loopback interference is strong. This is because the relay node prefers to allocate more power to the IP part in order to resist the effect of loopback interference. In systems where the self-interference mitigation

is more effective, the loopback interference after cancelation is weaker. Hence, allocating more power to EH translates to higher transmission power at the relay node, which in turn improves the SINR at the destination node. This improvement outweighs the loss in the received SINR at the relay node. Therefore, smaller ρ becomes more desirable in the case with weak residual self-interference.

The dashed line in Fig. 3.4 represents the the closed-form optimal ρ derived under the condition of sufficiently small residual self-interference channel gain in Proposition 3.2. As shown in the figure, it is almost the same with the solutions obtained by the numerical algorithm when the residual self-interference channel gain is smaller than -50 dB, which can be achieved by existing self-interference mitigation methods [25]. Therefore, the complexity of FD EH relay nodes in practical networks can be further reduced because the one-dimensional search for the optimal ρ is no longer necessary if the self-interference mitigation is reasonably effective.

3.4.2 Comparisons

In this set of simulations, we compare the performance of our proposed PS-FDR scheme with that of TS-FDR-I [20] and TS-FDR-II [22]. We set the simulation parameters as $P_S = 30$ dBm and $\mathbb{E}[|h_{SR}|^2] = \mathbb{E}[|h_{RD}|^2] = -60$ dB. All the channels follow Rayleigh fading and the noise power is set as the same in Secion 3.4.1. Note that TS-FDR-II performs better when the loopback interference is stronger, whereas TS-FDR-I and PS-FDR perform better when that is weaker. For the sake of fairness, the loopback interference is set to -15 dB for TS-FDR-II and -60 dB for TS-FDR-I and PS-FDR. Both the TS factor α in TS-FDR-I and the PS factor ρ in PS-FDR are optimized for each channel realization. The optimal ρ is

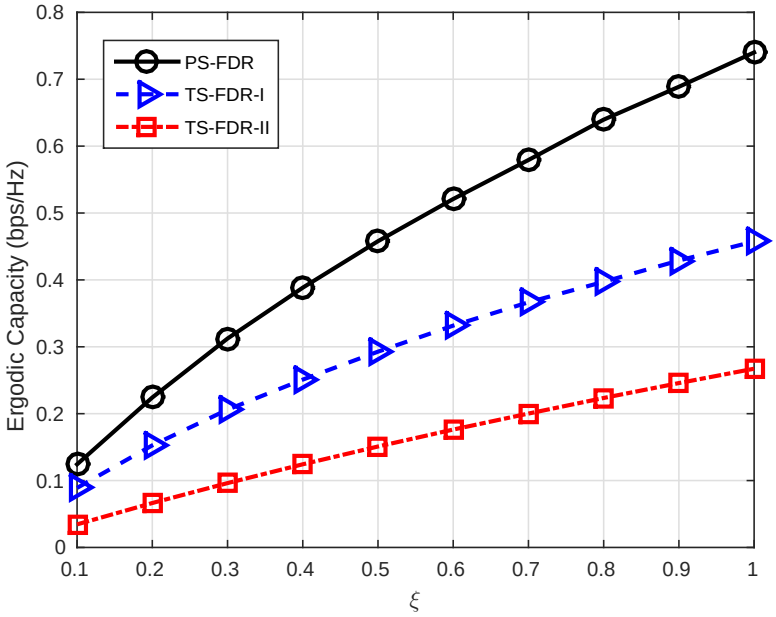

Figure 3.5: Performance comparisons of TS-FDR-I, TS-FDR-II, and PS-FDR with various values of ρ and ξ

obtained according to the closed-form solution in Proposition 3.2. As shown in Fig. 3.5, our proposed scheme PS-FDR performs much better than the TS based alternatives uniformly with all the values of the EH efficiency ξ.

3.5 Conclusions

In this chapter, we introduced SWIPT with PS into the study of full-duplex relay networks. The high spectrum efficiency of full-duplex relaying scheme is exploited. Combined with the SWIPT technology, we achieved sustainable operation of the relay node. PS, instead of TS in existing related works, is employed in our proposed scheme. Hence, truly full-duplex operation can be achieved in the entire transmission cycle. Compared with existing EH FD relaying schemes, our proposed scheme significantly improves the source-to-destination ergodic capacity, as verified by theoretical analysis and simulations.

CHAPTER 4

RELAY SELECTION IN FULL-DUPLEX ENERGY-HARVESTING ONE-WAY RELAY NETWORKS

4.1 Background

In wireless networks where multiple relays are available, relay selection (RS) is a practical method of exploiting the cooperative diversity. It was first introduced to HD relay networks in [28], and has been a fruitful research area henceforth [8, 9, 29–32]. Relay selection in FD relay networks was introduced in [29] and further investigated in [30]. Most existing work focus on the RS problem in networks where orthogonal channels are allocated to the relays, and independent power constraints at different relays are assumed. In this case, selecting only one relay is the optimal scheme in terms of spectrum efficiency, as the relay with the highest S-D signal-to-interference-and-noise ratio (SINR) can achieve the highest rate when it occupies the entire bandwidth. The concept of relay selection was extended to multiple selected relays cooperating in a shared bandwidth, and superior performance has been reported in [8, 9].

The RS problem in EH relay networks is an emerging research topic. Most existing studies have focused on HD relay networks and single relay selection (SRS) [33, 34]. In our previous work [23, 35], we investigated the RS problem in FDEH two-way relay networks and considered multiple relay selection. In this study, we investigate the RS problem in PS-based FDEH one-way relay networks. Our contributions can be summarized as follows: i) To the best of the authors' knowledge, this is the first study that investigates the RS

problem in FDEH one-way relay networks; ii) we expand the RS problem in FDEH one-way relay networks by allowing multiple relays to be selected for transmission simultaneously, and find that SRS is not always optimal in FD EH relay networks; and iii) we propose an efficient greedy RS method that achieves near-optimal performance with significantly reduced complexity compared with the exhaustive-search-based optimal RS method.

The remainder of this paper is organized as follows. Section 4.2 describes the system model of our investigated networks. Subsequently, our proposed greedy RS method is introduced in Section 4.3. Simulations are presented in Section 4.4 to evaluate the performance of our proposed greedy RS method. Finally, the concluding remarks are provided in Section 4.5.

4.2 System Model

As shown in Figure 4.1, we investigate a PS-FDEH amplify-and-forward (AF) relay network. All the N available relays operate in FD mode. This means that they transmit and receive signals over the same wireless channel resource in terms of time and frequency. We assume that the direct link between the source and destination is blocked and ignored in this investigation. The source has perfect knowledge of all the channels. The RS is processed at the source, and the decisions are subsequently broadcast to the involved relays.

The selected relays receive signals from the source, amplify the received signals, and transmit the signals to the destination simultaneously. At each relay, the received signals are split according to a power ratio of $\rho_j : (1 - \rho_j)$ for IP and EH, respectively.

The selected relays are assumed to operate on orthogonal channels with equal bandwidth, such that the interference among them can be avoided. The received signals from multiple

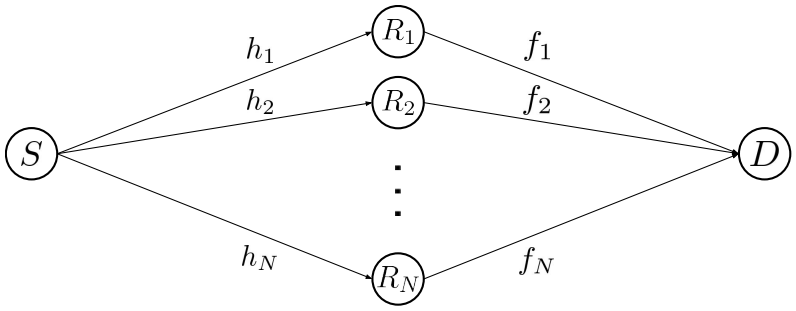

(a) System Diagram

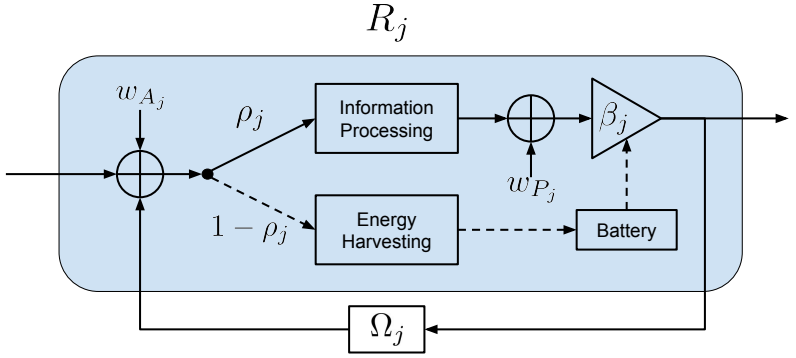

(b) Relay Node Diagram

Figure 4.1: Full-duplex energy-harvesting relay network

relays are combined at the destination. Let W denote the total bandwidth available to the network. Subsequently, each selected relay is allocated with a channel with bandwidth $W/|\mathcal{R}|$, where $\mathcal{R}$ is the set of the selected relays and $|\cdot|$ represents the cardinality of a set.

Let h_j denote the channel response between S and $R_j\,(j = 1, 2, \cdots, N)$, and f_j the channel response between R_j and D. The self-interference caused by the FD operation mode can be effectively suppressed by passive and active self-interference mitigation techniques [18]. The residual self-interference channel response is denoted as Ω_j. Note that these are the equivalent channel responses after self-interference mitigation is applied. The received signal at R_j can be derived as

$$y_{R_j}[n] = h_j x_S[n] + \Omega_j x_{R_j}[n] + w_{A_j}[n] \tag{4.1}$$

where x_{R_j} denotes the transmit signal of R_j. w_{A_j} and w_{P_j} denote the antenna noise and processing noise at the relays, respectively, whose distribution follows $\mathcal{CN}(0, \sigma_A^2)$ and $\mathcal{CN}(0, \sigma_P^2)$, respectively, where $\sigma_A^2 = N_A W/|\mathcal{R}|$ and $\sigma_P^2 = N_P W/|\mathcal{R}|$. N_A and N_P denote the corresponding noise power spectral density.

Subsequently, with a power ratio of $\rho_j : (1 - \rho_j)$, $\rho \in [0, 1]$, the received signal y_{R_j} at R_j is split for IP and EH, as described in

$$y_{\mathrm{IP}_j}[n] = \sqrt{\rho_j}\, y_{R_j}[n] \tag{4.2}$$

$$y_{\mathrm{EH}_j}[n] = \sqrt{1 - \rho_j}\, y_{R_j}[n]. \tag{4.3}$$

If R_j is selected, then y_{IP_j} is amplified and forwarded to the destination. Given the amplification factor at R_j, denoted by β_j, the transmit signal at R_j can be derived as

$$x_{R_j}[n] = \beta_j (y_{\mathrm{IP}_j}[n-1] + w_{P_j}[n]). \tag{4.4}$$

The required transmit power at R_j is

$$P_{R_j} = \mathbb{E}[|x_{R_j}|^2] = \beta_j^2 (\rho_j \mathbb{E}[|y_{R_j}|^2] + \sigma_P^2). \tag{4.5}$$

Note that the energy used for transmission at R_j should be exclusively supplied by the EH from y_{EH_j}. This means that the average transmit power should equal to the average harvested power. Given the EH efficiency ξ, the largest transmit power that R_j can support

is

$$P_{R_j} = \xi \, \mathbb{E}[|y_{\mathrm{EH}_j}|^2]. \tag{4.6}$$

Combining (4.5) and (4.6), we obtain the value of β_j as

$$\beta_j = \sqrt{\frac{\xi(1-\rho_j)\mathbb{E}[|y_{R_j}|^2]}{\rho_j \mathbb{E}[|y_{R_j}|^2] + \sigma_P^2}} \approx \sqrt{\frac{(1-\rho_j)\xi}{\rho_j}}. \tag{4.7}$$

This approximation is justified because $\rho_j \mathbb{E}[|y_{R_j}|^2] \gg \sigma_P^2$ in practical networks. Otherwise, the S-D SINR would be extremely small.

To obtain the source-to-destination capacity, we first derive the received signal at the destination via the jth relay

$$y_D^{(j)}[n] = f_j x_{R_j}[n] + w_D^{(j)}[n] \tag{4.8}$$

where $w_D^{(j)}$ is the noise at the destination in the frequency band allocated to R_j. The noise follows the distribution $\mathcal{CN}(0, \sigma_D^2)$ with $\sigma_D^2 = N_D W/|\mathcal{R}|$, and N_D is the noise power spectral density at the destination.

The received signals from multiple relays are combined at the destination. Let $\gamma_D^{(j)}$ denote the SINR of the received signal at D via R_j. Similar to [36], the capacity of the link from S to D can be calculated as

$$C_D = \frac{W}{|\mathcal{R}|} \log_2 \left(1 + \sum_{j \in \mathcal{R}} \gamma_D^{(j)} \right). \tag{4.9}$$

4.3 A Greedy Relay Selection Method

In this study, the performance objective of the RS is to maximize the source-to-destination capacity. Therefore, the RS problem can be formulated as follows:

$$\underset{\mathcal{R},\boldsymbol{\rho}}{\text{maximize}} \quad C_D(\mathcal{R}, \boldsymbol{\rho}) \tag{4.10a}$$

$$\text{subject to} \quad \rho_j \in [0,1], \quad j = 1, 2, \cdots, N \tag{4.10b}$$

where $\mathcal{R}$ is the set of selected relays and $\boldsymbol{\rho}$ denotes the vector of the corresponding PS factors.

Because the RS optimization problem is a 0-1 programming that is computationally intractable with exponential complexity, in the following, we propose a greedy RS method for the investigated FDEH relaying networks.

Our proposed greedy RS method starts with $\mathcal{R}_0 = \varnothing$ and gradually adds the relays one after another. At each step, we maintain the selected relays in the previous step and add one of the remaining relays that would achieve the maximum capacity if it were added to the selected relay set in the previous step. Let $\mathcal{R}_i$ denote the selected relays in the ith step. Hence, $\mathcal{R}_0 \subset \mathcal{R}_1 \subset \cdots \subset \mathcal{R}_N$. The detailed descriptions of the proposed method are presented in Algorithm 1. The intuition that inspired the algorithm is as follows. The relays selected in the previous step, with fewer relays cooperating, are expected to experience better channel conditions to the source and the destination. Other combinations of the same number of relays are unlikely to outperform this set of relays when adding an extra relay. Therefore, the relays selected in the previous step should be selected with priority in the current step as well. Although this is a heuristic algorithm, i.e., the optimality is

not guaranteed, our simulations demonstrate that its performance is almost identical to the exhaustive-search-based optimal algorithm.

The variable $\boldsymbol{\rho}^*$ in Line 14 of Algorithm 1 is the vector of the optimal PS factors for all the candidate relays. Each element of $\boldsymbol{\rho}^*$ is obtained in Line 11. Note that this optimization of ρ_j is irrelevant with the identities of the other selected relays or their related channel responses. However, it is relevant with the bandwidth allocated to R_j because the noise power is bandwidth dependent. Hence, only the number of selected relays $|\mathcal{R}|$, rather than the elements in $\mathcal{R}$, affects the optimization of ρ_j.

Therefore, given a fixed number of selected relays N', the joint optimization is equivalent to optimizing ρ_j first for each relay and subsequently selecting the best relays in the second step.

Finally, $\mathcal{R}^*$ is determined as the optimal set of relays to be selected among $\mathcal{R}_1, \mathcal{R}_2, \cdots, \mathcal{R}_N$ according to

$$\mathcal{R}^* = \underset{\mathcal{R}_n \in \{\mathcal{R}_1, \mathcal{R}_2, \cdots, \mathcal{R}_N\}}{\arg\max} C_D(\mathcal{R}_n, \boldsymbol{\rho}^*). \tag{4.11}$$

The computational complexity of the proposed greedy RS method in terms of the number of available relays N is $\mathcal{O}(N^2)$, which is significantly reduced compared with the exponential complexity of the exhaustive-search-based RS method. Because the performance gain of RS is more compelling when N is larger, the practical significance of the complexity reduction also becomes more attractive, especially for EH relays, whose computational power is typically limited.

To further investigate the properties of the optimization of ρ_j in Line 11 of Algorithm 1, we derive the analytical relationship between the objective function, the SINR of the received

Algorithm 1 Greedy RS for EHFD relay networks

Input: Available relay set $\Omega_R = \{R_1, R_2, \cdots, R_N\}$, CSI $\boldsymbol{h}$ and $\boldsymbol{f}$
Output: Selected relay set $\mathcal{R}^*$

$\mathcal{R}_0 \leftarrow \varnothing$
$\Omega \leftarrow \Omega_R$
$C_{\max} \leftarrow 0$
$N_{\max} \leftarrow 0$
for $n = 1, 2, \cdots, N$ **do**
  $C_n \leftarrow 0$
  for $j = 1, 2, \cdots, N$ **do**
    $\rho_j^* \leftarrow \underset{\rho_j \in [0,1]}{\arg\max}$
    $\gamma_D^{(j)}(\rho_j, h_j, f_j, |\mathcal{R}|)$
  end for
  for $R' \in \Omega$ **do**
    $C' = C_D(\mathcal{R}_{n-1} \cup \{R'\}, \boldsymbol{\rho}^*)$
    if $C_n < C'$ **then**
      $C_n \leftarrow C'$
      $\tilde{R}_n \leftarrow R'$
    end if
  end for
  $\mathcal{R}_n \leftarrow \mathcal{R}_{n-1} \cup \{\tilde{R}_n\}$
  $\Omega \leftarrow \Omega \setminus \{\tilde{R}_n\}$
  if $C_{\max} < C_n$ **then**
    $C_{\max} \leftarrow C_n$
    $N_{\max} \leftarrow n$
    $\mathcal{R}^* \leftarrow \mathcal{R}_n$
  end if
end for

signals at the destination $\gamma_D^{(j)}$, and the PS factor ρ_j. The power of the received signal at the destination $y_D^{(j)}$ can be obtained as

$$\begin{aligned}\mathbb{E}\left[\left|y_D^{(j)}\right|^2\right] &= \beta_j^2 \rho_j |f_j|^2 |h_j|^2 P_S \\ &\quad + |f_j|^2 |\Omega_j|^2 \beta_j^2 \rho_j P_{R_j} \\ &\quad + |f_j|^2 \beta_j^2 \rho_j \sigma_A^2 + |f_j|^2 \beta_j^2 \sigma_P^2 + \sigma_D^2 \end{aligned} \tag{4.12}$$

where the expectation is taken with respect to the source symbol realizations.

$$\gamma_D^{(j)} = \frac{|h_j|^2|f_j|^2 P_S}{\frac{(1-\rho_j)\xi|\Omega_j|^2|f_j|^2}{1-(1-\rho_j)\xi|\Omega_j|^2}(P_S|h_j|^2+\sigma_A^2)+(\sigma_A^2+\frac{\sigma_P^2}{\rho_j})|f_j|^2+\frac{\sigma_D^2}{(1-\rho_j)\xi}} \tag{4.13}$$

Only the first term on the right-hand side of (4.12) corresponds to the useful signal from the source. Hence, given the amplification factor in (4.7), the end-to-end SINR of the $S \to R_j \to D$ link is presented in (4.13). It can be proven that $\gamma_D^{(j)}$ is quasi-concave with respect to ρ_j, similarly to [37]. This means that the optimization of ρ_j is a maximization problem of a quasi-concave objective function. Therefore, the global optimizer ρ_j^* can be obtained by one-dimensional search methods without the concern of locally optimum traps [26].

4.4 Simulations

In this section, we present the simulations to evaluate the performance and characteristics of the proposed greedy RS method. The simulation parameters are set as in Table 4.1 and all the channels follow the Rayleigh fading. The residual self-interference channel gain at the relays $\mathbb{E}[|\Omega_j|^2]$ is set to -60 dB. This is a practical value as the self-interference channel gain without any mitigation is approximately -15 dB [22] and the existing self-interference mitigation can easily suppress the self-interference by 45 dB [18].

In Figures 4.2 and 4.3, we compare the performance of our proposed greedy RS method with the SRS method, the all-participate (AP) method, and the exhaustive search based optimal RS method. The performance metrics employed in this study are the source-to-destination capacity and the outage probability. The SRS method restricts the number of

Table 4.1: Simulation Parameters

Bandwidth	10 MHz
Noise Power Spectral Density	-174 dBm/Hz
Noise Figure	5 dB
Energy Harvesting Efficiency	90%
Residual Self-Interference Channel Gain	-60 dB
Number of Available Relays	$4, 8$

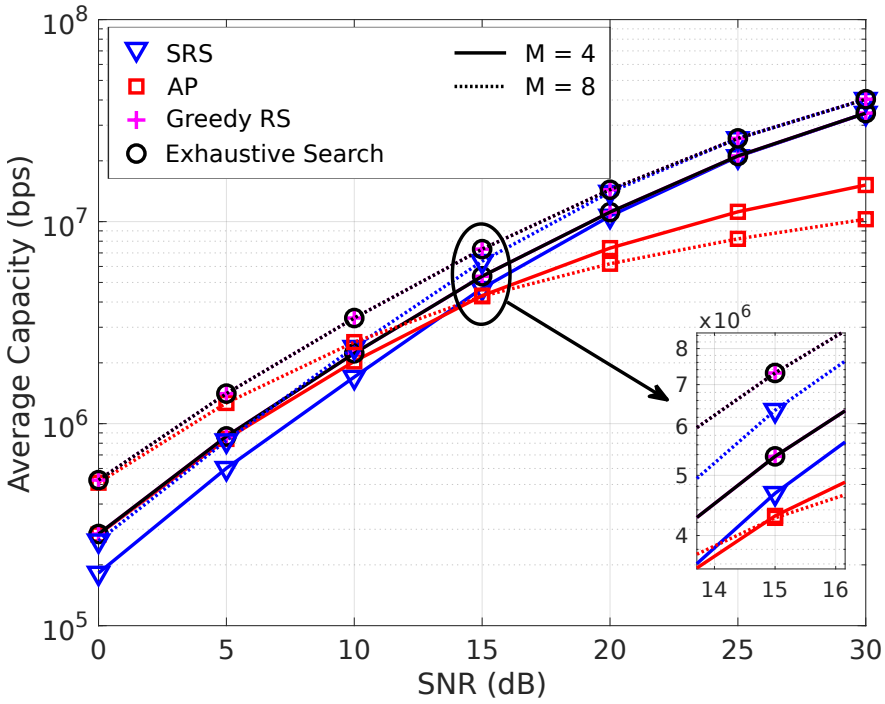

Figure 4.2: Average capacity comparison of the RS methods.

selected relays to one, whereas the AP method involves all the available relays into the transmission.

The AP method and the SRS method approach the optimal performance at the lower and higher ends of the SNR axis, respectively. This phenomenon can be explained as follows. Having more relays cooperating leads to more harvested energy overall for relaying. This is desirable when the source transmit power is low. On the other hand, selecting fewer relays results in a larger bandwidth for each of them. This is a more efficient way to utilize the spectrum while the source transmit power is relatively high. From another perspective, this

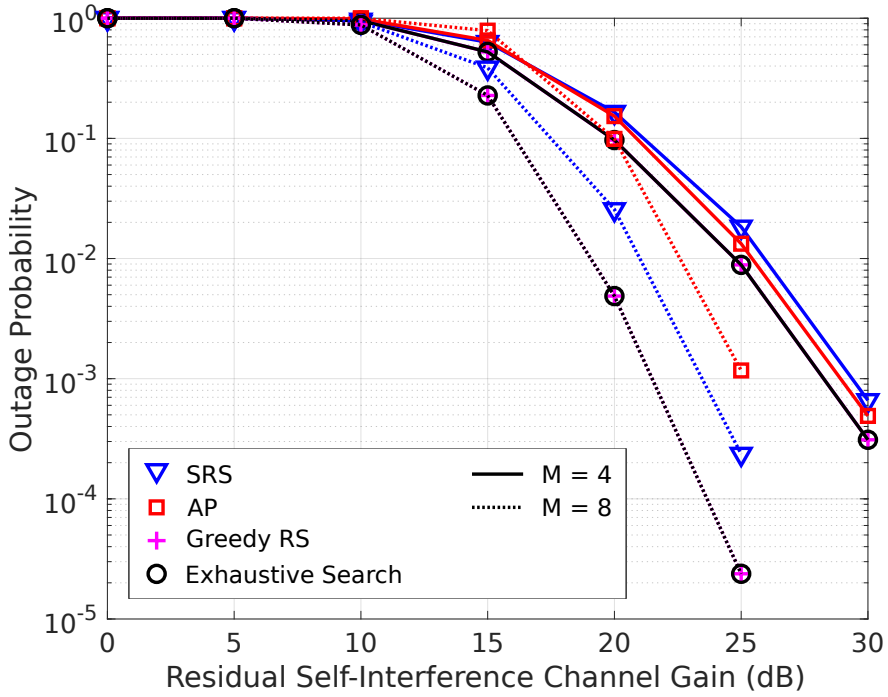

Figure 4.3: Outage probability comparison of the RS methods. The outage threshold is set to 0.5 bps/Hz.

observation is also supported by Figure 4.4, in which the average number of selected relays at different SNRs are presented. Figure 4.4 shows that both the greedy RS method and the exhaustive-search-based RS method tend to select more relays at low SNRs and fewer at high SNRs. This result also demonstrates that in FD EH relay networks, the SRS cannot always lead to the optimal capacity and/or outage probability as in most conventional relay networks.

Note that although the SRS method achieves similar average capacity to the exhaustive search RS method at high SNR, the outage probability gap between them cannot be ignored. This is because the capacity achieved by the two RS methods follow different distributions. The SRS method results in a distribution with a heavier tail at the lower end. Therefore, as the SNR increases, the outage probability of the SRS method does not decrease as quickly as that of the exhaustive search RS method.

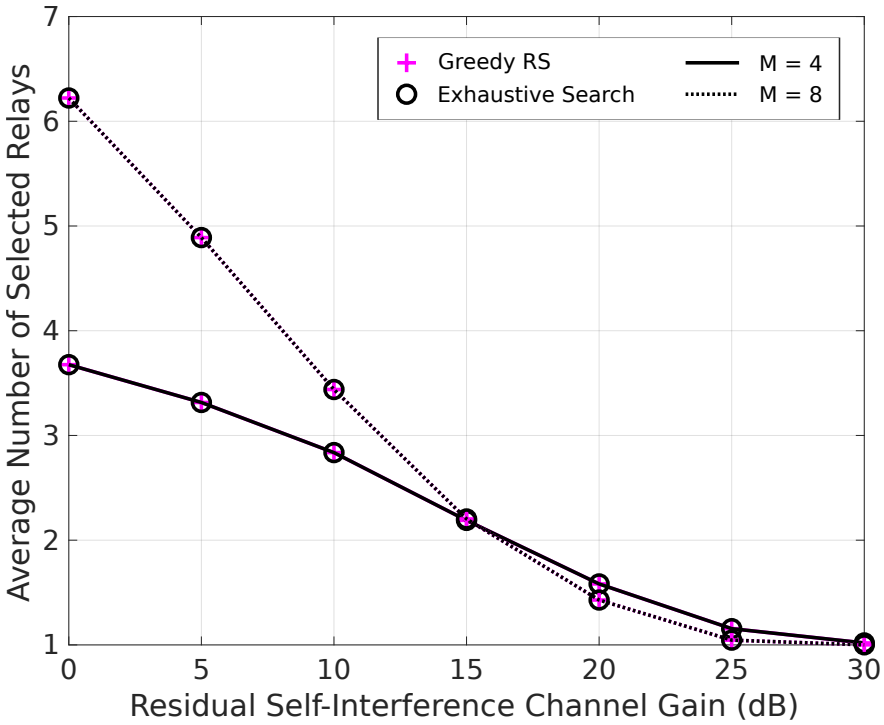

Figure 4.4: Average number of selected relays in FDEH1W relay networks.

Figures 4.2 and 4.3 also demonstrate that our proposed greedy RS method outperforms both the SRS and AP methods with different transmit SNRs at the source. It also achieves a performance similar to that of the optimal RS method based on exhaustive search. By changing from the exhaustive search RS method with exponential complexity to our proposed greedy RS method with a complexity of $\mathcal{O}(N^2)$, the computational burden can be significantly reduced, especially when the number of available relays is large.

The influence of residual self-interference on the performance of the network is investigated in Figure 4.5. The results show that the residual self-interference is always detrimental to the network capacity. Therefore, in practice, the self-interference at the FD relays should be mitigated as much as possible.

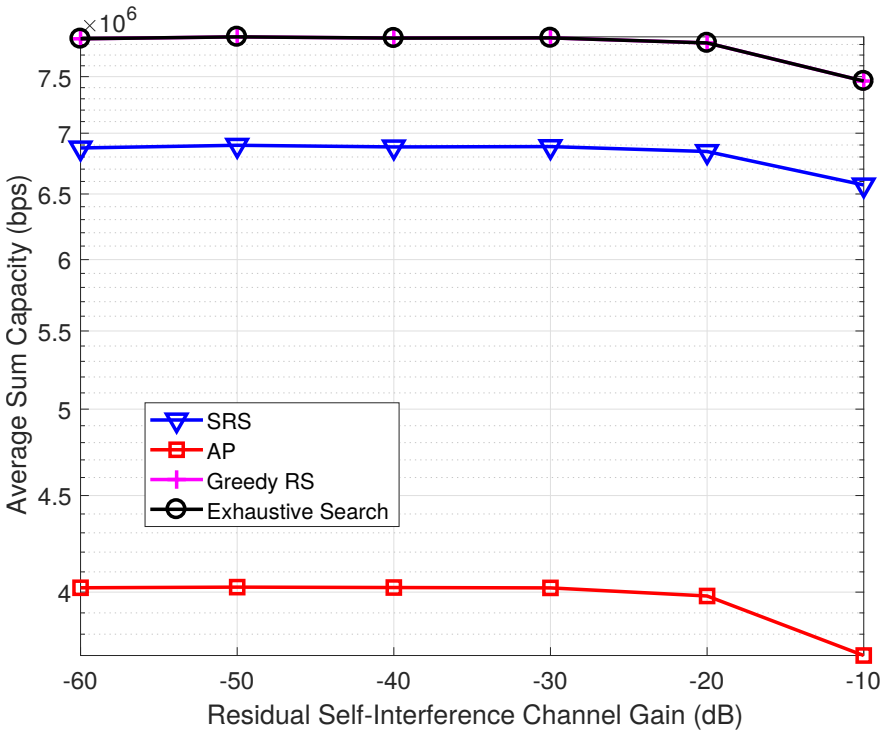

Figure 4.5: Influence of residual self-interference on average capacity in FDEH1W relay networks.

4.5 Conclusions

In this study, we investigated RS in FDEH1W relay networks. Compared with the existing work on the RS in EH relay networks, we expanded the investigation in two aspects. First, we investigated the RS in FDEH1W relay networks for the first time. Next, multiple relays were allowed to participate in the relaying process simultaneously. Because the optimal RS problem is computationally intractable, we proposed an efficient greedy RS method that achieved near-optimum performance with significantly reduced complexity.

CHAPTER 5

RELAY SELECTION IN FULL-DUPLEX ENERGY-HARVESTING TWO-WAY RELAY NETWORKS

5.1 Background

The relay selection (RS) problem in energy harvesting relay networks is relatively new. Most existing researches were conducted on HD or one-way relay networks [33, 34, 38]. However, the unique characteristics of FD EH two-way relay networks bring new insights to the RS problem. In EH relay networks, the transmit power of relays is not restricted by the volume of their batteries. Instead, the energy used for relaying is harvested from the received signals. Selecting more relays will not consume extra energy from the batteries as for conventional relays. On the contrary, it helps harvest more energy that can be used for relaying. On the other hand, selecting multiple relays still entails bandwidth splitting to avoid interference among the selected relays. Therefore, the RS problem under such a setup is both interesting and challenging.

Table 5.1: Related Work on EH Relay Networks

	SWIPT Method	Relaying Mode	Directions	Relay Selection
[15]	TS & PS	HD	One-Way	None
[20, 21]	TS	FD	One-Way	None
[22]	N/A	FD	One-Way	None
[33, 34]	PS	HD	One-Way	SRS
[38]	PS	HD	Two-Way	SRS
[23]	PS	FD	One-Way	None
[35]	PS	FD	Two-Way	SRS
This work [39]	PS	FD	Two-Way	GRS

Different from existing work in the literature, whose characteristics are summarized in Table 5.1, in this chapter, we investigate the characteristics and performance of PS-based full-duplex energy-harvesting two-way (PS-FDEH2W) relay networks and the relay selection problem therein. We focus on EH relays that employ PS as the coordinating method between IP and EH. The transmit power of the relays are exclusively provided by the energy harvesting at the relays themselves. We assume that the relays transmit over mutually orthogonal channels to avoid inter-relay interference in the FD mode. Both SRS and general relay selection (GRS) with an arbitrary number of selected relays are then investigated. Several near-optimal low-complexity RS methods are proposed and evaluated by simulations. Our contributions are summarized as follows.

1. To the best of the authors' knowledge, FDEH2W relay networks are investigated for the first time. We employ PS-based SWIPT at the EH relays, which can enable real FD information transmission in the investigated relaying network and improve the network spectrum efficiency effectively.

2. With PS-based SWIPT, we first derive the end-to-end SINR with respect to the PS factor for each EH relay and prove that the outage probability minimization is a quasi-convex optimization problem. Therefore, the optimal PS factor for each EH relay can be efficiently obtained by one-dimensional search algorithms.

3. As for the SRS problem, which is a simplified version of the GRS problem, the optimization of the PS factor and the relay selection is decoupled due to the fixed number of selected relays (i.e., 1). Based on the optimized PS factor at each relay, we propose two efficient SRS methods for the investigated FDEH2W relay network, aiming at out-

age probability minimization and sum capacity maximization, respectively. Both SRS methods can achieve near-optimal performance at high SNR.

4. As for the GRS problem, the optimal GRS can be obtained by an exhaustive search among all possible relay combinations. Unfortunately, the complexity is exponential in the number of relays, which prevents the method from being employed in practical applications. Therefore, we first propose three heuristic GRS methods based on the designed worse channel ordering (WCO), channel harmonic mean ordering (CHMO), and worse signal-to-interference-and-noise ratio ordering (WSINRO), respectively, which can achieve sub-optimal GRS with very low complexity. To further improve the performance of GRS methods with practical complexity, a greedy GRS method is then proposed that can find the optimal relay ordering so long as it exists. Although the optimal relay ordering does not always exist, all proposed GRS methods are shown to outperform both the SRS methods and the all participate (AP) method while achieving near-optimal performance.

The rest of this chapter is organized as follows. Section 5.2 introduces the system model of our proposed PS-FDEH2W relay network as well as the corresponding RS problem formulation. Section 5.3 presents the PS factor optimization and the SRS problem. The GRS problem is discussed in Section 5.4 and various GRS methods are proposed. Simulations and corresponding discussions are presented in Section 5.5 to evaluate the performance of our proposed RS methods in terms of the outage probability and the sum capacity. Finally, Section 5.6 concludes this chapter.

5.2 System Model and Problem Formulation

5.2.1 System Model

As shown in Fig. 5.1, in this work, we investigate a PS-FDEH2W AF relay network. All involved nodes, including two sources and N relays, operate in FD mode, which means that they transmit and receive signals simultaneously over the same frequency band. We assume that no direct link exists between the sources and the sources have perfect knowledge of all channels, while each relay only knows the channels related to itself. The relay selection is processed at the sources and the decisions are then broadcast to the involved relays.

The relays receive signals from both sources. The selected relays amplify the received signals and transmit the combined signals back to the sources simultaneously, so that the sources can extract the information sent from the other side. At each relay, the received signals are split according to a power ratio of $\rho_j : (1 - \rho_j)$ for IP and EH, respectively. The harvested energy is transferred to the batteries for temporary storage and then used to power the transmission circuits.

In order to avoid the potential inter-relay interference due to the FD operation mode of the relays, we assume that orthogonal channels with equal bandwidth are allocated to the selected relays, and the received signals from multiple relays are combined at the sources.[1] Let $\mathcal{R}$ denote the set of the selected relays. The total bandwidth available to the network is W. Then, each selected relay occupies a channel with bandwidth $W/|\mathcal{R}|$, where $|\cdot|$ represents the cardinality of a set. Note that such bandwidth allocation for the relays is different from

[1]One should note that the performance of the network could be improved if the network beamforming technique was implemented by phase compensation and power adjustment at the relays. Network beamforming in EH relay networks will be investigated in Chapter 6.

many RS-oriented work in the literature. This difference, along with the EH components of the relays, results in interesting variations in the optimal RS strategy. We will discuss these variations in detail in Section 5.2.2 and Section 5.4.

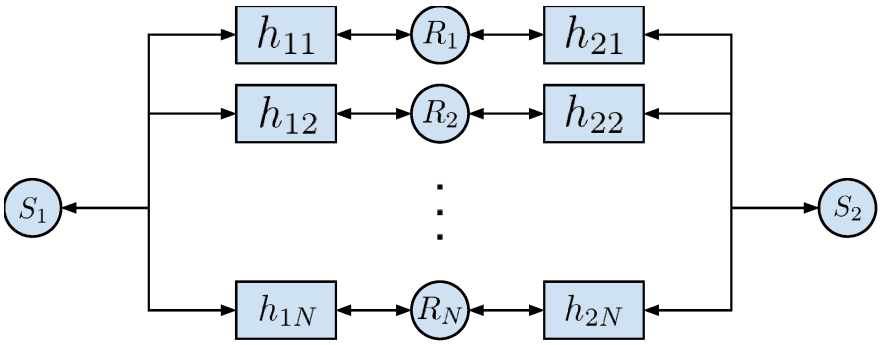

(a) System Diagram

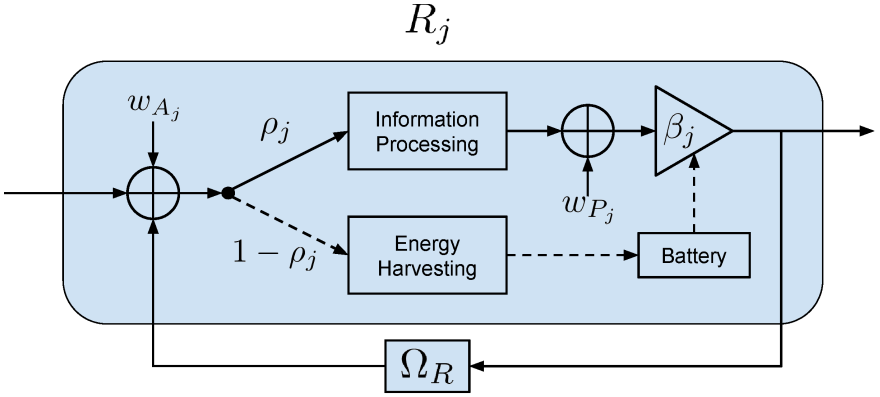

(b) Relay Node Diagram

Figure 5.1: A full-duplex energy-harvesting relay network.

The channel response between $S_i\,(i = 1, 2)$ and $R_j\,(j = 1, 2, \cdots, N)$ is denoted by h_{ij}. The self-interference due to the FD operation mode can be effectively suppressed by various self-interference mitigation methods [18]. However, the residual self-interference still plays an important role in the performance of the network. Therefore, in order to investigate the impact of residual self-interference, it is necessary to model it at each FD node explicitly. In this work, the residual self-interference channel response of S_i and R_j are denoted as Ω_{S_i} and Ω_{R_j}, respectively. Note that these are the equivalent channel responses after self-interference

mitigation. Then, the received signal at R_j is

$$y_{R_j}[n] = \sum_{i=1}^{2} h_{ij} x_{S_i}[n] + \Omega_{R_j} x_{R_j}[n] + w_{A_j}[n] \tag{5.1}$$

where x_{R_j} denotes the transmitted signal from R_j. The antenna noise and processing noise at the relays are represented by w_{A_j} and w_{P_j}, whose distribution follows $\mathcal{CN}(0, \sigma_A^2)$ and $\mathcal{CN}(0, \sigma_P^2)$, respectively, where $\sigma_A^2 = N_A W/|\mathcal{R}|$ and $\sigma_P^2 = N_P W/|\mathcal{R}|$. N_A and N_P denote the corresponding noise power spectral density. The received signal y_{R_j} at R_j is then split for IP and EH with a power ratio of $\rho_j : (1 - \rho_j)$, $\rho \in [0, 1]$, as described in

$$y_{\mathrm{IP}_j}[n] = \sqrt{\rho_j}\, y_{R_j}[n] \tag{5.2}$$

$$y_{\mathrm{EH}_j}[n] = \sqrt{1 - \rho_j}\, y_{R_j}[n]. \tag{5.3}$$

If R_j is selected to cooperate, then y_{IP_j} is amplified and forwarded to the sources. Let β_j denote the amplification factor at R_j. The transmit signal at R_j is

$$x_{R_j}[n] = \beta_j (y_{\mathrm{IP}_j}[n-1] + w_{P_j}). \tag{5.4}$$

Then the required transmit power at R_j with amplification factor β_j is

$$P_{R_j} = \mathbb{E}[|x_{R_j}|^2] = \beta_j^2 (\rho_j \mathbb{E}[|y_{R_j}|^2] + \sigma_P^2). \tag{5.5}$$

Note that the investigated EH relays do not rely on additional power sources and all the energy used for transmission at R_j is harvested from y_{EH_j}. This means that the transmit

power equals to the harvested power on average. Given the EH efficiency ξ, the allowable transmit power at R_j is

$$P_{R_j} = \xi \, \mathbb{E}[|y_{\mathrm{EH}_j}|^2]. \tag{5.6}$$

Combining (5.5) and (5.6), we obtain the value of β_j as

$$\beta_j = \sqrt{\frac{\xi(1-\rho_j)\mathbb{E}[|y_{R_j}|^2]}{\rho_j \mathbb{E}[|y_{R_j}|^2] + \sigma_P^2}} \approx \sqrt{\frac{(1-\rho_j)\xi}{\rho_j}}. \tag{5.7}$$

This approximation is justified as $\rho_j \mathbb{E}[|y_{R_j}|^2] \gg \sigma_P^2$ in practical networks. Otherwise, the end-to-end SINR would be very small if the signal and interference could not dominate the received power at the relays.

The received signal at S_i via the jth relay is

$$y_{S_i}^{(j)}[n] = h_{ij} x_{R_j}[n] + \Omega_{S_i} x_{S_i}[n] + w_{ij}[n] \tag{5.8}$$

where w_{ij} is the noise at S_i, which follows the distribution $\mathcal{CN}(0, \sigma_S^2)$ with $\sigma_S^2 = N_S W/|\mathcal{R}|$ and N_S is the noise power spectral density at the sources.

The received signals from multiple relays are combined at the sources. Let $\gamma_{S_i}^{(j)}$ denote the SINR of the received signal at S_i via R_j. The capacity of the link from S_2 to S_1 can be calculated as

$$C_{S_1} = \frac{W}{|\mathcal{R}|} \log_2 \left(1 + \sum_{j \in \mathcal{R}} \gamma_{S_1}^{(j)} \right) \tag{5.9}$$

and same for the link from S_1 to S_2, mutatis mutandis.

5.2.2 The Relay Selection Problem

In this chapter, we consider two important performance metrics for the relay selection problem, that is the outage probability and the ergodic sum capacity. The outage probability is defined as

$$P_{\text{out}} = \Pr\{\min(C_{S_1}, C_{S_2}) < C_{\text{th}}\} \tag{5.10}$$

where C_{th} is the outage threshold below which the capacity is considered as unacceptable.

The ergodic sum capacity is defined as

$$C_E = \mathbb{E}[C_{S_1} + C_{S_2}] \tag{5.11}$$

in which the expectation is taken with respect to channel realizations.

The relay selection problem can be formulated as

$$\underset{\mathcal{R},\boldsymbol{\rho}}{\text{minimize}} \quad J(\mathcal{R}, \boldsymbol{\rho}) \tag{5.12a}$$

$$\text{subject to} \quad \rho_j \in [0,1], \quad k = 1, 2, \cdots, N \tag{5.12b}$$

where $J(\mathcal{R}, \boldsymbol{\rho})$ is an objective function whose value varies with the set of selected relays $\mathcal{R}$ and the corresponding PS factors $\boldsymbol{\rho}$. The specific forms of the objective function will be discussed in detail in Sections 5.3 and 5.4.

For conventional relay networks without energy harvesting, the relays operate on their own battery. Therefore, selecting more than one relay to cooperate may not be desirable in terms of energy efficiency. For energy-harvesting relay networks, however, each relay harvests

energy from its received signals independently. Consequently, selecting more relays would not increase the energy consumption. Instead, more energy would be harvested from the signals transmitted by the sources and the received SINR would be enhanced.

The downside of selecting more than one relay is that the selected relays still need to transmit and to receive over orthogonal channels, meaning that different segments of the frequency spectrum are assigned to different relays. As a result, the AP method is not necessarily optimal for EH relay networks either. This tradeoff between the SINR and the bandwidth utilization makes the investigated RS problem more interesting.

On the other hand, the general RS problem is a nonlinear 0-1 programming problem, which is known to be intractable in practice due to its exponentially increasing complexity with respect to the number of relays. For simplicity, we first focus on the SRS methods in Section 5.3. Then, we further study the more complicated GRS problem in Section 5.4.

5.3 Single Relay Selection

We first consider a scenario where only one relay is selected each time, i.e., $|\mathcal{R}| = 1$. With this additional constraint, solving the RS optimization problem is computationally tractable, with the complexity of merely $\mathcal{O}(N)$. To achieve different goals, we present the following two SRS criteria: the outage probability, which captures the fairness of the selection method, and the sum capacity, which captures the overall network performance.

Note that for these criteria, the optimization of the PS factor is independent of the relay selection. Therefore, the joint optimization is equivalent to optimizing ρ_j first for each relay and selecting the best relay in the second step.

5.3.1 Minimum Outage Probability

First, we consider the SRS methods aiming to minimize the outage probability of the network. Note that for each channel realization, minimizing the outage probability is equivalent to maximizing $\min(C_{S_1}, C_{S_2})$, which in turn is equivalent to maximizing $\min\left(\gamma_{S_1}^{(j)}, \gamma_{S_2}^{(j)}\right)$. Therefore, the SRS problem with minimum outage probability is formulated as

$$j^* = \underset{j\in\{1,2,\cdots,N\}}{\arg\min} \min_{\rho_j\in[0,1]} J_{P_{\text{out}}}^{(j)}(\rho_j) \tag{5.13}$$

where $J_{P_{\text{out}}}^{(j)}(\rho_j) = -\min\left(\gamma_{S_1}^{(j)}, \gamma_{S_2}^{(j)}\right)$ is the objective function if the jth relay was selected, i.e., $\mathcal{R} = \{R_j\}$.

For each relay R_j, we first find the optimal PS factor that minimizes the outage probability if R_j is selected. Then we find the best relay with their respective ρ_j^*.

To investigate the properties of this optimization problem, we first derive the SINR of the received signals at the sources. The power of $y_{S_i}^{(j)}$ can be obtained as

$$\begin{aligned}\mathbb{E}\left[\left|y_{S_i}^{(j)}\right|^2\right] &= \beta_j^2\rho_j|h_{ij}|^2|h_{\bar{i}j}|^2P_S \\ &\quad + |h_{ij}|^2|\Omega_{R_j}|^2\beta_j^2\rho_jP_{R_j} + |h_{ij}|^2\beta_j^2\rho_j\sigma_A^2 + |\Omega_{S_i}|^2P_S \\ &\quad + |h_{ij}|^2\beta_j^2\sigma_P^2 + \sigma_S^2\end{aligned} \tag{5.14}$$

where P_S denotes the source transmit power and $\bar{i}$ is the index of the other source. The expectation is taken with respect to source symbol realizations.

Only the first term on the right-hand side of (5.14) corresponds to the useful signal from the other source $S_{\bar{i}}$. Hence, given the amplification factor in (5.7), the end-to-end SINR of

the $S_{\bar{i}} \to R_j \to S_i$ link is

$$\gamma_{S_i}^{(j)} = \frac{\beta_j^2 \rho_j |h_{ij}|^2 |h_{\bar{i}j}|^2 P_S}{|h_{ij}|^2 |\Omega_{R_j}|^2 \beta_j^2 \rho_j P_{R_j} + |h_{ij}|^2 \beta_j^2 \rho_j \sigma_A^2 + |\Omega_{S_i}|^2 P_S + |h_{ij}|^2 \beta_j^2 \sigma_P^2 + \sigma_S^2} \tag{5.15}$$

$$= \frac{|h_{ij}|^2 |h_{\bar{i}j}|^2 P_S}{\frac{(1-\rho_j)\xi |\Omega_{R_j}|^2}{1-(1-\rho_j)\xi |\Omega_{R_j}|^2} |h_{ij}|^2 [P_S(|h_{ij}|^2 + |h_{\bar{i}j}|^2) + \sigma_A^2] + (\sigma_A^2 + \frac{\sigma_P^2}{\rho_j})|h_{ij}|^2 + \frac{|\Omega_{S_i}|^2 P_S + \sigma_S^2}{(1-\rho_j)\xi}}. \tag{5.16}$$

Proposition 5.1 *The objective function $J_{P_{\text{out}}}^{(j)}$ for R_j is quasi-convex with respect to the power splitting factor ρ_j over the open interval $(0, 1)$.*

Proof. See Appendix. ■

Apparently, neither $\rho_j = 0$ nor $\rho_j = 1$ is the minimizer of $J_{P_{\text{out}}}^{(j)}$. Therefore, Proposition 5.1 guarantees that we can find a ρ_j that achieves the globally minimum outage probability for $\rho_j \in [0, 1]$ by local search methods, such as the method of gradient descent or the Newton-Raphson method [26]. Since these methods are well-studied and are suitable for quasi-convex optimization problems, we will not expand our discussion on this subject in this chapter.

5.3.2 Maximum Sum Capacity

In this subsection, we discuss the RS criteria that maximize the sum capacity in both directions. Hence, the problem is formulated as

$$j^* = \underset{j \in \{1,2,\cdots,N\}}{\arg\max} \max_{\rho_j \in [0,1]} \left(C_{S_1}^{(j)} + C_{S_2}^{(j)} \right). \tag{5.17}$$

Note that the conclusion drawn from Proposition 5.1 is not applicable to the maximum sum capacity SRS. Although we can always apply the same optimization algorithm to this

problem, the solution is not necessarily the global optimum. However, through our simulations in Section 5.5, we find that the obtained solutions almost always yield good results in terms of sum capacity.

5.4 General Relay Selection

As explained in Section 5.2.2, neither the SRS methods nor the AP method is the optimal RS method under all circumstances. Therefore, it is necessary to further investigate the GRS problem for EH relay networks.

In this chapter, we focus on the networks in which relays transmit over mutually orthogonal channels. Compared with relays that transmit over a shared channel, this type of networks is easier to implement and have smaller overhead. Although sharing the same bandwidth provides higher rate, it requires carrier-level synchronization at the relays, which allows precise phase adjustment of the relay transmission signals so that coherent combining at the receivers is possible [12].

Since the optimal GRS problem is computationally intractable with exponential complexity, some heuristic algorithms have been proposed to solve the GRS problem for conventional relay networks without energy harvesting [8, 9, 40]. In this section, we also propose two types of heuristic GRS methods for the investigated FDEH2W relaying networks.

5.4.1 GRS Methods Based on Relay Ordering

An intuitive way to simplify the GRS problem is to find an optimal relay ordering in which the predecessors should always have higher priorities to be selected than the successors. More rigorously, for an optimal relay ordering $(\tau_1, \tau_2, \cdots, \tau_N)$, the relay selection $\mathcal{R}^*_{N'} =$

$\left\{R_{\tau_1}, R_{\tau_2}, \cdots, R_{\tau_{N'}}\right\}$ is optimal among all relay selection sets with N' relays, where $1 \leqslant N' \leqslant N$. Correspondingly, a function $\psi(h_{1j}, h_{2j})$ that could induce such an ordering by a descending sort is called an optimal relay ordering function.

After the optimal relay ordering is obtained, the remainder of the problem is to determine the number of relays to select. Finding the number of cooperating relays can be achieved with N iterations. Therefore, the complexity is linear in the number of candidate relays N, which is much lower than the exponential complexity of the original GRS problem.

In [9] and [40], the existence of such optimal relay ordering was discussed for conventional relay networks in which the selected relays transmit over the same channel resource through network beamforming. The results therein show that: when the options for each relay is to cooperate with full power or not to cooperate at all, the optimal relay ordering does not exist; whereas the optimal relay ordering does exist in cases where the relays can cooperate with arbitrary power within their individual power limits. This is because that cooperating with the maximum available power does not necessarily provide the optimal beamforming SNR. Therefore, flexible adjustment of the transmit power is beneficial to the performance improvement in network beamforming. For the investigated networks in this research, however, the transmission of each cooperating relay is decoupled since the relays transmit over mutually orthogonal channels. It is always desirable for the relays to transmit with as much power as possible. Therefore, the existence of the optimal relay ordering in the investigated networks entails further investigation.

Proposition 5.2 *For FDEH2W relay networks with more than* 2 *available relays, the optimal relay ordering does not always exist.*

Proof. Let $\mathcal{R}_n^*$ denote the optimal relay selection set when n relay(s) is/are selected. If the optimal relay order does exist, we have $\mathcal{R}_i^* \subset \mathcal{R}_j^*$ for any $1 \leqslant i < j \leqslant N$. First we prove this proposition for the case of $N = 3$ by finding an example in which $\mathcal{R}_1^*$ is not a subset of $\mathcal{R}_2^*$. In this case, the transmit SNR is 30 dB, $|h_{11}|^2 = 0.2308$, $|h_{12}|^2 = 0.1025$, $|h_{13}|^2 = 0.0167$, $|h_{21}|^2 = 0.0220$, $|h_{22}|^2 = 0.0428$, and $|h_{23}|^2 = 0.2813$. By exhaustive search, we find that $\mathcal{R}_1^* = \{R_1\}$ and $\mathcal{R}_2^* = \{R_2, R_3\}$. Obviously, $\mathcal{R}_1^* \not\subset \mathcal{R}_2^*$ and, hence, the optimal relay ordering does not exist in this case. This example can be easily extended to cases where $N > 3$ by making $|h_{ij}|^2 \to 0, \forall i \in \{1, 2\}$ and $j > 3$. Therefore, the optimal relay ordering does not always exist for FDEH2W relay networks with 2 or more available relays. ■

In fact, the simulations in Section 5.5.2 also demonstrate that the optimal relay ordering does not always exist.

Although the optimal relay ordering may not exist in some cases, we can still adopt the idea of relay ordering to achieve sub-optimal RS with low complexity. Therefore, we propose three sub-optimal relay ordering functions for the investigated FDEH2W relaying networks.

5.4.1.1 Worse Channel Ordering (WCO)

The WCO function is defined as the lower channel gain between the $S_1 \leftrightarrow R_j$ and the $S_2 \leftrightarrow R_j$ channels

$$\psi_{\text{WCO}}(h_{1j}, h_{2j}) = \min\{|h_{1j}|^2, |h_{2j}|^2\}. \tag{5.18}$$

5.4.1.2 Channel Harmonic Mean Ordering (CHMO)

The CHMO function is defined as the harmonic mean of the same two channel gains

$$\psi_{\text{CHMO}}(h_{1j}, h_{2j}) = \left(\frac{1}{|h_{1j}|^2} + \frac{1}{|h_{2j}|^2} \right)^{-1}. \tag{5.19}$$

5.4.1.3 Worse SINR Ordering (WSINRO)

Given that only R_j is selected to cooperate, the WSINRO function takes value as the lower SINR between the $S_1 \to S_2$ and the $S_2 \to S_1$ links

$$\psi_{\text{WSINRO}}(h_{1j}, h_{2j}) = \min \left(\gamma_{S_1}^{(j)}, \gamma_{S_2}^{(j)} \right). \tag{5.20}$$

5.4.2 A Greedy GRS Method

The relay ordering functions proposed in the previous subsection are heuristic and sub-optimal. And simulations show that they do not perform as well as the optimal GRS method. In order to improve the performance of GRS, we further propose a greedy GRS method to achieve near-optimal RS. The greedy GRS method starts with $\mathcal{R}_0 = \emptyset$ and gradually adds the relays one by one as $\mathcal{R}_{N'} = \mathcal{R}_{N'-1} \cup \left\{ R_{j_{N'}^*} \right\}$, where

$$j_{N'}^* = \underset{j,\, R_j \in \{R_1, R_2, \cdots, R_N\} \setminus \mathcal{R}_{N'-1}}{\arg\min} J(\mathcal{R}_{N'-1} \cup \{R_j\}, \boldsymbol{\rho}^*) \tag{5.21}$$

and $\boldsymbol{\rho}^*$ is the vector of optimal PS factors for all the candidate relays. Finally, we choose $\mathcal{R}^*$ as the optimal set of relays to be selected among $\mathcal{R}_1, \mathcal{R}_2, \cdots, \mathcal{R}_N$ according to

$$\mathcal{R}^* = \underset{\mathcal{R}_n \in \{\mathcal{R}_1, \mathcal{R}_2, \cdots, \mathcal{R}_N\}}{\arg\min} J(\mathcal{R}_n, \boldsymbol{\rho}^*). \tag{5.22}$$

The computational complexity of this greedy GRS method in terms of the number of available relays is obviously $\mathcal{O}(N^2)$.

Note that $\mathcal{R}_i \subset \mathcal{R}_j$ for $i < j$. Hence, the greedy GRS method would find the optimal relay ordering if it does exist. In other words, the proposed greedy GRS method should perform at least equally well as the relay ordering based methods presented in Section 5.4.1.

5.5 Simulations

In this section, we present simulations to evaluate the performance and characteristics of the proposed RS methods. In the simulations, parameters are set as in Table 5.2 and all channels follow Rayleigh fading. As for the residual self-interference channel gain, -85 dB to -15 dB is considered as a pragmatic range. The self-interference channel gain without cancellation is approximately -15 dB [22] and practical self-interference cancellation can already suppress the interference by 70 dB or more [18]. Therefore, we set $\mathbb{E}[|\Omega_{S_i}|^2]$ to -85 dB as the self-interference is unambiguously harmful at the sources. $\mathbb{E}[|\Omega_{R_j}|^2]$ is set to -85 dB except for the simulation in Section 5.5.3, where the effect of self-interference cancellation is under investigation.

Table 5.2: Simulation Parameters

Bandwidth	10 MHz
Noise Power Spectral Density	-174 dBm/Hz
Noise Figure	5 dB
Energy Harvesting Efficiency	90%
Residual Self-Interference Channel Gain	-85 dB
Outage Threshold	0.5 bps/Hz

5.5.1 Performance Comparison

We first investigate the performance of the proposed RS methods with various source transmit SNR as presented in Figs. 5.2-5.4.

When the source transmit power is low, the AP method performs better than the SRS method in terms of sum capacity. This is mainly because the AP method could harvest more energy and enhance the overall SINR at the sources. Whereas when the source transmit power is high, selecting the best relay that could utilize the channel bandwidth more efficiently becomes more important, since the best relay can harvest considerable amount of energy by itself already. As a result, the SRS method outperforms the AP method, at the cost of marginally increased complexity.

In Fig. 5.3, however, the AP method yields better outage probability than the SRS at high SNR. This is on the contrary to the performance shown in Fig. 5.2. To further investigate this phenomenon, we plot the empirical cumulative distribution function (CDF) of the minimum capacity of the two directions in Fig. 5.4. Note that, by definition, the value of the CDF at C_{th} is the outage probability if C_{th} is chosen as the threshold. We can see clearly from this figure that the choice of the outage threshold affects the relative relationship of the outage probability of the RS methods. At the transmit SNR of 25 dB, the SRS method has higher outage probability than the AP method if the threshold is small. The order is reversed if a

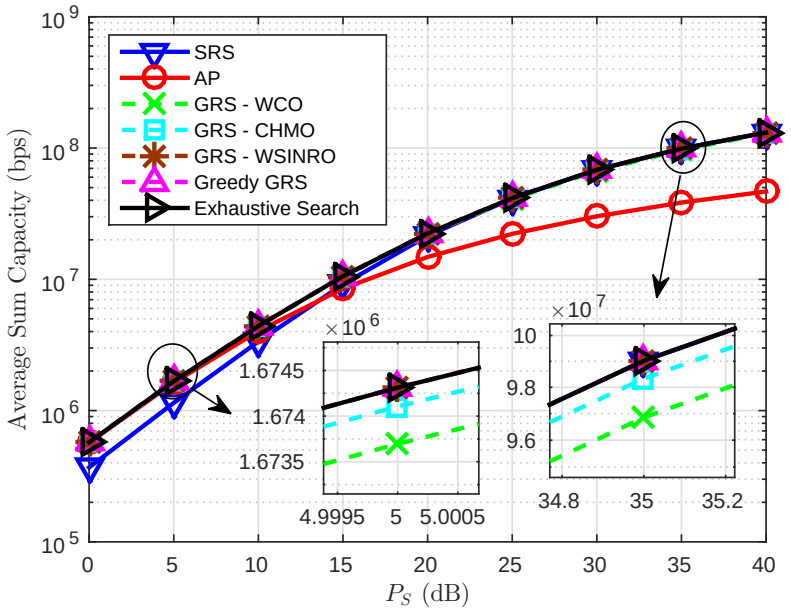

Figure 5.2: Sum capacity comparisons with varying source transmission SNR

higher threshold is chosen at the same SNR. The threshold for outage is set to 0.5 bps/Hz while plotting Fig. 5.3. And that explains why, at high SNR, the SRS method yields higher outage probability in Fig. 5.3 while achieving higher average sum capacity in Fig. 5.2.

As for the proposed GRS methods, all of them achieve at least as good performance as the SRS and the AP methods uniformly across different source transmit power. Also from Figs. 2 and 3, we find that all the proposed GRS methods based on WCO, CHMO, and WSINRO, as well as the greedy GRS method achieve very close performance in terms of sum capacity and outage probability compared with the optimal RS method based on exhaustive search.

From this set of simulations, we can conclude that the SRS and the AP methods are near-optimal for high SNR and low SNR situations, respectively. This observation is corroborated in the following two aspects. In Fig. 5.2, the AP method has similar performance with the GRS methods at low SNR and the SRS methods achieves similar performance with the

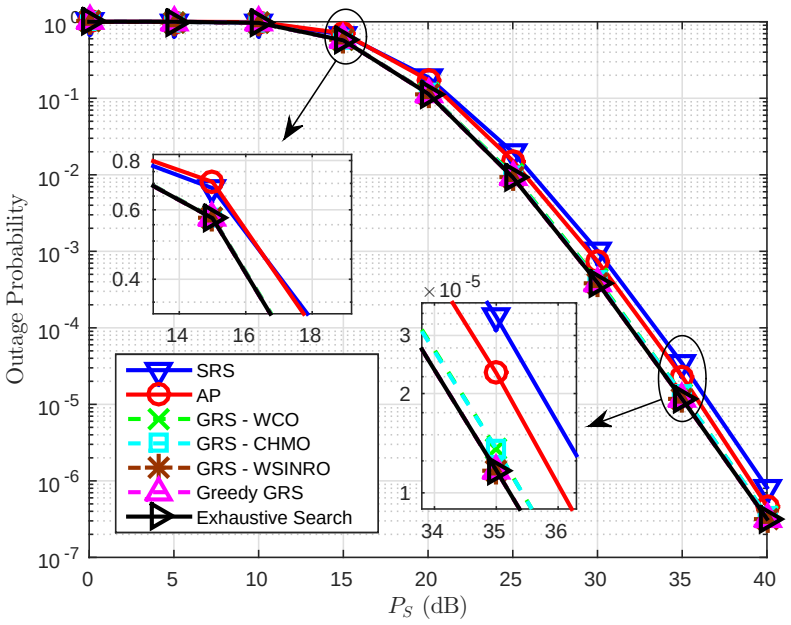

Figure 5.3: Outage probability comparisons with varying source transmission SNR

GRS methods at high SNR. From another perspective, it is also supported by simulation results presented in Fig. 5.5. The average number of selected relays by the GRS methods, including the exhaustive search method, eventually reduces to 1 as the source transmission power increases. This observation is fundamentally different from that in the conventional RS problem, where SRS is always optimal [7].

In all these figures, all of the proposed GRS methods achieve near-optimum performance in terms of both the sum capacity and the outage probability, especially for the WSINRO based GRS method and the greedy GRS method. Although difficult to observe from the figures, the gap between the WSINRO based GRS method and the exhaustive search does exist. This means that the WSINRO is not the optimal relay ordering and the GRS method based on it is not optimal either. From a practical perspective, however, we believe the WSINRO based GRS method and the greedy GRS method achieve good compromise between complexity and performance.

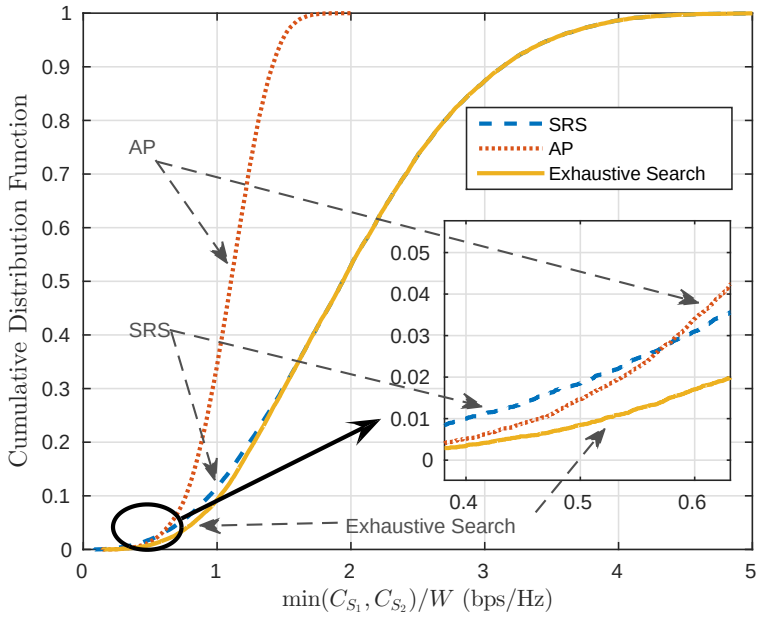

Figure 5.4: The cumulative distribution functions of the min capacity at 25 dB.

5.5.2 Number of Relays

The number of available relay candidates that are available for selection also affects the performance of the RS methods. As shown in Fig. 5.6 and Fig. 5.7, because of the diversity gain brought by the relays, increasing the number of relay candidates benefits all the RS methods except the AP one. When the number of available relays is large, selecting all of them causes the bandwidth to be split into too many subbands. As a result, the SINR gain brought by the extra power harvested by the relays is no longer large enough to overcome the capacity loss due to the bandwidth reduction, especially at high SNR. Therefore, the performance of AP is not monotonically increasing with the number of relays.

The GRS methods also uniformly outperforms both the SRS and the AP methods. In addition, in terms of both the sum capacity and the outage probability, the performance gap between the GRS methods and the SRS methods increases when the number of relays N

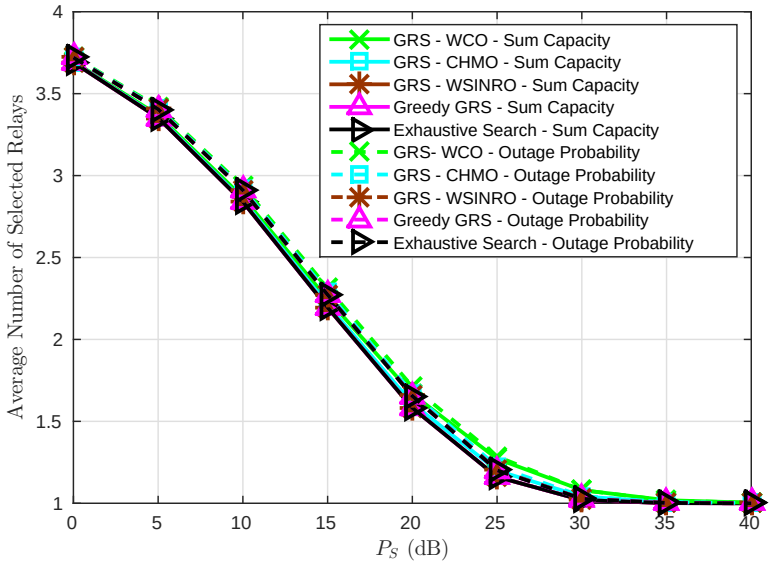

Figure 5.5: Number of selected relays versus the source transmit SNR

increases from 2 to 6 and stabilizes thereafter. When N is small, the GRS methods tend to select all "good" relays and the number of selected relays increases along with N. When N is large, the number of selected relays stops growing as N keep increasing. Hence, increasing N will not provide as much extra benefit for GRS over SRS as it does when N is small. As a result, the performance gap gradually stops increasing. This statement is corroborated by Fig. 5.8, which shows the average number of selected relays of the four proposed GRS methods while optimizing sum capacity and outage probability, respectively. In fact, the number even slightly declines when $N > 6$. This is reasonable since the chance of having "better" candidate relays increases as N increases and fewer relays tend to be selected. It is similar as the phenomenon presented in Section 5.5.1.

Another important insight that can be drawn from this set of simulations is that the greedy GRS method is demonstrated to be sub-optimal. As observed in the zoom-in windows in Figs. 5.6-5.8, the greedy GRS method does not perform as well as the optimal

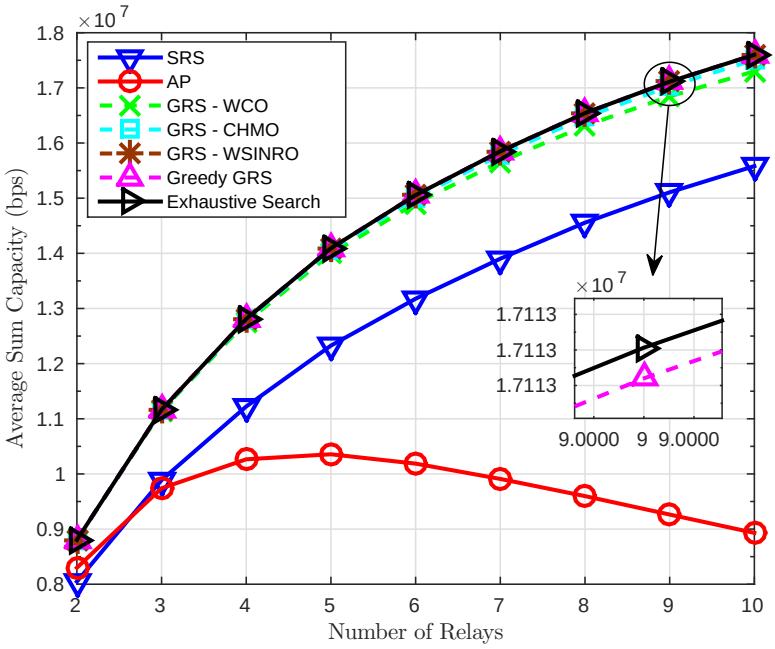

Figure 5.6: Sum capacity comparisons with different number of relays

GRS method. In addition, the average number of selected relays by these two methods are also different. These observations indicate that the greedy GRS method, at least in some occasions, selects different subsets of relays with the optimal GRS method. Furthermore, because the greedy GRS method is guaranteed to find the optimal relay ordering if it does exist, these phenomena corroborate Proposition 5.2 that an optimal relay ordering does not always exist.

5.5.3 Effects of Self-Interference at the Relays

The sum capacity and the outage probability with different self-interference channel gains are shown in Fig. 5.9 and Fig. 5.10, respectively. $\mathbb{E}[|\Omega_{R_j}|^2]$ varies from -55 dB to -15 dB. The transmit SNR is set to 20 dB, with other settings unchanged.

In Fig. 5.9, we observe that the sum capacity is monotonically increasing when the residual self-interference channel gain becomes weaker. And it begins to plateau when $\mathbb{E}[|\Omega_{R_j}|^2]$

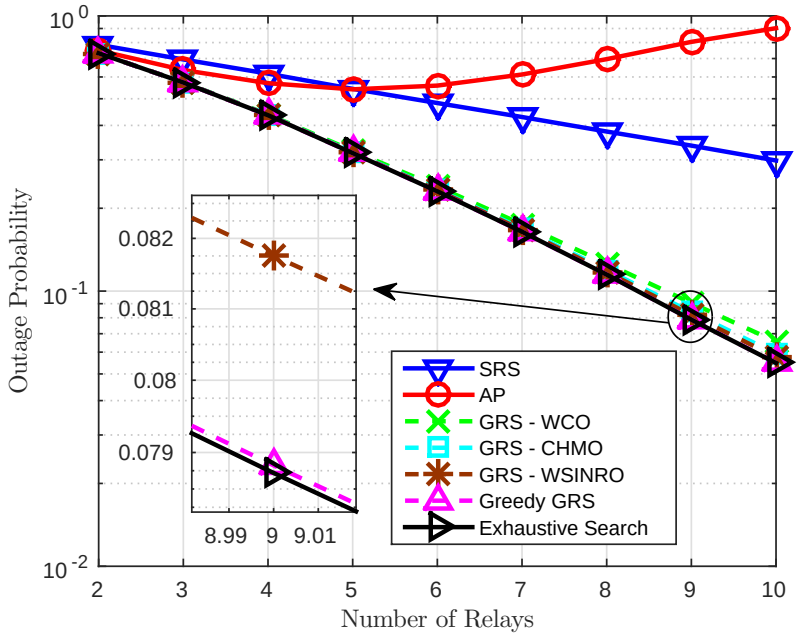

Figure 5.7: Outage probability comparisons with different number of relays

is below -30 dB. Intuitively, however, there should be a non-zero optimal $\mathbb{E}[|\Omega_{R_j}|^2]$ for such EH relay networks, since the system could benefit from the loopback interference at the relays as an additional source of energy that can be harvested. Nonetheless, as we can see in (5.16), the end-to-end SINR is monotonically decreasing with $\mathbb{E}[|\Omega_{R_j}|^2]$. This is caused by the approximation made in (5.7), which assumes the power of the received signals at the relays is much larger than that of the processing noise. In this case, the power harvested from the self-interference is simply too little to overcome its undesirable effect, namely the SINR degradation at the relays.

In Fig. 5.10, the outage probability curves of the SRS and the AP methods cross over each other between -20 dB and -15 dB. This phenomenon is absent in the sum capacity performance in Fig. 5.9. The reason is similar to that explained in Section 5.5.1. That is the behavior of the outage probability is highly sensitive to the threshold of outage capacity,

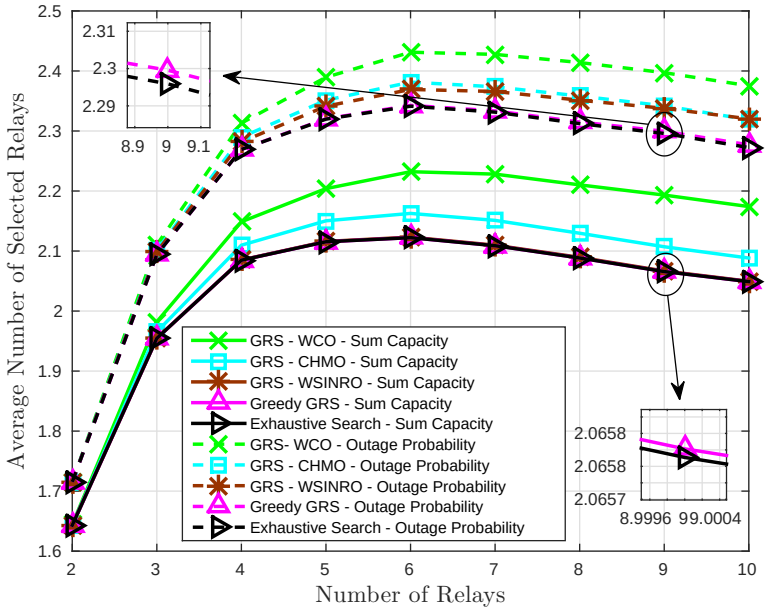

Figure 5.8: Comparisons of the average number of relays with different number of relays

especially for the AP method whose capacity distribution is more concentrated around its mean than the SRS method.

5.6 Conclusions

In this chapter, we studied the relay selection problem in two-way FD PS-SWIPT-based EH relay networks. Based on the received SINR at the sources in FDEH2W networks, the quasi-convexity of the PS factor optimization was proved, and the optimal PS factor for each relay was obtained by one-dimensional search. In addition, we proposed two efficient SRS methods based on the optimized PS factor at each relay. Both SRS methods perform almost identically to the exhaustive search based optimal RS at high SNR. Then we investigated the GRS problem. Given the fundamental differences of the FDEH2W networks from conventional multi-relay networks, we proved the suboptimality of SRS. Nonetheless, the optimal GRS can only be obtained by exhaustive search with exponential complexity in

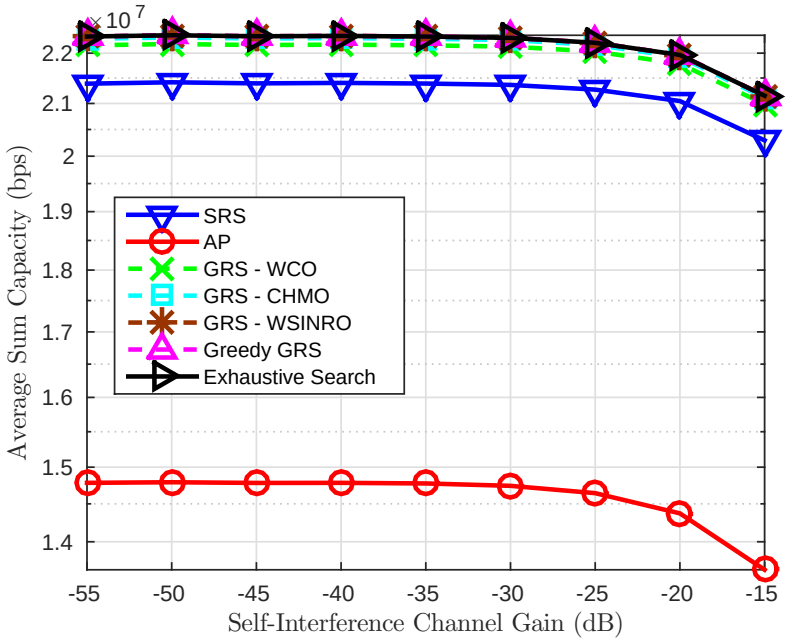

Figure 5.9: Sum capacity comparisons with varying residual self-interference channel gain

the number of available relays. Hence, three relay ordering based GRS methods with linear complexity and a greedy GRS method with quadratic complexity were proposed. Despite the fact that the optimal relay ordering does not always exist, our proposed GRS methods achieve near-optimal performance with much lower complexity than the exhaustive search.

5.7 Proof of Proposition 5.1

Proof. Let $\tilde{\gamma}_{S_i}^{(j)}$ denote the denominator in (5.16), so that $\gamma_{S_i}^{(j)} = |h_{ij}|^2|h_{\bar{i}j}|^2 P_S/\tilde{\gamma}_{S_i}^{(j)}$.

$$J_{P_{\text{out}}}^{(j)} = \max\left(-\gamma_{S_1}^{(j)}, -\gamma_{S_2}^{(j)}\right) \tag{5.23}$$

$$= \max\left(-\frac{|h_{1j}|^2|h_{2j}|^2 P_S}{\tilde{\gamma}_{S_1}^{(j)}}, -\frac{|h_{2j}|^2|h_{1j}|^2 P_S}{\tilde{\gamma}_{S_2}^{(j)}}\right) \tag{5.24}$$

Since both maximization and composition with a non-decreasing function preserve quasi-convexity, and $f(x) = -\frac{|h_{ij}|^2|h_{\bar{i}j}|^2 P_{\bar{i}}}{x}$ is a non-decreasing function for $x > 0$, $J_{P_{\text{out}}}^{(j)}$ is quasi-

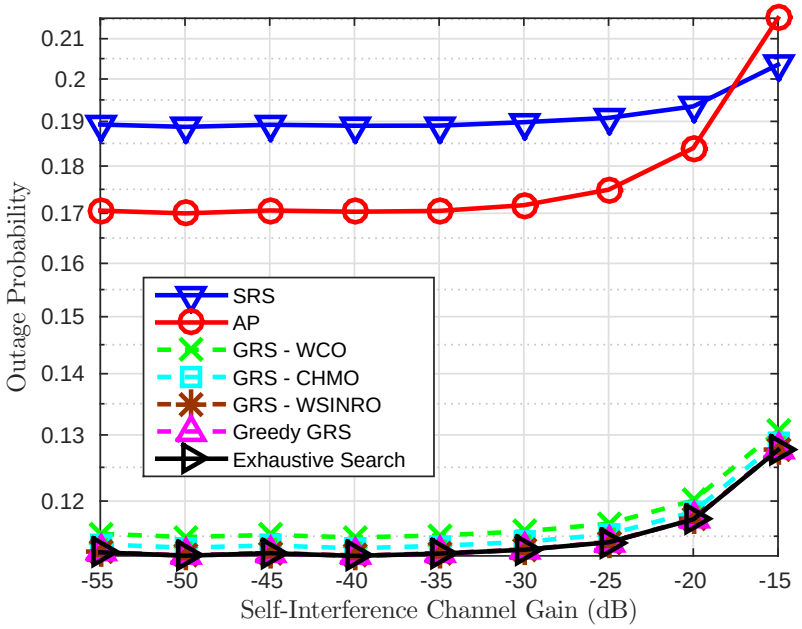

Figure 5.10: Outage probability comparisons with varying residual self-interference channel gain

convex if both $\tilde{\gamma}_{S_1}^{(j)}$ and $\tilde{\gamma}_{S_2}^{(j)}$ are positive and quasi-convex. Since $(1-\rho_j)\xi|\Omega_{R_j}|^2 \ll 1$, we can approximate $\tilde{\gamma}_{S_i}^{(j)}$ as

$$\tilde{\gamma}_{S_i}^{(j)} \approx (1-\rho_j)\xi|\Omega_{R_j}|^2|h_{ij}|^2(P_S(|h_{ij}|^2+|h_{\bar{i}j}|^2)+\sigma_A^2)+(\sigma_A^2+\frac{\sigma_P^2}{\rho_j})|h_{ij}|^2+\frac{|\Omega_{S_i}|^2P_S+\sigma_S^2}{(1-\rho)\xi}.$$

$\tilde{\gamma}_{S_i}^{(j)}$ is obviously positive because it is the denominator of the SINR. To prove that it is quasi-convex, we derive its second derivative as

$$\frac{\partial^2\tilde{\gamma}_{S_i}^{(j)}}{\partial\rho_j^2} \approx \frac{2\sigma_P^2|h_{ij}|^2}{\rho_j^3}+\frac{2(|\Omega_{S_i}|^2P_S+\sigma_S^2)}{(1-\rho_j)^3\xi}. \tag{5.25}$$

It is obvious that $\frac{\partial^2\tilde{\gamma}_{S_i}^{(j)}}{\partial\rho_j^2} > 0$ for $\rho_j \in (0,1)$. Consequently, $\tilde{\gamma}_{S_i}^{(j)}$ is convex. And a convex function is also quasi-convex. Therefore, $\tilde{\gamma}_{S_i}^{(j)}$ is quasi-convex and that concludes the proof.

■

CHAPTER 6

NETWORK BEAMFORMING IN ENERGY-HARVESTING RELAY NETWORKS

In previous chapters, we have investigated RS in networks with multiple EH relays. It is a technique that exploits the cooperative diversity with relatively low complexity and the relays use orthogonal channels. Network beamforming, on the other hand, is a more effective technique in exploiting the cooperative diversity with shared bandwidth. In this chapter, we propose a network beamforming scheme for EH relay networks with jointly optimized PS factors.

6.1 Background

Beamforming is one of the most successful multi-antenna techniques that increases the SNR at the receiver without increasing the transmit power. In EH relay networks, the beamforming in EH systems has been an active research area in recent years. An comprehensive survey on this subject can be found in [41]. Most of existing work consider networks with a single multi-antenna relay. However, installing and operating multiple antennas can be impractical for many wireless mobile devices, especially the ones rely on EH, due to limitations on size, power, and cost.

Network/distributed beamforming in conventional networks has been a heated topic in the literature. The optimization of the beamforming weights is studied assuming perfect channel state information (CSI) [40] or only second-order statistics of the CSI [42] with

the objective of SNR maximization or transmit power minimization. In cases where SNR maximization is the objective, a total power constraint leads to an optimal solution that reaches the total power limit, whereas individual power constraints yield relay transmit powers that are not necessarily at their maximum allowable values.

For networks with SWIPT or EH, network/distributed beamforming by multiple single-antenna relays is a relatively new research topic. In [43], a network with multiple sources, relays, and destinations is considered. The relays facilitate the communications in the network cooperatively by distributed beamforming. The PS-based EH is done at the destinations.

In this chapter, we propose a network beamforming scheme for networks with multiple single-antenna PS-based EH relays. In such networks, the issue of power constraint becomes more complicated compared to conventional relay networks. The relay transmit power is neither constrained by a total limit nor individual limits. Instead, it is determined by the PS factors because the power relays used to transmit is obtained through EH. Thus, the optimization of PS factors becomes the most intriguing problem. In this research, we formulate the joint optimization of PS factors at all relays and convert it to a quasi-convex optimization problem with semidefinite relaxation (SDR). Hence, the globally optimal solution can be obtained efficiently. We also propose a distributed, but sub-optimal, scheme with closed-form solutions that only require local CSI at each relay. Simulations show that both proposed schemes outperform the optimal RS schemes.

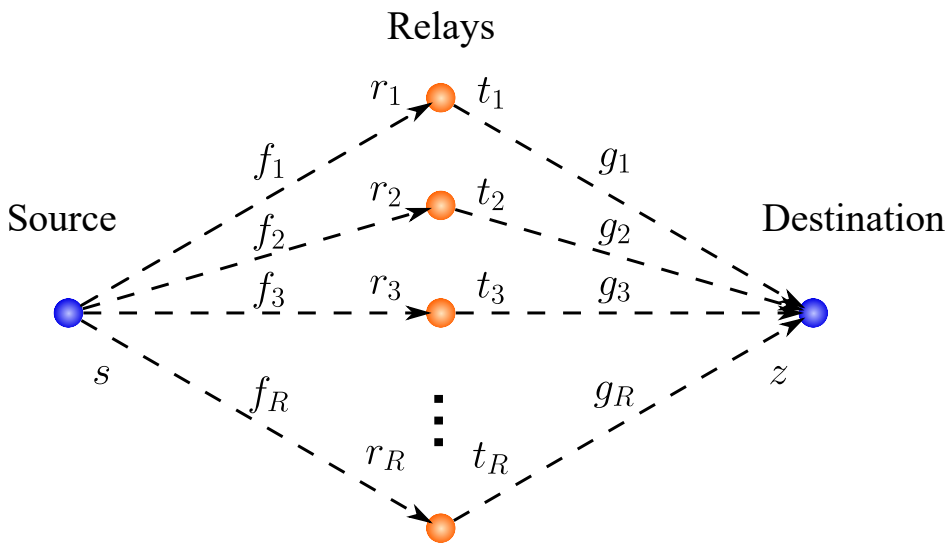

Figure 6.1: Wireless Relay Network

6.2 System Model

The network we consider consists of $R+2$ nodes, each of which is equipped with a single antenna, as shown in Fig. 6.1. Among these nodes, one is the source, one is the destination, and all else are relays. All relays operate under the HD AF protocol.

The received signal at Relay i

$$r_i = \sqrt{P_S} f_i s + v_{i,A} \tag{6.1}$$

which is split for IP and EH respectively according to PS factor $\rho_i \in [0, 1]$, so that the signal for IP

$$d_i = \sqrt{\rho_i} r_i + v_{i,P}$$

and the signal for EH

$$\bar{d}_i = \sqrt{1 - \rho_i} r_i.$$

Relay i amplifies the received signal r_i with a factor of β_i and adjust the phase by θ_i before forwarding to the destination. Thus, the transmit signal at Relay i is

$$t_i = \beta_i e^{j\theta_i} d_i. \tag{6.2}$$

The average transmit power of Relay i is

$$\mathbb{E}[|t_i|^2] = \beta_i^2(\rho_i P_S |f_i|^2 + \rho_i \sigma_A^2 + \sigma_P^2) \tag{6.3}$$

and the average power of the signal split for EH at Relay i is

$$\mathbb{E}[|\bar{d}_i|^2] = (1-\rho_i)(P_S|f_i|^2 + \sigma_A^2). \tag{6.4}$$

To maintain sustainable operation, the harvested power should equal to the transmit power, that is,

$$\mathbb{E}[|t_i|^2] = \xi \mathbb{E}[|\bar{d}_i|^2] \tag{6.5}$$

where ξ denotes the energy conversion efficiency for EH. Therefore,

$$\beta_i = \sqrt{\frac{\xi(1-\rho_i)(P_S|f_i|^2 + \sigma_A^2)}{\rho_i(P_S|f_i|^2 + \sigma_A^2) + \sigma_P^2}} \approx \sqrt{\frac{\xi(1-\rho_i)}{\rho_i}}.$$

The received signal at the destination

$$x = \sum_{i=1}^{R} g_i t_i + w = \boldsymbol{g}^\top \boldsymbol{t} + w \tag{6.6}$$

$$= \sqrt{\xi P_S} \left(\sum_{i=1}^{R} \sqrt{1-\rho_i} f_i g_i e^{j\theta_i} \right) s + \sqrt{\xi} \sum_{i=1}^{R} \sqrt{1-\rho_i} g_i e^{j\theta_i} \left(v_{i,A} + \frac{v_{i,P}}{\sqrt{\rho_i}} \right) + w. \tag{6.7}$$

Therefore, the SNR at the destination is

$$\gamma = \frac{P_S |\sum_{i=1}^{R} \sqrt{1-\rho_i} f_i g_i e^{j\theta_i}|^2}{\sum_{i=1}^{R} (1-\rho_i)|g_i|^2 \left(\sigma_A^2 + \frac{\sigma_P^2}{\rho_i} \right) + \frac{\sigma_D^2}{\xi}}. \tag{6.8}$$

Obviously, the SNR is maximized where $\theta_i = -\arg f_i - \arg g_i$. Substituting θ_i in (6.8), we have

$$\gamma = \frac{P_S (\sum_{i=1}^{R} \sqrt{1-\rho_i} |f_i g_i|)^2}{\sum_{i=1}^{R} (1-\rho_i)|g_i|^2 \left(\sigma_A^2 + \frac{\sigma_P^2}{\rho_i} \right) + \frac{\sigma_D^2}{\xi}} \tag{6.9}$$

and the only variables to be optimized are the PS factors $\rho_i, i = 1, 2, \cdots, R$.

6.3 PS Factor Optimization

6.3.1 Joint optimization

Our objective is to find the PS factors that maximizes γ. However, the non-concavity of γ renders this optimization problem non-convex. To solve the problem efficiently, we first convert the problem to a quasi-convex one. Then, the solution to the orignal problem can be obtained with arbitrary accuracy by employing the bisection method and evaluating a series of convex feasibility problems.

For clearer presentation, let $a_i = |f_i g_i|$, $b_i = |g_i|^2$, $x_i = \sqrt{1-\rho_i}$, and $y_i = \dfrac{x_i^2}{1-x_i^2}$. γ can then be rewritten as

$$\gamma = \frac{P_S(\sum_{i=1}^{R} a_i x_i)^2}{\sigma_A^2 \sum_{i=1}^{R} b_i x_i^2 + \sigma_P^2 \sum_{i=1}^{R} b_i y_i + \dfrac{\sigma_D^2}{\xi}}. \tag{6.10}$$

Let vector $\boldsymbol{a} = [a_1, a_2, \cdots, a_R]^\top$ and similarly for $\boldsymbol{b}$, $\boldsymbol{x}$, and $\boldsymbol{y}$, we have

$$\gamma = \frac{P_S \boldsymbol{a}^\top \boldsymbol{x}\boldsymbol{x}^\top \boldsymbol{a}}{\sigma_A^2 \sum_{i=1}^{R} b_i x_i^2 + \sigma_P^2 \boldsymbol{b}^\top \boldsymbol{y} + \dfrac{\sigma_D^2}{\xi}} \tag{6.11}$$

Let $\boldsymbol{X} = \boldsymbol{x}\boldsymbol{x}^\top$, then $X_{ii} = x_i^2$ and

$$\gamma = \frac{P_S \boldsymbol{a}^\top \boldsymbol{X} \boldsymbol{a}}{\sigma_A^2 \sum_{i=1}^{R} b_i X_{ii} + \sigma_P^2 \boldsymbol{b}^\top \boldsymbol{y} + \dfrac{\sigma_D^2}{\xi}} = \frac{P_S \boldsymbol{a}^\top \boldsymbol{X} \boldsymbol{a}}{\sigma_A^2 \mathrm{tr}\{\boldsymbol{B}\boldsymbol{X}\} + \sigma_P^2 \boldsymbol{b}^\top \boldsymbol{y} + \dfrac{\sigma_D^2}{\xi}} \tag{6.12}$$

where

$$\boldsymbol{B} = \begin{bmatrix} b_1 & & & \\ & b_2 & & \\ & & \ddots & \\ & & & b_R \end{bmatrix}.$$

The righthand-side of (6.12) is quasi-convex in $\boldsymbol{X}$ and $\boldsymbol{y}$, that is, the sub-level set $\{\boldsymbol{X}, \boldsymbol{y} | \gamma < t\}$ is convex for all $t \in \mathbb{R}$. This can be trivially shown since the numerator and the denominator are both linear in $\boldsymbol{X}$ and $\boldsymbol{y}$.

The optimization problem can be equivalently reformulated as

$$\underset{\boldsymbol{X},\boldsymbol{y}}{\text{maximize}} \quad \frac{P_S \boldsymbol{a}^\top \boldsymbol{X} \boldsymbol{a}}{\sigma_A^2 \text{tr}\{\boldsymbol{B}\boldsymbol{X}\} + \sigma_P^2 \boldsymbol{b}^\top \boldsymbol{y} + \frac{\sigma_D^2}{\xi}} \tag{6.13a}$$

$$\text{subject to} \quad \boldsymbol{X} = \boldsymbol{x}\boldsymbol{x}^\top, \tag{6.13b}$$

$$y_i = \frac{X_{ii}}{1 - X_{ii}}, \tag{6.13c}$$

$$0 \leqslant X_{ii} \leqslant 1, \tag{6.13d}$$

$$i = 1, 2, \cdots, R. \tag{6.13e}$$

Note that although the objective function in (6.13) is quasi-convex in $\boldsymbol{X}$ and $\boldsymbol{y}$, the constraints $\boldsymbol{X} = \boldsymbol{x}\boldsymbol{x}^\top$ and $y_i = \frac{X_{ii}}{1 - X_{ii}}, i = 1, 2, \cdots, R$ are all non-convex. We propose to convexify them by the following relaxations:

1. Semidefinite relaxation, i.e., replace $\boldsymbol{X} = \boldsymbol{x}\boldsymbol{x}^\top$ by $\boldsymbol{X} \succ 0$ and

2. Replace $y_i = \frac{X_{ii}}{1 - X_{ii}}$ by $y_i \geqslant \frac{X_{ii}}{1 - X_{ii}}$.

The first relaxation is tight if the resultant optimal $\boldsymbol{X}$ has rank 1. In our extensive simulations, the rank of the solutions of $\boldsymbol{X}$ has always been 1. For the case where $rank(\boldsymbol{X}) > 1$, if it exists, the relaxation is no longer tight, i.e. the transformation is not exact. Nonetheless, there are randomization techniques proposed in the literature that provide a good approximation to the original problem using the solution to the relaxed problem [42].

As for the second relaxation, the maximization process drives y_i toward zero since $b_i > 0$. Hence, $y_i^* = \frac{X_{ii}}{1 - X_{ii}}$ always holds for the optimal solution; otherwise, any $y_i' \in \left[\frac{X_{ii}}{1 - X_{ii}}, y_i^*\right)$ would yield a larger objective function value. Therefore, the second relaxation is also tight.

A maximization problem with a quasi-concave objective function and convex constraints can be solved with the bisection method by solving a series of convex feasibility problems of the form

$$\underset{\boldsymbol{X},\boldsymbol{y}}{\text{maximize}} \quad 0 \tag{6.14a}$$

$$\text{subject to} \quad P_S \boldsymbol{a}^\top \boldsymbol{X} \boldsymbol{a} \geqslant c \left(\sigma_a^2 \text{tr}\{\boldsymbol{b}\boldsymbol{x}\} + \sigma_p^2 \boldsymbol{b}^\top \boldsymbol{y} + \frac{\sigma_d^2}{\xi} \right) \tag{6.14b}$$

$$\boldsymbol{X} \succ 0, \tag{6.14c}$$

$$y_i \geqslant \frac{X_{ii}}{1 - X_{ii}}, \tag{6.14d}$$

$$0 \leqslant X_{ii} \leqslant 1, \tag{6.14e}$$

$$i = 1, 2, \cdots, R. \tag{6.14f}$$

It is feasible if and only if the optimal SNR $\gamma^* \geqslant c$. In the meantime, we known that

$$\gamma^* = \frac{P_S (\sum_{i=1}^R \sqrt{1-\rho_i^*} |f_i g_i|)^2}{\sum_{i=1}^R (1-\rho_i^*) |g_i|^2 \left(\sigma_A^2 + \frac{\sigma_P^2}{\rho_i^*} \right) + \frac{\sigma_D^2}{\xi}} \leqslant \frac{\xi P_S (\sum_{i=1}^R |f_i g_i|)^2}{\sigma_D^2} \tag{6.15}$$

and

$$\gamma^* \geqslant \gamma \Big|_{\rho_1 = \rho_2 = \cdots = \rho_R = \frac{1}{2}}. \tag{6.16}$$

Therefore, with know upper and lower bounds, γ^* can be found with arbitrary accuracy with the bisection method and henceforth the corresponding $\boldsymbol{X}$. The detailed description of the algorithm is presented in Algorithm 2, where ϵ is a positive number denoting the tolerance. The optimal PS factors can then be obtained by $\rho_i = 1 - X_{ii}$.

Algorithm 2 PS factor optimization for network beamforming

Calculate the upper bound u and lower bound l of the SNR according to (6.15) and (6.16), respectively.
repeat
  $c \leftarrow \dfrac{u+l}{2}$;
  Solve the feasibility problem in (6.14);
  if feasible **then**
    $l \leftarrow c$;
    $\boldsymbol{X}^* \leftarrow \boldsymbol{X}$;
  else
    $u \leftarrow c$;
  end if
until $u - l < \epsilon$
$\rho_i \leftarrow 1 - X_{ii}, i = 1, 2, \cdots, R$.

6.3.2 Separate Optimization

To obtain the optimal PS factors requires a joint optimization with all channel responses available. In some scenarios, one may prefer a distributed scheme where each relay determines its own PS factor with CSI related to itself alone. In such cases, a sub-optimal solution can be obtained by optimizing the PS factor at each relay separately. Relay i optimizes ρ_i by maximizing the SNR γ_i at the destination as if only Relay i is available.

$$\gamma_i = \frac{P_S(1-\rho_i)|f_i g_i|^2}{(1-\rho_i)|g_i|^2\left(\sigma_A^2 + \dfrac{\sigma_P^2}{\rho_i}\right) + \dfrac{\sigma_D^2}{\xi}} = \frac{P_S|f_i g_i|^2}{|g_i|^2\left(\sigma_A^2 + \dfrac{\sigma_P^2}{\rho_i}\right) + \dfrac{\sigma_D^2}{\xi(1-\rho_i)}} \tag{6.17}$$

Maximizing γ_i is equivalent to minimizing its denominator, which is denoted as $\tilde{\gamma}_i = |g_i|^2\sigma_A^2 + \dfrac{|g_i|^2\sigma_P^2}{\rho_i} + \dfrac{\sigma_D^2}{\xi(1-\rho_i)}$. Obviously,

$$\frac{\partial^2 \tilde{\gamma}_i}{\partial \rho_i^2} = \frac{2\,b\sigma_P^2}{\rho_i^3} + \frac{2\,\sigma_D^2}{(1-\rho_i)^3\xi} > 0 \tag{6.18}$$

where $0 \leqslant \rho_i \leqslant 1$. Therefore, $\tilde{\gamma}_i$ is convex in $\rho_i \in [0,1]$. Let

$$\frac{\partial \tilde{\gamma}_i}{\partial \rho_i} = -\frac{|g_i|^2 \sigma_P^2}{\rho_i^2} + \frac{\sigma_D^2}{(1-\rho_i)^2 \xi} = 0. \tag{6.19}$$

Considering $0 \leqslant \rho_i \leqslant 1$, we have $\rho_i^* = \dfrac{|g_i|\sigma_P\sqrt{\xi}}{|g_i|\sigma_P\sqrt{\xi} + \sigma_D}$.

6.4 Simulations

We evaluate the performance of our proposed network beamforming scheme by simulations and compare it with that of SRS and greedy GRS in the same network. Simulation parameters are presented in Table 6.1. The transmit SNR at the source ranges from -4 dB to 10 dB and the pathloss effect is ignored.

Table 6.1: Simulation Parameters

Bandwidth	10 MHz
Noise Power Spectral Density	-174 dBm/Hz
Noise Figure	5 dB
Energy Harvesting Efficiency	90%
Outage SNR Threshold	5 dB

We first consider a simple network with only 2 relays and compare the average capacity of our proposed SDR-based PS factor optimization method for NB with that of the grid search. The results are presented in Fig. 6.2. The average capacity curves of these two methods are almost identical. And the same is true for the 5- and 95-percentile curve pairs. These observations demonstrate that our relaxations are tight and the relaxed optimization problem is a very good approximation to the original one.

Then we compare the average capacities of different cooperative schemes with varying source transmit SNR and numbers of relays. The results are shown in Fig. 6.3. Our proposed

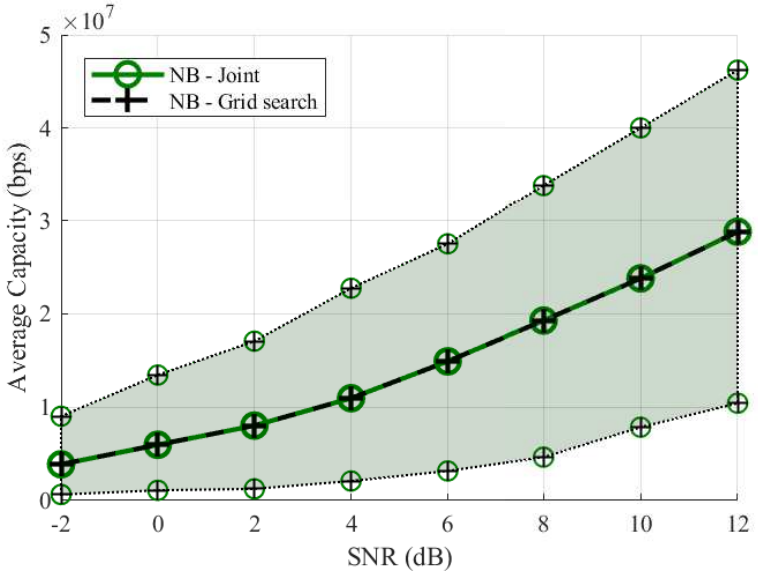

Figure 6.2: NB capacity comparisons between our proposed SDR-based PS optimization method and the grid search. The dotted lines with corresponding markers show the 5- and 95-percentiles of the data.

jointly optimal NB scheme outperforms all other schemes. The separately optimized NB scheme performs slightly worse than the jointly optimal one. In particular, the jointly optimal NB scheme has a $7 - 8$ dB gain compared with the greedy GRS scheme for the network with 10 relays. This shows that the shared-bandwidth NB schemes can achieve a much higher rate than even the best orthogonal-channel cooperative scheme. Of course, such gain is obtained at the cost of additional complexity of synchronization among relays.

Comparing scenarios with 4 and 10 relays, the differences among schemes are more significant when more relays are available. For example, the gain of the jointly optimal NB scheme with respect to the separately optimized one is approximately 1 dB when there are 10 relays, while the same gain is about 0.5 dB in the scenario with 4 relays. This is mainly because that, when more relays are available, the jointly optimal transmit power control, implemented by PS factor adjustments, among relays can contribute more to the SNR at the destination.

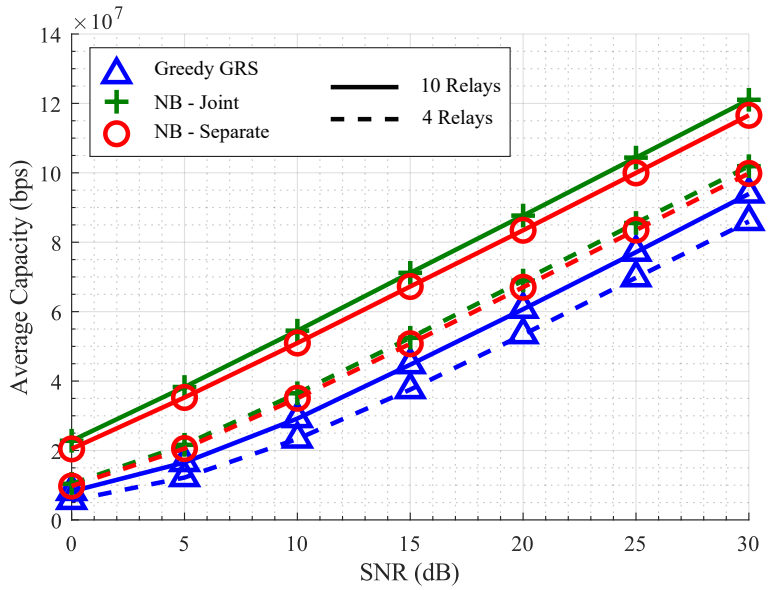

Figure 6.3: Capacity comparisons among cooperative schemes with varying source transmission SNR

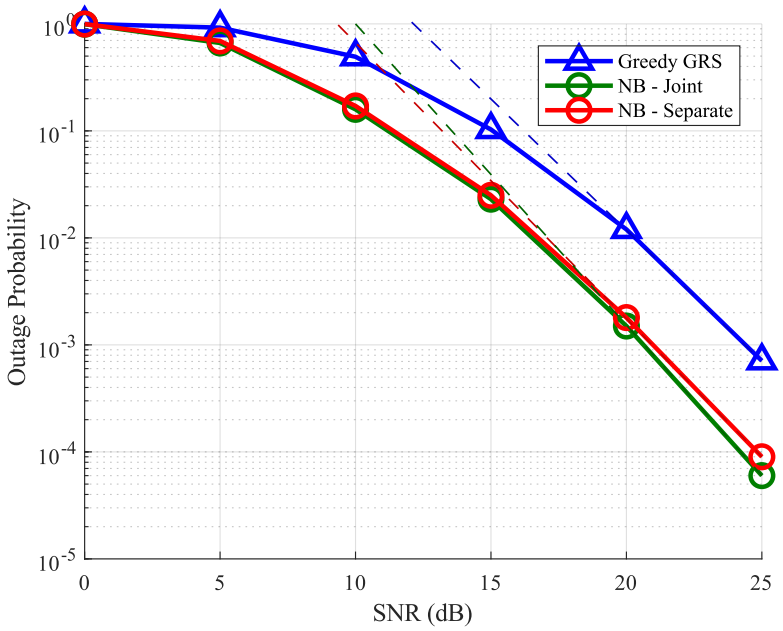

Figure 6.4: Outage probability comparisons among cooperative schemes with varying source transmission SNR in a network with 3 relays.

The outage probability performance comparisons among the same set of schemes are presented in Fig. 6.4. We see a similar trend here that both NB schemes outperform the RS ones. One interesting observation is that the gain of the NB schemes are even larger, especially at high SNR. This means that the improvement of NB schemes in reliability is even more significant than that in average capacity. Furthermore, the NB schemes is demonstrated to achieve higher diversity orders than the RS schemes, because their corresponding curves have a steeper slope at high SNR.

6.5 Conclusions

In this chapter, we investigate the network beamforming technique in HD EH relay networks. We formulated the joint optimization of PS factors and converted in to a quasi-convex one using SDR to enable an efficient solution. The jointly optimal PS factors are obtained with arbitrary accuracy by a combination of the bisection method and a series of convex feasibility problem. We also proposed a sub-optimal distributed solution in closed-form that optimizes the PS factor of each relay separately. Simulations demonstrated the superiority of both NB schemes compared with RS schemes.

CHAPTER 7

JOINT POWER ALLOCATION AND SPLITTING UNDER DOUBLY-SELECTIVE CHANNELS

Vehicular communications is an emerging research area that has been the focus of many researchers in recent years [44, 45] and it is a typical scenario in which SWIPT can facilitate the communications of energy constrained sensors. For example, direct connection to the power grid may be unavailable for roadside units (RSUs) in rural areas or along remote highways [46]. These RSUs rely on batteries to power themselves. SWIPT is a viable and affordable solution to extend the lifetime of these RSUs and reduce their maintenance cost. For future vehicles with a rapidly growing number of on-board sensors, SWIPT is more meaningful for sustainable communications of their on-board sensors, whose power can be supplied from other vehicles with excess power or grid-connected RSUs. And this is especially true for electric vehicles as their power is usually more stringent and precious. Moreover, this is also relevant in cooperative communications, where the relay node consumes its own energy to help enhance the communication performance among other nodes. In the setting we presented in the manuscript, the wireless energy transferred via SWIPT can serve as an incentive for cooperation. Nonetheless, the time-invariant channel assumption in existing studies on power allocation and splitting for SWIPT is generally invalid in vehicular communications. It is well-recognized that channel fading is a major factor that limits the performance of wireless communication systems. Channel estimation works well under slow fading conditions. Under fast fading conditions, however, the CSI estimated by the receiver

often becomes obsolete at the time of transmission. In vehicular communications, as the movement speed of the vehicles increases, the channel coherence time decreases [47–50]. For a vehicle moving at highway speed (75 mph or 120 km/h) with carrier frequency of 5.9 GHz, the 50% channel coherence time is only 0.65 ms. For time-variant channels, the proposition in [5] that static power splitting (SPS) scheme is the optimal dynamic power splitting (DPS) scheme no longer holds. On the other hand, the existing schemes could not accommodate the time-variant channel condition with optimal performance. The issue of channel prediction was brought up in [51, 52]. This has led to significant improvement in the performance of communication systems [53].

Frequency selectiveness, caused by the multi-path effect, is another aspect of channel fading that affects the performance of wireless communication systems, especially for wide-band systems such as VANETs. The tradeoff between power allocation principles favoring information and power transfer, respectively, was investigated in [4].

Therefore, studying the optimization of power allocation and splitting factor for SWIPT over doubly-selective channels is necessary for the application of SWIPT in practical scenarios.

7.1 Background

Grover et al. studied the inherent and non-trivial rate-energy tradeoff in the power allocation problem in SWIPT for frequency-selective channels [4]. The compromise between the optimal allocation for the highest Shannon capacity and that for the highest efficiency of power transfer was investigated. Traditionally, power allocation across subcarriers of different

frequencies is investigated to improve the overall information transmission capacity. In the context of SWIPT, power allocation over frequency selective channels was investigated by some researchers in [4, 54]. Waterfilling has long been known as the optimal power allocation scheme for information transmission, whereas power transfer favors a single-tone signal at the subcarrier with the largest channel response.

In [4], however, it was assumed that there is no loss of power on observing the signal for information decoding (ID). To the best of the authors' knowledge, however, practical circuits for EH from radio signals are not yet capable of directly decoding the carried information. As a result, two practical circuit designs, namely TS and PS, were proposed in [55]. In [5] and [56], the authors extended the work to a DPS scheme, which dynamically splits the received signal into two streams, for ID and EH respectively, with varying splitting factors over time. The rate-energy tradeoff is investigated by means of the rate-energy (R-E) region in the context of flat-fading time-invariant channel.

In this chapter, we investigate the power allocation at the transmitter and power splitting at the receiver for SWIPT over doubly-selective (i.e., selective in both the time and frequency domains) channels in a point-to-point vehicular communications system. Compared with existing work in the literature, we aim to improve the R-E region of the SWIPT system by exploiting the time and frequency diversity. Our contributions can be summarized as follows:

1. We propose a two-step scheme, named as joint power allocation and splitting (JoPAS), that optimizes the power allocation and power splitting over doubly-selective channels. Since the original problem is non-convex and difficult to solve directly, we propose to solve the problem along the time and frequency dimensions in a sequential manner.

The power allocation and splitting are first optimized over multiple slots in a time window while treating the channels as flat-fading. Then, the transmit power in each time slot is allocated to all the subcarriers according to the waterfilling algorithm, which is the optimal power allocation algorithm for traditional multi-carrier wireless communications. We further reformulate the original optimization problem in the first step of JoPAS, which is still non-convex, into a convex one, so that it can be solved efficiently by existing algorithms in polynomial time.

2. We derive the dual problem of the optimization across the time dimension in the first step of JoPAS. And then, by applying the KKT conditions, we discover some interesting resemblance between the optimal solution for SWIPT and the waterfilling scheme. Such observations are theoretically proved and corroborated by simulations.

3. In light of these observations, we propose a suboptimal heuristic algorithm named decoupled power allocation and splitting (DePAS). In contrast to JoPAS, it first splits the total transmit power in the time window into two parts for ID and EH, respectively. Then, the two parts of power are allocated to each time slot separately, with different strategies optimized for ID and EH respectively. Simulations demonstrate that DePAS achieves near-optimum performance with dramatically reduced computational complexity.

The rest of the chapter is organized as follows. The system model and assumptions are introduced in Section 7.2. The JoPAS is proposed and analyzed in Section 7.3. Section 7.4 proposes a low-complexity sub-optimal heuristic algorithm, named as DePAS, that achieves near-optimal solution. Simulations presented in Section 7.5 demonstrate the correctness of

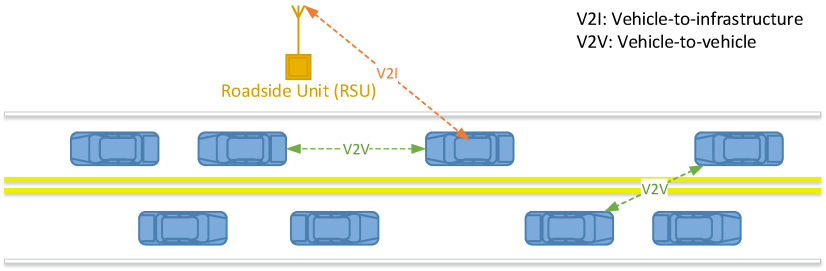

Figure 7.1: An illustrated vehicular communications scenario.

our derivations and proofs. Comparisons between the proposed algorithms and the DPS [5] are also conducted to show the improvement of our proposed algorithms. Finally, Section 7.6 concludes the chapter.

7.2 System Model

In this chapter, we focus on the optimization of the power allocation and the power splitting factors for PS-based SWIPT over doubly-selective vehicular channels, as shown in Fig. 7.1. As discussed above, the wireless channels in vehicular communications are highly selective in both frequency and time dimensions due to high speed movement of vehicles and the multipath effect.

Different from the traditional PS problem with time-invariant channels [5], we model the problem as a joint optimization of power allocation, across time and frequency, and SWIPT PS factors, across time slots, to maximize the data rate within a window of N time slots and K sub-bands. The channel response at the ith subcarrier in the jth time slot is denoted by h_{ij}. We assume that perfect CSI is available at the transmitter. Note that although the channel responses are different across both time and frequency, the PS factor can only vary across time, as the PS is implemented at the RF band before any digital processing.

The formulation of the optimization problem is

$$\underset{\boldsymbol{P},\boldsymbol{\rho}}{\text{maximize}} \quad \sum_{j=0}^{N-1}\sum_{i=0}^{K-1} \log_2\left(1+\frac{(1-\rho_j)|h_{ij}|^2 P_{ij}}{\sigma^2}\right) \tag{7.1a}$$

$$\text{subject to} \quad \sum_{j=0}^{N-1}\sum_{i=0}^{K-1} P_{ij} \leqslant E_{\text{total}}, \tag{7.1b}$$

$$\rho_k \in [0,1], \tag{7.1c}$$

$$\sum_{j=0}^{N-1} \rho_j \sum_{i=0}^{K-1} h_{ij} P_{ij} \geqslant E_{\text{del}}, \tag{7.1d}$$

$$0 \leqslant \sum_{i=0}^{K-1} P_{ij} \leqslant P_{\max}, \tag{7.1e}$$

$$j = 0, 1, \cdots, N-1, \tag{7.1f}$$

where P_{ij} denotes the transmit power for subcarrier i at time slot j and σ^2 is the variance of the additive white Gaussian noise generated by the down conversion circuits at the receiver. The antenna noise is usually much weaker than the down conversion noise. Hence, it is ignored in this work as in [54]. The symbol $\boldsymbol{P}$ represents the vector whose elements are $P_1, P_2, \cdots, P_N$. Likewise, $\boldsymbol{\rho}$ and other symbols in bold face in the rest of this chapter have similar meanings. Without loss of generality, the energy harvest efficiency is assumed to be 1 for simplicity of the analysis, since it is just a constant positive scalar that does not affect the formulation and properties of the problem.

The constraint (7.1b) limits the total energy consumed by the transmitter during the N-slot time window. It can also be deemed as a limit on the average power consumption at the transmitter because the transmitter could also be energy-constrained. The variable ρ_j represents the portion of power split to energy harvesting at the receiver in the jth time

slot and (7.1c) ensures it falls in the range from 0 to 1. The constraint (7.1d) states that the total delivered power to the receiver must exceed P_{del}. The constraints in (7.1e) describe the hardware limitations of instantaneous transmit power for each time slot.

7.3 Joint Power Allocation and Splitting

Since the objective function of the maximization problem in (7.1) is non-concave, it is a non-convex optimization problem and, hence, is difficult to solve efficiently. In this section, we propose a two-stage solution to this problem, named joint power allocation and splitting (JoPAS) and present it in Algorithm 3.

In the first stage, the power allocation and the power splitting factors across the N time slots are jointly optimized. The frequency selectiveness of the channels is ignored and the average channel response is used in the optimization. More specifically, we denote the average channel gain in the jth time slot as $\eta_j = \frac{1}{K}\sum_{i=0}^{K-1}|h_{ij}|^2$ and treat the channel as flat-fading.

In the second stage, the equivalent power allocated for ID in each time slot $(1-\rho_j)P_j$ is further distributed to each subcarrier by employing the waterfilling algorithm, which is known for the optimal power allocation for information transmission over frequency selective channels.

Finally, the transmit power for each subcarrier is obtained by scaling the equivalent power for ID by a factor of $\frac{1}{1-\rho_j}$. In the following, we will look into the two stages in more detail, respectively.

7.3.1 JoPAS Across Time

The JoPAS problem across time can be formulated as

$$\underset{\boldsymbol{P},\boldsymbol{\rho}}{\text{maximize}} \quad K\sum_{j=0}^{N-1}\log_2\left(1+\frac{(1-\rho_j)\eta_j P_j}{\sigma^2 K}\right) \tag{7.2a}$$

$$\text{subject to} \quad \sum_{j=0}^{N-1} P_j \leqslant E_{\text{total}}, \tag{7.2b}$$

$$\sum_{j=0}^{N-1} \rho_j\eta_j P_j \geqslant E'_{\text{del}}, \tag{7.2c}$$

$$\rho_j \in [0,1], \tag{7.2d}$$

$$0 \leqslant P_j \leqslant P_{\max}, \tag{7.2e}$$

$$j = 0, 1, \cdots, N-1. \tag{7.2f}$$

Note that (7.2) is still a non-convex problem. However, we can equivalently reformulate it to a convex optimization by substituting each cross term $(1-\rho_j)P_j$ with an auxilliary variable Q_j. After some mathematical manipulations, the reformulated problem is presented as

$$\underset{\boldsymbol{P},\boldsymbol{Q}}{\text{minimize}} \quad -\sum_{j=0}^{N-1}\ln(K\sigma^2+\eta_j Q_j) \tag{7.3a}$$

$$\text{subject to} \quad \sum_{j=0}^{N-1} P_j \leqslant E_{\text{total}}, \tag{7.3b}$$

$$\sum_{j=0}^{N-1} \eta_j\left(P_j - Q_j\right) \geqslant E'_{\text{del}}, \tag{7.3c}$$

$$P_k \leqslant P_{\max}, \tag{7.3d}$$

$$0 \leqslant Q_k \leqslant P_k, \tag{7.3e}$$

$$k = 0, 1, \cdots, N-1, \tag{7.3f}$$

and ρ_j^* can then be obtained by $\rho_j^* = 1 - \frac{Q_j^*}{P_j^*}$, where $P_j^* \neq 0$. ρ_j^* is set to zero if $P_j^* = 0$. After the reformulation, (7.3) can be solved in polynomial time by many existing algorithms, such as the interior point method [57].

7.3.2 Power Allocation Across Frequency

In the second stage, the power allocated to each time slot P_j^* can be distributed to each subcarrier by employing waterfilling algorithm with $(1-\rho_j^*)P_j^* = Q_j^*$, which is the equivalent transmit power for ID. Let Q_{ij} denote the allocated equivalent transmit power for ID at subcarrier i in time slot j. And the actual transmit power for SWIPT can be obtained by $P_{ij}^* = \frac{1}{1-\rho_j^*} Q_{ij}^*$.

Obviously, the optimal solution of (7.3) should satisfy the equality in constraint (7.3c). If the power is evenly distributed to all the subcarriers in a time slot, the delivered energy should also equal to E'_{del}. However, when the transmit power is distributed to each subcarrier according to waterfilling, the actual delivered energy will be larger, since the waterfilling algorithm allocates higher power to subcarriers with larger channel gains. Therefore, we need to adjust the intermediate energy delivery objective E'_{del} so that the actual delivered energy matches E_{del}. Detailed description of the adjustment process is presented in Algorithm 3.

7.4 Decoupled Power Allocation and Splitting

The convex optimization problem in (7.3) can be solved by many existing numerical algorithms in polynomial time [57], which is typically considered computationally efficient. Nonetheless, it is still considerably slower than the waterfilling algorithm when N becomes large. In this section, we propose a faster power allocation and splitting algorithm that

Algorithm 3 JoPAS

Initialize $E'_{\text{del}} \leftarrow E_{\text{del}}$;
repeat
  Solve (7.3) and obtain the optimizers $\boldsymbol{P}^*$ and $\boldsymbol{Q}^*$.
  for all $j = 1, 2, \cdots, N$ **do**
    if $P_j^* > 0$ **then**
      $\rho_j^* \leftarrow 1 - \frac{Q_j^*}{P_j^*}$.
    else
      $\rho_j^* \leftarrow 0$.
    end if
    if $Q_j^* > 0$ **then**
      Obtain Q_{ij}^* by distributing Q_j^* to all subcarriers with the waterfilling algorithm
      $P_{ij}^* \leftarrow Q_{ij}^*/(1 - \rho_j^*)$
    else
      Allocate P_j^* to the subcarrier with the largest $|h_{ij}|^2$.
    end if
  end for
  Compute $\tilde{E}_{\text{del}} \leftarrow \sum_{j=0}^{N-1} \rho_j^* \sum_{i=0}^{K-1} |h_{ij}|^2 P_{ij}^*$.
  if $\tilde{E}_{\text{del}} < E_{\text{del}}$ **then**
    Increase E'_{del}
  else
    Decrease E'_{del}
  end if
until The delivered energy $\tilde{E}_{\text{del}}$ matches E_{del}
Calculate $\rho_k = 1 - \frac{Q_k}{P_k}$.

has comparable complexity with the traditional waterfilling algorithm. To achieve this goal, we first derive the dual problem and apply the Karush-Kuhn-Tucker (KKT) conditions to develop a deeper understanding of the problem.

To derive an interesting dual problem, we first reformulate (7.3) once more. Let vector inequality $\boldsymbol{a} > \boldsymbol{b}$, with respect to two vectors of equal length, represent that $a_i > b_i$ for all elements. The problem can be reformulated as

$$
\begin{aligned}
\underset{\boldsymbol{P},\boldsymbol{Q}}{\text{minimize}} \quad & \tilde{R}(\boldsymbol{Q}) = \begin{cases} -\sum_{j=0}^{N-1} \ln(K\sigma^2 + \eta_j Q_j), & \boldsymbol{Q} \geqslant \mathbf{0}; \\ \infty, & \text{otherwise.} \end{cases} \\
\text{subject to} \quad & Q_j - P_j \leqslant 0, j = 0, 1, \cdots, N-1, \\
& P_k - P_{\max} \leqslant 0, j = 0, 1, \cdots, N-1, \\
& P_{\text{del}} - \sum_{j=0}^{N-1} \eta_j \left(P_j - Q_j\right) \leqslant 0, \\
& \sum_{j=0}^{N-1} P_j - P_{\text{total}} \leqslant 0.
\end{aligned}
\tag{7.4}
$$

By moving the lower bound on $\boldsymbol{Q}$ to the objective function, fewer dual variables will be introduced and, thus, facilitate our analysis of the problem.

Proposition 7.1 *The dual problem of* (7.4) *is*

$$
\underset{\boldsymbol{\lambda},\boldsymbol{\mu},\alpha,\beta}{\text{maximize}} \quad g(\boldsymbol{\lambda}, \boldsymbol{\mu}, \alpha, \beta) \tag{7.5a}
$$

$$
\text{subject to} \quad \alpha + \mu_k - \eta_k \lambda_k - \eta_k \beta = 0, \tag{7.5b}
$$

$$
\boldsymbol{\lambda} \geqslant \mathbf{0}, \boldsymbol{\mu} \geqslant \mathbf{0}, \alpha \geqslant 0, \beta \geqslant 0. \tag{7.5c}
$$

where

$$
\begin{aligned}
g(\boldsymbol{\lambda}, \boldsymbol{\mu}, \alpha, \beta) = & \sum_{k=0}^{N-1} \ln(\lambda_k + \beta) - \sigma^2 \sum_{k=0}^{N-1} (\lambda_k + \beta) \\
& - P_{\max} \sum_{k=0}^{N-1} \mu_k - P_{\text{total}} \alpha + P_{\text{del}} \beta + N.
\end{aligned}
\tag{7.6}
$$

Proof. See Section 7.7. ■

By applying the KKT conditions to the primal-dual pair and exploiting the zero duality gap, we have

Proposition 7.2 *For any P_j^* strictly less than $P_{\max}$,*

$$(1-\rho_j^*)P_j^* = \left(\frac{1}{\alpha^*} - \frac{\sigma^2}{\eta_j}\right)^+ \tag{7.7}$$

where $(\cdot)^+$ denotes $\max(0,\cdot)$ and α^* is the optimizer of the dual problem (7.5).

Proof. See Section 7.8. ■

Note that α^* is a constant with respect to j. The right-hand side of (7.7) is of the same form of the waterfilling scheme in conventional communication systems. Therefore, Proposition 7.2 tells us that the power allocated for ID follows a pattern similar to the waterfilling scheme over time when the maximum transmit power is not reached. Intuitively, it is desirable for the purpose of EH to allocate all the power to the time slot with the largest η_j, referred to as the best time slot. Whereas for the purpose of ID, the optimal power allocation is waterfilling, which favors time slots with larger η_j by allocating more power to them, but also allocates some power to time slots with smaller η_j to exploit the extra transmission time.

Therefore, the optimal power allocation for SWIPT would only use the best time slot for power transfer and allocate the remaining power with the waterfilling scheme, should the constraints on maximum instantaneous transmit power (7.3d) did not exist. Nonetheless, with the constraints in (7.3d), ID and EH will have to compete for the transmit power at time slots with larger η_j-s when the maximum instant transmit power is reached, meaning $P_j = P_{\max}$. In such situations, neither the ID nor the EH part can transmit the ideal amount of power. Instead, they will have to compromise to achieve the optimal solution. Part of the

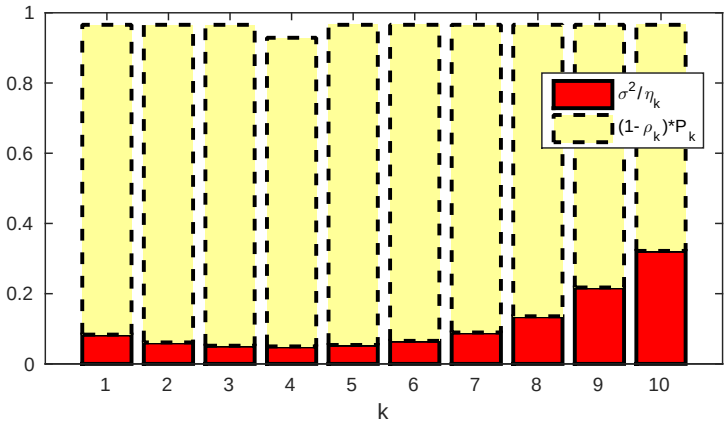

(a) Transmit power allocated for ID.

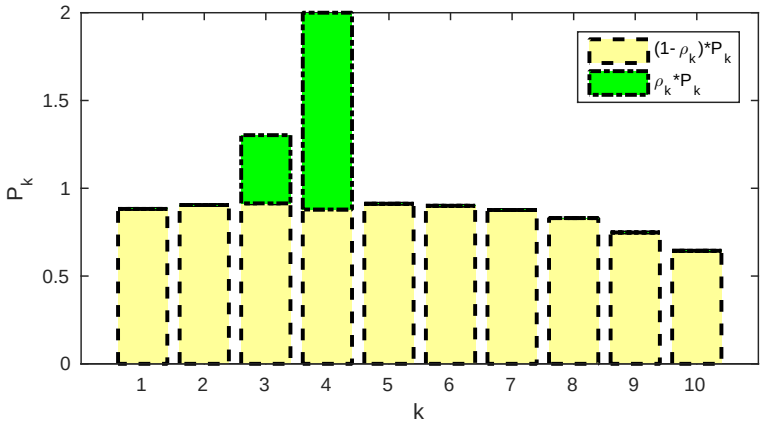

(b) Transmit power for ID and EH.

Figure 7.2: JoPAS solutions at high SNR.

power to be transmitted for EH will shift to other time slots with lower η_j. And that for ID will also deviate from the waterfilling solution.

Figs. 7.2 and 7.3 show the optimal transmit power allocation and power splitting factors at the receiver. In the figures, the black bars denote the ratios $\frac{\sigma^2}{\eta_k}$, which is a visualization of the channel conditions at each time slot. In the meantime, it is the varying term at the right-hand side of (7.7), which can be regarded as the "riverbed" of the waterfilling scheme. The blue bars stacked on the black bars represent the power allocated to the respective time slots.

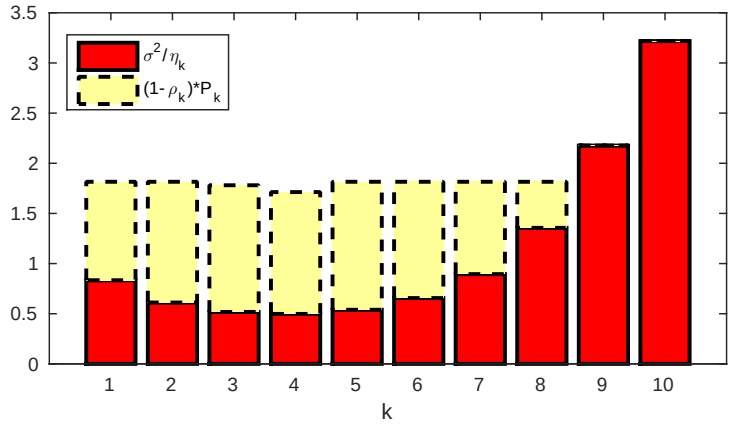

(a) Transmit power allocated for ID.

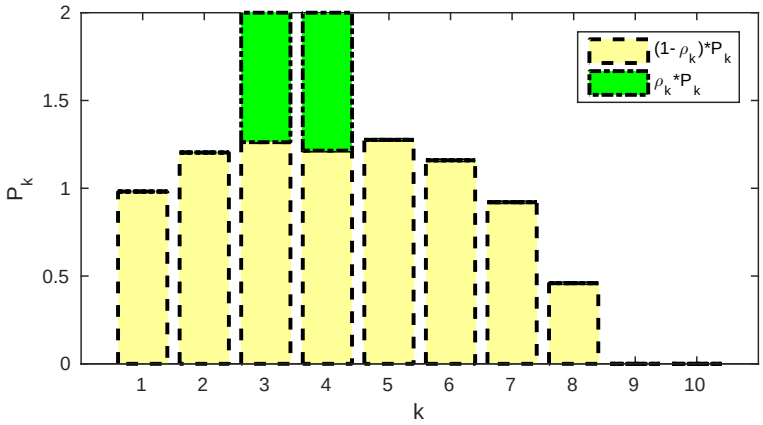

(b) Transmit power for ID and EH.

Figure 7.3: JoPAS solutions at low SNR.

We observe the same phenomenon as described in Proposition 7.2. The optimal power allocation for information transfer, represented by the blue bars in the figures, always shows similar pattern as the regular waterfilling scheme wherever the maximum transmit power limit is not reached. At the time slots where $P_{\max}$ is reached, on the other hand, the power allocation shows obvious differences from the waterfilling scheme, e.g., the time slot where $k = 4$ in Fig. 7.2 and the time slots where $k = 3, 4$ in Fig. 7.3. This simulation verifies the correctness of our derivation and the proof of Proposition 7.2.

Although the first stage of JoPAS algorithm is a convex optimization problem, the complexity to find the optimum solution is still polynomial with respect to the number of time slots N. Whereas the complexity of the waterfilling algorithm for traditional power allocation problems is only linear to N. On the other hand, according to Proposition 7.2, the power allocation for ID follows a pattern similar to waterfilling except at time slots where $P_k = P_{\max}$. In the following, we propose a heuristic low-complexity algorithm, named DePAS, to obtain a sub-optimal solution to the problem in (7.3), which formulates the sub-problem of the first stage of the overall problem.

In this algorithm, we first split the total transmit power in the N time slots according to a factor ρ. For the part of power split for ID, waterfilling scheme is adopted to calculate the power for ID at each time slot. For the other part of power split for EH, time slots with higher η_k are adopted with priority. If the transmit power at the best time slot reaches $P_{\max}$, the channel with the next largest η_k is used for the remaining power and so on. Then the value of the overall power splitting factor ρ is adjusted until the required power delivery P_{del} is achieved. The detailed algorithm description is presented in Algorithm 4. In Section 7.5, simulations show that the performance of the DePAS is almost as good as that of the JoPAS.

7.5 Simulations

Without loss of generality, we consider a vehicle-to-infrastructure link in vehicular communications, with the vehicle moving at a speed of 120 km/h, which is the typical speed on highways. The carrier frequency is set to 5.9 GHz and the bandwidth is 10 MHz. The ITU channel model for vehicular test environment Channel A is adopted and the variation

Algorithm 4 DePAS

Initialize $\rho \leftarrow \rho_0$;
repeat
  Split $(1-\rho)P_{\text{total}}$ for ID and allocate Q_j by the waterfilling algorithm
  for all $Q_j > P_{\max}$ **do**
    $Q_j \leftarrow P_{\max}$
  end for
  Prioritize the time slots with larger η_j-s when allocating the remaining power for EH as long as the constraints $P_j \leqslant P_{\max}$ hold.
  for all $j = 1, 2, \cdots, N$ **do**
    if $P_j > 0$ **then**
      $\rho_j \leftarrow 1 - \frac{Q_j}{P_j}$.
    else
      $\rho_j \leftarrow 0$.
    end if
    if $Q_j > 0$ **then**
      Obtain Q_{ij} by distributing Q_j to all subcarriers with the waterfilling algorithm
      $P_{ij} \leftarrow Q_{ij}/(1-\rho_j)$
    else
      Allocate P_j to the subcarrier with the largest $|h_{ij}|^2$.
    end if
  end for
  Compute $\tilde{E}_{\text{del}} \leftarrow \sum_{j=0}^{N-1} \rho_j^* \sum_{i=0}^{K-1} |h_{ij}|^2 P_{ij}^*$.
  if $\tilde{E}_{\text{del}} < E_{\text{del}}$ **then**
    Increase ρ
  else
    Decrease ρ
  end if
until The delivered energy $\tilde{E}_{\text{del}}$ matches E_{del}

in time is generated according to the Jake's model [58]. To demonstrate the effectiveness of JoPAS and DePAS, we compare them with the DPS scheme [5], which allocates transmit power evenly and optimizes the splitting factor ρ_k at each time slot.

7.5.1 Flat-Fading Time-Variant Channels

In this comparison, we assume the channel responses are flat across all subcarriers but variant across time. The total transmit energy E_{total} is set to N units and E_{del} is set to vary

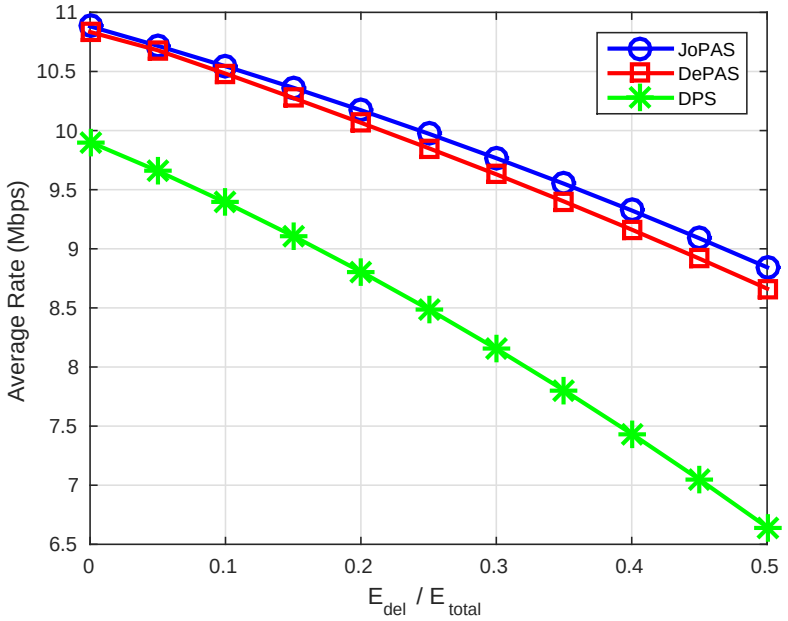

Figure 7.4: Average rate (Mbps) achieved by JoPAS and DePAS in comparison with DPS under flat-fading channels.

from 0 to $0.5E_{\text{total}}$. The average rates for ID are shown in Fig. 7.4. From the results, we observe that, compared with DPS, both JoPAS and DePAS improve the capacity for ID while satisfying the same requirement on EH, especially when larger amount of EH is required. This is because that the DPS only utilizes the CSI for power splitting factor optimization and the power allocation is not adapted according to the CSI. Additionally, the achievable rate of DePAS is close to that of JoPAS with dramatically reduced computational complexity from $\mathcal{O}(N^3)$ to $\mathcal{O}(N)$.

Besides the comparison of the average rate, we take a closer look at the rate-energy tradeoff for a given channel. For a realization of the time-variant channel $\boldsymbol{\eta}$ in $N = 10$ time slots, the achievable R-E regions at high SNR and low SNR are presented in Fig. 7.5. At the high-rate end of the curves in Fig. 7.5, where $E_{\text{del}} = 0$, the difference between JoPAS and DPS in achievable rate decreases as SNR increases. This is reasonable since the optimal

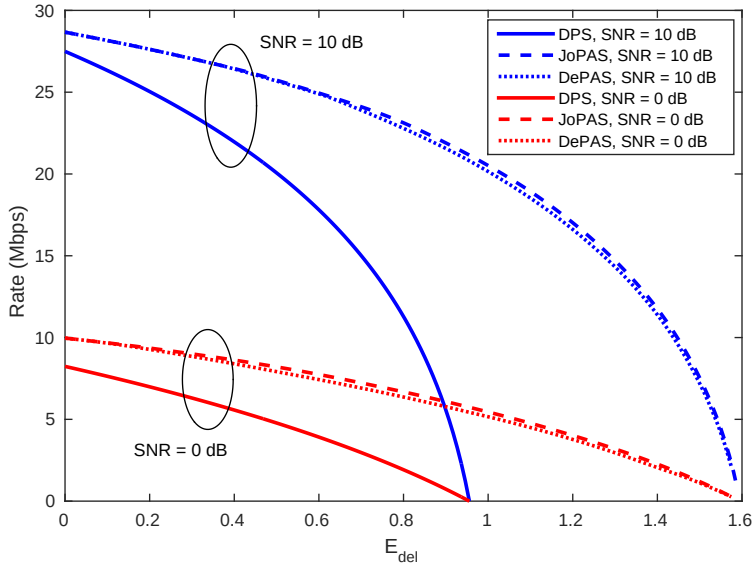

Figure 7.5: Achievable rate-energy regions of JoPAS, DePAS, and DPS.

power allocation in JoPAS, i.e., the waterfilling scheme, is close to uniform allocation since σ^2/η_k is almost zero across all k-s, and the DPS just allocates E_{total}/N to each time slot.

Fig. 7.5 shows that both DePAS and JoPAS achieves much larger R-E region than DPS. For this given channel $\boldsymbol{\eta}$, the R-E region difference between DePAS and JoPAS is negligible.

7.5.2 Doubly-Selective Channels

In this set of simulations, our proposed algorithms will be evaluated under scenarios with frequency-selective channels. The average rate vs. the energy delivery requirement is presented in Fig. 7.6. We observe similar trend with the scenarios with flat-fading channels, although the improvement of JoPAS and DePAS is not as dramatic. This is because the JoPAS algorithm is optimal for flat-fading channels, whereas it is no longer the case for frequency-selective channels. Therefore, for scenarios with frequency-selective channels, the heuristic algorithms cannot perfectly realize the potential benefits of joint power allocation and power splitting.

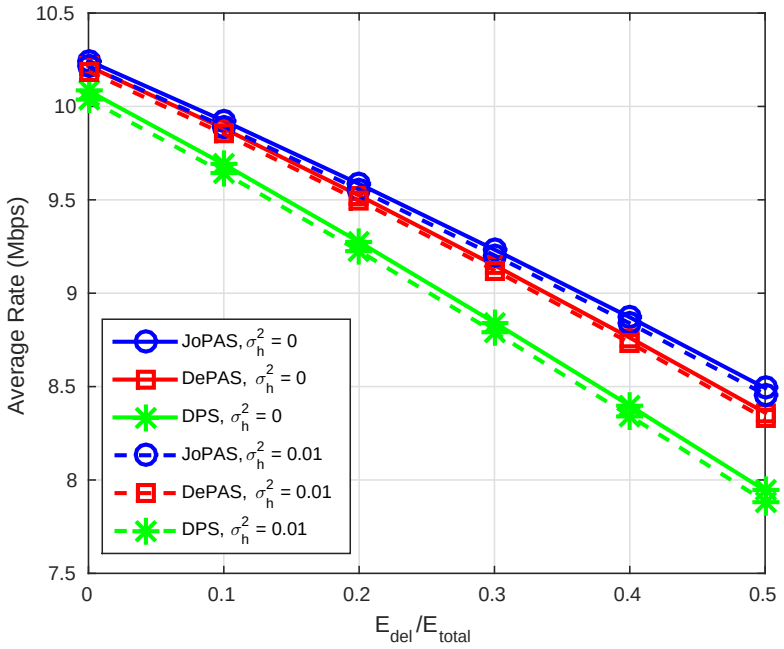

Figure 7.6: Average rate (Mbps) achieved by JoPAS and DePAS in comparison with DPS under frequency-selective channels. Solid lines represent cases with perfect channel prediction. Dashed lines represent cases with Gaussian channel prediction error with variance 0.01.

Fig. 7.6 also presents the performance when Gaussian distributed channel prediction errors are added. The performance degradation caused by channel prediction errors is negligible with the error covariance set to 0.01. This is a very conservative simulation setting for channel prediction errors, since most existing channel prediction methods could achieve such accuracy within at least half wavelength, which is approximately 5 cm for carrier frequency of 5.9 GHz. The vehicle movement during one time slot, on the other hand, is less than 0.3 mm.

7.5.3 Effect of Window Length

The effect of window length in terms of the number of time slots N is investigated in this subsection. Simulations demonstrate that the average rate achieved by all three

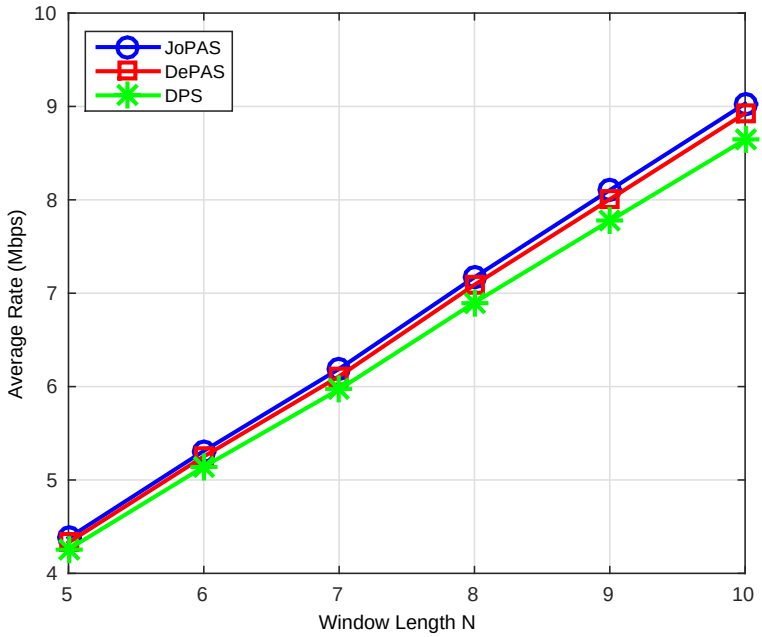

Figure 7.7: Average rate vs. window length.

algorithms increases while longer window length is employed in the power allocation and splitting optimization, as presented in Fig. 7.7. The results match the intuition that when longer time window is considered during the optimization, the better will the performance be, given perfect CSI at the transmitter. In practice, however, the transmitter only has predicted imperfect CSI. In this case, longer time window inevitably involves larger channel prediction errors and, henceforth, affects the performance negatively. The problem of optimal window length and the tradeoffs therein in such scenarios are out of the scope of this work and require a dedicated study.

7.5.4 Effect of Speed

The relative speed between the transmitter and the receiver is also an important factor to the performance of the system. As shown in Fig. 7.8, an interesting phenomenon is that the

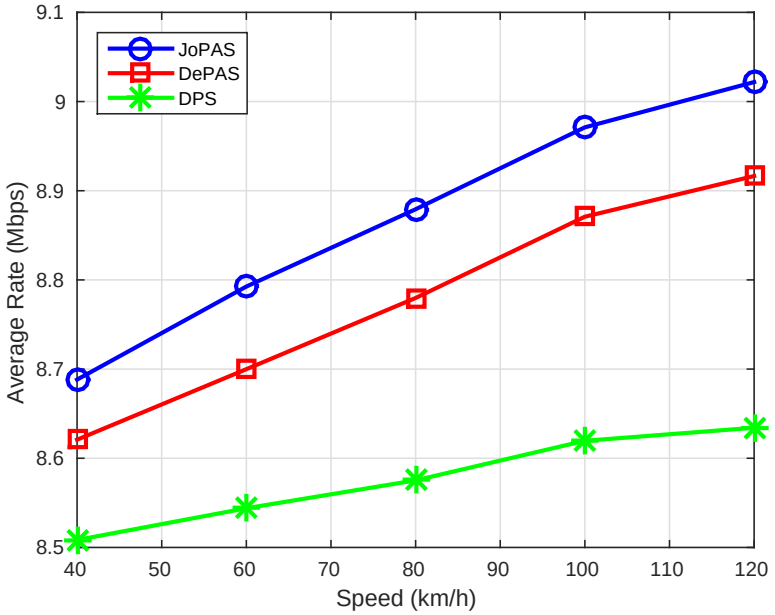

Figure 7.8: Average rate vs. relative speed.

average rate of all the algorithms increases as the relative speed increases. Although this is rather counter intuitive at the first glance, it is actually a result of stronger diversity. When the relative speed is higher, the channel response changes faster since the coherence time of the channel becomes smaller. Consequently, the considered time window with length N is more probable to include time slots with higher channel gains. With the power allocation and splitting optimization, the transmitter can exploit such diversity and improve the rate of communication. In addition, we can observe that the larger time variance of the channel responses further generates greater superiority of our proposed algorithms, which involve more sophisticated optimization along the dimension of time than the DPS.

7.6 Conclusions

In this chapter, we investigated the power allocation and splitting factor optimization for simultaneous information and power transfer over doubly-selective vehicular channels. Since

the problem is difficult to solve directly due to its non-convexity, we proposed a two-step approach, named JoPAS, to the problem along the time and frequency dimensions sequentially. In the first step, the optimization along the time dimension is transformed into a convex problem. In the second step, the optimization along the frequency dimension is solved in a manner similar to the waterfilling algorithm in traditional wireless communications systems. To further simplify the solution to the optimization problem in the first step, we then derived its dual problem and proved that the power allocated for ID follows the waterfilling scheme at time slots when the maximum instant transmit power constraint is inactive. Following this observation, a heuristic algorithm DePAS was proposed that decouples the optimization of power allocation and power splitting. Simulations verified our analyses and demonstrated that JoPAS achieves much larger R-E region than DPS over time-variant channels and, henceforth, provides improved flexibility and more efficient usage of the channel, especially at low SNR. In addition, simulations also indicated that our proposed DePAS algorithm achieves similar performance with JoPAS despite significantly reduced computational complexity.

7.7 Proof of Theorem 7.1

The Lagrangian is

$$\begin{aligned} L(\boldsymbol{P},\boldsymbol{Q},\boldsymbol{\lambda},\boldsymbol{\mu},\alpha,\beta) &= \tilde{R}(\boldsymbol{Q})+\sum_{k=0}^{N-1}\lambda_k(Q_k-P_k)+\sum_{k=0}^{N-1}\mu_k(P_k-P_{\max})+\alpha(\sum_{k=0}^{N-1}P_k-P_{\text{total}}) \\ &\quad+\beta(P_{\text{del}}-\sum_{k=0}^{N-1}\eta_k P_k+\sum_{k=0}^{N-1}\eta_k Q_k) \\ &= \tilde{R}(\boldsymbol{Q})+\sum_{k=0}^{N-1}(\lambda_k+\eta_k\beta)Q_k+\sum_{k=0}^{N-1}(\alpha+\mu_k-\lambda_k-\eta_k\beta)P_k \\ &\quad-P_{\max}\sum_{k=0}^{N-1}\mu_k-P_{\text{total}}\alpha+P_{\text{del}}\beta. \end{aligned} \tag{7.8}$$

Let

$$\frac{\partial L}{\partial Q_k}=-\frac{\eta_k}{\sigma^2+\eta_k Q_k}+\lambda_k+\beta\eta_k=0 \tag{7.9}$$

we have

$$Q_k^*=\left(\frac{1}{\lambda_k+\beta\eta_k}-\frac{\sigma^2}{\eta_k}\right)^+ \tag{7.10}$$

where Q_k^* is the optimum Q_k that miminizes the Lagrangian (7.8) and $(\cdot)^+$ denotes the function $\max(0,\cdot)$. Therefore, we have

$$\tilde{g}(\boldsymbol{\lambda},\boldsymbol{\mu},\alpha,\beta)=\inf_{\boldsymbol{P},\boldsymbol{Q}}L(\boldsymbol{P},\boldsymbol{Q},\boldsymbol{\lambda},\boldsymbol{\mu},\alpha,\beta) \tag{7.11}$$

Substituting (7.10) into (7.8) yields

$$\tilde{g}(\boldsymbol{\lambda}, \boldsymbol{\mu}, \alpha, \beta) = \begin{cases} g(\boldsymbol{\lambda}, \boldsymbol{\mu}, \alpha, \beta), & \alpha + \mu_k - \lambda_k - \eta_k \beta = 0, \forall k; \\ -\infty, & \text{otherwise.} \end{cases}$$

Therefore, the dual problem

$$\text{maximize} \quad \tilde{g}(\boldsymbol{\lambda}, \boldsymbol{\mu}, \alpha, \beta)$$

is equivalent to (7.5).

7.8 Proof of Theorem 7.2

Obviously, Slater's condition holds as there exist a strictly feasible point for the primal problem. Let $(\boldsymbol{\lambda}^*, \boldsymbol{\mu}^*, \alpha^*, \beta^*)$ represents the optimizer of the dual problem (7.5). Therefore, the optimizer for the primal problem is

$$(\boldsymbol{P}^*, \boldsymbol{Q}^*) = \arg \inf_{\boldsymbol{P}, \boldsymbol{Q}} L(\boldsymbol{P}, \boldsymbol{Q}, \boldsymbol{\lambda}^*, \boldsymbol{\mu}^*, \alpha^*, \beta^*). \tag{7.12}$$

Given the Q_k^* in (7.10) and substitute λ_k according to the constraints in (7.5b), we have

$$Q_k^* = \left(\frac{1}{\mu_k^* + \alpha^*} - \frac{\sigma^2}{\eta_k} \right)^+. \tag{7.13}$$

On the other hand, by applying the KKT condition on the primal dual pair (7.4) and (7.5), we have complementary slackness [57].

$$\mu_k^*(P_k^* - P_{\max}) = 0. \tag{7.14}$$

Therefore, for any P_k^* strictly less than $P_{\max}$, $\mu_k = 0$ and, hence, $Q_k^* = \left(\frac{1}{\alpha^*} - \frac{\sigma^2}{\eta_k}\right)^+$, which exactly is the form of waterfilling solutions.

CHAPTER 8

CONCLUSIONS AND FUTURE WORK

8.1 Conclusions

In this dissertation, we investigated the application of SWIPT in EH relay networks with various configurations and assumptions.

First, we proposed PS-SWIPT-based FD EH relay networks. Truly FD operation can be achieved in the entire transmission cycle because of the employment of PS, instead of TS in existing work in the literature. Compared with existing state-of-the-art FD EH relaying schemes, our proposed scheme significantly improves the source-to-destination ergodic capacity, as verified by theoretical analysis and simulations.

Secondly, we proposed two cooperative schemes in networks with multiple EH relays, namely RS and network beamforming. Based on the received SINR at the sources in FDEH2W networks, we proved the quasi-convexity of the PS factor optimization, and the optimal PS factor for each relay was obtained by one-dimensional search. In addition, we proposed two efficient SRS methods based on the optimized PS factor at each relay. Both SRS methods perform almost identically to the exhaustive search based optimal RS at high SNR. In addition, given the fundamental differences of the EH networks from conventional multi-relay networks, we proved the suboptimality of SRS. Since, unfortunately, the optimal GRS can only be obtained by exhaustive search with exponential complexity, we proposed three relay ordering based GRS methods with linear complexity and a greedy GRS method with quadratic complexity. Our proposed GRS methods achieve near-optimal performance

uniformly in a wide range of transmit SNR with much lower complexity than the exhaustive search. For HD EH relay networks, we proposed network beamforming and the joint optimization of PS factors therein. To solve the optimization problem efficiently, it was converted to a quasi-convex one with the help of SDR. In addition to this centralized solution, we also proposed a distributed beamforming scheme in which the PS factor at each relay is optimized separately using only CSI related to the relay itself. Simulations show that both schemes outperform the RS schemes and achieve higher rate and reliability at various SNR levels.

Finally, we expanded our research to include the time dimension and investigated the power allocation and splitting factor optimization for SWIPT over doubly-selective vehicular channels. Since the problem is difficult to solve directly due to its non-convexity, we proposed a two-step approach, named JoPAS, to the problem along the time and frequency dimensions sequentially. Inspired by the dual problem and one of the KKT conditions, we also proposed a heuristic algorithm DePAS that decouples the optimization of power allocation across time and frequency and power splitting. Simulations verified our analyses and demonstrated that JoPAS provides improved flexibility and more efficient usage of the channel, especially at low SNR. Our proposed DePAS algorithm also demonstrated similar performance with JoPAS despite significantly reduced computational complexity.

8.2 Future Work

In this dissertation, we mainly studied the cooperative techniques in dual-hop EH relay networks under simplified channel conditions, except the work presented in Chapter 7, where

point-to-point SWIPT over doubly-selective channels is studied. The impact of doubly-selective channels on communications in EH relay networks is more complicated and interesting. The objective is no longer to transfer sufficient amount of information and energy via a particular link. Instead, maximizing the end-to-end capacity becomes the objective and EH relays become intermediate nodes that rely on the energy harvested in the process to power themselves. Therefore, the power allocation across time and frequency dimensions, the power splitting/time switching factor, and the selection of relays require sophisticated investigation.

Furthermore, enabling energy storage for EH relays can significantly enhance the network performance. However, more flexible usage of harvested energy inevitably brings more complexity in the optimization of relaying schemes, as the system states become relevant to historical events instead of the ones occurring in the current transmission cycle alone. Existing work in the literature is far from sufficient, and abundant problems related to energy storage in EH relay networks are waiting to be investigated.

On the other hand, in existing work on cooperative relay networks, the relays are assumed to be selfless in the sense that they consume their own power to facilitate the communications between other nodes. The RS problem is usually approached from the perspective of the sources and destinations in a totalitarian manner. In practice, the motivations of the cooperating relays need to be considered as well, and fairness can be guaranteed by a competitive RS schemes with individual rationality of every node in mind. In this context, the energy harvested from the received signals may serve as an incentive for the relays to cooperate as their energy consumption is completely covered by the harvested energy, with

even some extra energy left to charge their own battery. And such incentives can further serve as a foundation of a game-theoretic approach to the RS problem.

REFERENCES

[1] D. Ross, "Battery bottleneck [editorial]," *Engineering & Technology*, vol. 5, no. 9, 2010.

[2] B. Gurakan, O. Ozel, J. Yang, and S. Ulukus, "Energy cooperation in energy harvesting communications," *IEEE Trans. Communications*, vol. 61, no. 12, pp. 4884–4898, December 2013.

[3] L. Varshney, "Transporting information and energy simultaneously," in *Proc. Intl. Symp. Information Theory*, Toronto, Ontario, Canada, July 6-11, 2008, pp. 1612–1616.

[4] P. Grover and A. Sahai, "Shannon meets Tesla: Wireless information and power transfer," in *Proc. Intl. Symp. Information Theory*, Austin, TX, June 13-18, 2010, pp. 2363–2367.

[5] X. Zhou, R. Zhang, and C. K. Ho, "Wireless information and power transfer: Architecture design and rate-energy tradeoff," *IEEE Trans. Communications*, vol. 61, no. 11, pp. 4754–4767, November 2013.

[6] K. Singh, A. Gupta, T. Ratnarajah, and M.-L. Ku, "A General Approach Toward Green Resource Allocation in Relay-Assisted Multiuser Communication Networks," *IEEE Trans. Wireless Commun.*, vol. 1276, no. c, pp. 1–1, 2017.

[7] H. Cui, M. Ma, L. Song, and B. Jiao, "Relay selection for two-way full duplex relay networks with amplify-and-forward protocol," *IEEE Trans. Wireless Communications*, vol. 13, no. 7, pp. 3768–3777, July 2014.

[8] L. Blanco and M. Najar, "Subset relay selection in wireless cooperative networks using sparsity-inducing norms," in *Intl. Symp. Wireless Communications Systems*, Barcelona, Spain, August 26-29, 2014, pp. 501–505.

[9] Y. Jing and H. Jafarkhani, "Single and multiple relay selection schemes and their achievable diversity orders," *IEEE Trans. Wireless Communications*, vol. 8, no. 3, pp. 1414–1423, March 2009.

[10] S. Talwar, Y. Jing, and S. Shahbazpanahi, "Joint relay selection and power allocation for two-way relay networks," *IEEE Signal Processing Letters*, vol. 18, no. 2, pp. 91–94, February 2011.

[11] I. Maric and R. Yates, "Bandwidth and power allocation for cooperative strategies in Gaussian relay networks," *IEEE Trans. Information Theory*, vol. 56, no. 4, pp. 1880–1889, April 2010.

[12] S. Atapattu, Y. Jing, H. Jiang, and C. Tellambura, "Relay selection schemes and performance analysis approximations for two-way networks," *IEEE Trans. Communications*, vol. 61, no. 3, pp. 987–998, March 2013.

[13] M. Wen, X. Cheng, V. Poor, and B. Jiao, "Use of SSK modulation in two-way amplify-and-forward relaying," *IEEE Trans. Vehicular Technology*, vol. 63, no. 3, pp. 1498–1504, March 2014.

[14] M. Zhang, M. Wen, X. Cheng, and L. Yang, "A dual-hop virtual MIMO architecture based on hybrid differential spatial modulation," *IEEE Trans. Wireless Communications*, vol. 15, no. 9, pp. 6356–6370, September 2016.

[15] A. Nasir, X. Zhou, S. Durrani, and R. Kennedy, "Relaying protocols for wireless energy harvesting and information processing," *IEEE Trans. Wireless Communications*, vol. 12, no. 7, pp. 3622–3636, July 2013.

[16] M. Duarte and A. Sabharwal, "Full-duplex wireless communications using off-the-shelf radios: Feasibility and first results," in *Proc. Asilomar Conf. Signals, Systems, and Computers*, Pacific Grove, CA, November 7-10, 2010, pp. 1558–1562.

[17] M. Duarte, C. Dick, and A. Sabharwal, "Experiment-driven characterization of full-duplex wireless systems," *IEEE Trans. Wireless Communications*, vol. 11, no. 12, pp. 4296–4307, December 2012.

[18] S. Li and R. Murch, "An investigation into baseband techniques for single-channel full-duplex wireless communication systems," *IEEE Trans. Wireless Communications*, vol. 13, no. 9, pp. 4794–4806, September 2014.

[19] N. Shende, O. Gurbuz, and E. Erkip, "Half-duplex or full-duplex relaying: A capacity analysis under self-interference," in *Annual Conf. Information Sciences and Systems (CISS)*, Baltimore, MD, March 20-22, 2013, pp. 1–6.

[20] C. Zhong, H. Suraweera, G. Zheng, I. Krikidis, and Z. Zhang, "Wireless information and power transfer with full duplex relaying," *IEEE Trans. Communications*, vol. 62, no. 10, pp. 3447–3461, October 2014.

[21] M. Mohammadi, H. Suraweera, G. Zheng, C. Zhong, and I. Krikidis, "Full-duplex MIMO relaying powered by wireless energy transfer," in *IEEE International Workshop on Sig-*

nal Processing Advances in Wireless Communications (SPAWC), Stockholm, Sweden, June 28 - July 1, 2015, pp. 296–300.

[22] Y. Zeng and R. Zhang, "Full-duplex wireless-powered relay with self-energy recycling," *IEEE Wireless Communications Letters*, vol. 4, no. 2, pp. 201–204, April 2015.

[23] D. Wang, R. Zhang, X. Cheng, and L. Yang, "Capacity-Enhancing Full-Duplex Relay Networks based on Power-Splitting (PS-)SWIPT," *IEEE Trans. Veh. Technol.*, vol. 66, no. 6, pp. 5445–5450, Jun. 2017.

[24] W. Xu, J. Zhang, and P. Zhang, "Outage probability of two-hop fixed-gain relay with interference at the relay and destination," *IEEE Communications Letters*, vol. 15, no. 6, pp. 608–610, June 2011.

[25] M. Duarte, A. Sabharwal, V. Aggarwal, R. Jana, K. K. Ramakrishnan, C. W. Rice, and N. K. Shankaranarayanan, "Design and characterization of a full-duplex multiantenna system for WiFi networks," *IEEE Transactions on Vehicular Technology*, vol. 63, no. 3, pp. 1160–1177, March 2014.

[26] E. Chong and S. Żak, *An Introduction to Optimization*, 2nd ed. Wiley, 2001.

[27] I. S. Gradshteyn and I. M. Ryzhik, *Table of integrals, series, and products*, 7th ed. Elsevier/Academic Press, Amsterdam, 2007.

[28] A. Bletsas, A. Khisti, D. Reed, and A. Lippman, "A simple cooperative diversity method based on network path selection," *IEEE Journal on Selected Areas in Communications*, vol. 24, no. 3, pp. 659–672, mar 2006.

[29] X. Rui, J. Hou, and L. Zhou, "On the performance of full-duplex relaying with relay selection," *Electronics Letters*, vol. 46, no. 25, p. 1674, 2010.

[30] I. Krikidis, H. Suraweera, P. Smith, and C. Yuen, "Full-duplex relay selection for amplify-and-forward cooperative networks," *IEEE Trans. Wireless Communications*, vol. 11, no. 12, pp. 4381–4393, December 2012.

[31] C.-L. Wang and J.-Y. Chen, "Power allocation and relay selection for AF cooperative relay systems with imperfect channel estimation," *IEEE Transactions on Vehicular Technology*, vol. 65, no. 9, pp. 7809–7813, sep 2016.

[32] C. H. M. de Lima, H. Alves, P. H. J. Nardelli, and M. Latva-aho, "Effects of relay selection strategies on the spectral efficiency of wireless systems with half- and full-duplex nodes," *IEEE Transactions on Vehicular Technology*, vol. 66, no. 8, pp. 7578–7583, aug 2017.

[33] K.-H. Liu, "Outage-optimal relay selection for energy-harvesting relays based on power splitting," in *International Conf. on Wireless Communications & Signal Processing (WCSP)*, Nanjing, China, October 15-17, 2015, pp. 1–6.

[34] J. Men, J. Ge, and C. Zhang, "A joint relay-and-antenna selection scheme in energy-harvesting MIMO relay networks," *IEEE Signal Processing Letters*, vol. 23, no. 4, pp. 532–536, April 2016.

[35] D. Wang, R. Zhang, X. Cheng, and L. Yang, "Relay Selection in Two-Way Full-Duplex Energy-Harvesting Relay Networks," in *IEEE Glob. Commun. Conf.*, Dec. 2016, pp. 1–6.

[36] L. Song, "Relay selection for two-way relaying with amplify-and-forward protocols," *IEEE Trans. Vehicular Technology*, vol. 60, no. 4, pp. 1954–1959, May 2011.

[37] D. Wang, R. Zhang, X. Cheng, and L. Yang, "Relay selection in power splitting based energy-harvesting half-duplex relay networks," in *IEEE Veh. Technol. Conf.*, Sydney, NSW, Australia, Jun. 2017.

[38] J. Men, J. Ge, C. Zhang, and J. Li, "Joint optimal power allocation and relay selection scheme in energy harvesting asymmetric two-way relaying system," *IET Communications*, vol. 9, no. 11, pp. 1421–1426, July 2015.

[39] D. Wang, R. Zhang, X. Cheng, L. Yang, and C. Chen, "Relay Selection in Full-Duplex Energy-Harvesting Two-Way Relay Networks," *IEEE Trans. Green Commun. Netw.*, vol. 1, no. 2, pp. 182–191, Jun. 2017.

[40] Y. Jing and H. Jafarkhani, "Network beamforming using relays with perfect channel information," *IEEE Trans. Information Theory*, vol. 55, no. 6, pp. 2499–2517, June 2009.

[41] Y. Alsaba, S. K. A. Rahim, and C. Y. Leow, "Beamforming in wireless energy harvesting communications systems: A survey," *IEEE Communications Surveys & Tutorials*, vol. 20, no. 2, pp. 1329–1360, 2018.

[42] V. Havary-Nassab, S. Shahbazpanahi, A. Grami, and Z.-Q. Luo, "Distributed beamforming for relay networks based on second-order statistics of the channel state information," *IEEE Transactions on Signal Processing*, vol. 56, no. 9, pp. 4306–4316, September 2008.

[43] O. T. Demir and T. E. Tuncer, "Distributed beamforming in relay networks for energy harvesting multi-group multicast systems," in *IEEE International Conference on Acoustics, Speech and Signal Processing (ICASSP)*, March 2016.

[44] X. Cheng, L. Yang, and X. Shen, "D2D for intelligent transportation systems: A feasibility study," *IEEE Transactions on Intelligent Transportation Systems*, vol. 16, no. 4, pp. 1784–1793, Aug 2015.

[45] X. Cheng, C. Chen, W. Zhang, and Y. Yang, "5G-enabled cooperative intelligent vehicular (5GenCIV) framework: When benz meets marconi," *IEEE Intelligent Systems*, vol. 32, no. 3, pp. 53–59, May 2017.

[46] R. Atallah, M. Khabbaz, and C. Assi, "Energy harvesting in vehicular networks: a contemporary survey," *IEEE Wireless Communications*, vol. 23, no. 2, pp. 70–77, apr 2016.

[47] J. Fernandez, K. Borries, L. Cheng, B. Kumar, D. Stancil, and F. Bai, "Performance of the 802.11p physical layer in vehicle-to-vehicle environments," *IEEE Trans. Vehicular Technology*, vol. 61, no. 1, pp. 3–14, January 2012.

[48] X. Cheng, C. X. Wang, D. I. Laurenson, S. Salous, and A. V. Vasilakos, "An adaptive geometry-based stochastic model for non-isotropic MIMO mobile-to-mobile channels," *IEEE Transactions on Wireless Communications*, vol. 8, no. 9, pp. 4824–4835, September 2009.

[49] X. Cheng, Q. Yao, M. Wen, C. X. Wang, L. Y. Song, and B. L. Jiao, "Wideband channel modeling and intercarrier interference cancellation for vehicle-to-vehicle communication

systems," *IEEE Journal on Selected Areas in Communications*, vol. 31, no. 9, pp. 434–448, September 2013.

[50] X. Cheng, C. X. Wang, B. Ai, and H. Aggoune, "Envelope level crossing rate and average fade duration of nonisotropic vehicle-to-vehicle ricean fading channels," *IEEE Transactions on Intelligent Transportation Systems*, vol. 15, no. 1, pp. 62–72, February 2014.

[51] J.-K. Hwang and J. Winters, "Sinusoidal modeling and prediction of fast fading processes," in *Proc. Global Telecommunications Conf.*, vol. 2, Sydney, Australia, November 8-12, 1998, pp. 892–897.

[52] G. Giannakis and C. Tepedelenlioglu, "Basis expansion models and diversity techniques for blind identification and equalization of time-varying channels," *Proc. the IEEE*, vol. 86, no. 10, pp. 1969–1986, October 1998.

[53] A. Duel-Hallen, "Fading channel prediction for mobile radio adaptive transmission systems," *Proc. the IEEE*, vol. 95, no. 12, pp. 2299–2313, December 2007.

[54] G. Huang, Q. Zhang, and J. Qin, "Joint time switching and power allocation for multi-carrier decode-and-forward relay networks with SWIPT," *IEEE Signal Processing Letters*, vol. 22, no. 12, pp. 2284–2288, December 2015.

[55] R. Zhang and C. K. Ho, "MIMO broadcasting for simultaneous wireless information and power transfer," *IEEE Trans. Wireless Communications*, vol. 12, no. 5, pp. 1989–2001, 2013.

[56] L. Liu, R. Zhang, and K.-C. Chua, "Wireless information and power transfer: A dynamic power splitting approach," *IEEE Trans. Communications*, vol. 61, no. 9, pp. 3990–4001, 2013.

[57] S. Boyd and L. Vandenberghe, *Convex optimization*. Cambridge University Press, 2004.

[58] R. I.-R. M.1225, "Guidelines for evaluation of radio transmission technologies for imt-2000," International Telecommunications Union, Tech. Rep., 1997.

LIST OF ABBREVIATIONS

A	Amplify-and-forward
AP	All-participate
CDF	Cumulative distribution function
CHMO	Channel harmonic mean ordering
CSI	Channel state information
DePAS	Decoupled power allocation and splitting
DF	Decode-and-forward
DPS	Dynamic power splitting
EE	Energy efficiency
EH	Energy harvesting
FD	Full-duplex
FDEH2W	Full-duplex energy-harvesting two-way
GRS	General relay selection
HD	Half duplex
ID	Information decoding
IP	Information processing
JoPAS	Joint power allocation and splitting
KKT	Karush-Kuhn-Tucker
MIMO	Multiple-input multiple-output
NB	Network beamforming
PDF	Probability density function

PS	Power splitting
PSR	Power-splitting relaying
R-D	Relay-to-destination
RF	Radio frequency
RS	Relay selection
RSU	Roadside unit
S-R	Source-to-relay
SDR	Semi-definite relaxation
SE	Spectral efficiency
SINR	Signal-to-interference-and-noise ratio
SNR	Signal-to-noise ratio
SPS	Static power splitting
SRS	Single relay selection
SWIPT	Simultaneous wireless information and power transfer
TS	Time switching
TSR	Time-switching relaying
VANET	Vehicular ad-hoc network
WCO	Worse channel ordering
WSINRO	Worse signal-to-interference-and-noise ratio ordering